KAUNAS UNIVERSITY OF TECHNOLOGY

ANDRIUS RAPALIS

PHYSIOLOGICAL SIGNAL PROCESSING ALGORTIHMS FOR SHORT-TERM HEART RATE AND BLOOD PRESSURE VARIABILITY ESTIMATION

Doctoral dissertation

Technological Sciences, Electrical and Electronics Engineering (01T)

2017, Kaunas

This doctoral dissertation was prepared at Kaunas University of Technology, Biomedical Engineering Institute during the period of 2012–2017.

Scientific Supervisor:

Dr. Artūras JANUŠAUSKAS (Kaunas University of Technology, Technological Sciences, Electrical and Electronics Engineering – 01T).

Doctoral dissertation has been published in:
http://ktu.edu

Editor:

Dovilė Dumbrauskaitė (Publishing House "Technologija")

ISBN 978-609-02-1332-2

The bibliographic information about the publication is available in the National Bibliographic Data Bank (NBDB) of the Martynas Mažvydas National Library of Lithuania

KAUNO TECHNOLOGIJOS UNIVERSITETAS

ANDRIUS RAPALIS

FIZIOLOGINIŲ SIGNALŲ APDOROJIMO ALGORITMAI TRUMPALAIKIAM ŠIRDIES RITMO IR KRAUJO SPAUDIMO VARIABILUMUI VERTINTI

Daktaro disertacija

Technologijos mokslai, elektros ir elektronikos inžinerija (01T)

2017, Kaunas

Disertacija rengta 2012-2017 metais Kauno technologijos universiteto Biomedicininės inžinerijos institute.

Mokslinis vadovas:

Dr. Artūras JANUŠAUSKAS (Kauno technologijos universitetas, technologijos mokslai, elektros ir elektronikos inžinerija – 01T).

Interneto svetainės, kurioje skelbiama disertacija, adresas:
http://ktu.edu

Redagavo:

Dovilė Dumbrauskaitė (Leidykla "Technologija")

ISBN 978-609-02-1332-2

Leidinio bibliografinė informacija pateikiama Lietuvos nacionalinės Martyno Mažvydo bibliotekos Nacionalinės bibliografijos duomenų banke (NBDB)

CONTENTS

ABBREVIATIONS

ACC – Accelerometer
ANAM4 – Automated neuropsychological assessment metrics
ANS – Autonomic nervous system
BP – Blood pressure
BPV – Blood pressure variability
C1D1 – Control1 day1
C1D2 – Control1 day2
CD – Coefficient of determination
CV – Coefficient of variation
CVDs – Cardiovascular diseases
DBP – Diastolic blood pressure
DQ – Direct quadrature
E1D1 – Experiment1 day1
E1D2 – Experiment1 day2
E2D1 – Experiment2 day1
E2D2 – Experiment2 day2
ECG – Electrocardiogram
EEMD – Ensemble empirical mode decomposition
EMD – Empirical mode decomposition
HF – High frequency
HF norm – HF power in normalized units
HHT – Hilbert-Huang transform
HR – Heart rate
HRV – Heart rate variability
HT – Hilbert transform
IF – Instantaneous frequency
IF1 – 1st extracted instantaneous PPG frequency
IF2 – 2nd extracted instantaneous PPG frequency
IFe – Instantaneous frequencies from PPG extraction algorithm
IMF1 – first decomposed intrinsic mode function
IMF2 – second decomposed intrinsic mode function
IMFs – Intrinsic mode functions
LF – Low frequency
LF norm – LF power in normalized units
LF/HF ratio – LF and HF ratio
MD – Mean difference
NHFA – National Heart Foundation of Australia
NN – normal-to-normal
NN50 – Number of pairs of adjacent NN intervals differing by more than 50 ms in the entire recording
PAT – Blood volume pulse arrival time

PATca – Classical PAT estimation algorithm based on the maximum of 1st PPG signal derivative
PATdp – Diastole-patching pulse arrival time estimation algorithm
PATht – Pulse arrival time estimation algorithm based on the Hilbert transform
PEP – Pre-ejection period
pNN50 – NN50 count divided by the total number of all NN intervals
PPG – Photoplethysmogram
PSD – Power spectral density
PTT – Pulse transit time
PWV – Pulse wave velocity
RMSSD – Square root of mean squared differences of NN intervals
RRI – The interval between successive peaks of the ECG R waves
SBP – Systolic blood pressure
SD – Standard deviation
SDANN – Standard deviation of mean of short period (5 min) intervals
SDNN – Standard deviation of NN intervals
SDNN index – Mean of the SD of all NN intervals for all 5 min segments of the entire recording
SNR – Signal to noise ratio
SSD – Sum of square differences
TP – Total power
VLF – Very low frequency
WHO – World Health Organization
r_S – Spearman correlation coefficient

INTRODUCTION

Relevance of the research

Cardiovascular diseases (CVDs) is the number one cause of death in the world and was responsible for 17.5 million deaths in 2012 (31% of all deaths) (WHO, 2014a). Deaths of CVDs mainly consist of coronary heart disease (7.4 million) and stroke (6.7 million). In Europe CVDs are responsible for over 4 million deaths every year (47% of all deaths), including 1.9 million in the European Union (Nichols et al., 2012). Population growth and improved longevity lead to an increased number of older people in almost all parts of the world. For this reason, the number of deaths from CVDs is increasing as well, from 17.5 million in 2012 to the estimated 22.2 million in 2030 (WHO, 2014b).

Hypertension is a raised blood pressure (BP), which is a major risk factor of cardiovascular diseases and end organ damage: chronic kidney disease, stroke, myocardial infarction, heart failure, and other (NHFA, 2016). Each year, about 9.4 million people in the world die from the complications of hypertension (about 58% of all cardiovascular deaths) (WHO, 2013). Currently hypertension is diagnosed using non-invasive cuffless blood pressure devices. The absolute value of blood pressure and its changes over time are assessed. Blood pressure varies not only in long-term but also in short-term. The interaction between several cardiovascular regulatory systems (baroreceptor reflex, renin-angiotensin system, vascular myogenic response, and the release of nitric oxide from the endothelium) causes the beat-to-beat changes in blood pressure (Höcht, 2013). The changes of heart rate (HR) and blood pressure variability (HRV and BPV, respectively) are related to an increased risk of cardiovascular events (Greiser et al., 2005; Hillebrand et al., 2013; Thayera et al., 2010; Parati et al., 2012; Parati et al., 2013b). BPV influencers can be identified using spectral analysis and may provide important information about individual blood pressure control mechanisms (Stauss, 2007). Variability of blood pressure in ultra-short or very short (beat-to-beat) and short (within a 24 h period) term mainly reflect: the influences of reflex and central autonomic modulation (Mancia et al., 1986; Conway et al., 1984; Parati et al., 1995), the elastic properties of arteries (increased or reduced arterial compliance) (Parati et al., 2006; Kotsis et al., 2011; Fukui et al., 2013), and the diverse nature and duration effects of humoral (angiotensin II, bradykinin, endothelin-1, insulin, nitric oxide), rheological (blood viscosity), and emotional factors (psychological stress) (Parati et al., 2013a). The detection of beat-to-beat BP fluctuations (BPV) can help to select antihypertensive drugs for hypertensive patients because elevated BPV in low frequency spectral component can show an increased vascular tone sympathetic modulation and response to sympatholytic drugs (Stauss, 2007).

However, the assessment of short-term BPV is quite complicated because continuous (beat-to-beat) blood pressure recording is needed (Mancia, 2012). Continuous blood pressure may be recorded invasively (commonly used in intensive care unit) and non-invasively. Nevertheless, current non-invasive BP recording devices are very expensive and are used only in laboratories or under ambulatory

conditions. For these reasons, it becomes necessary: 1) to improve the techniques and devices of non-invasive continuous blood pressure recording, to make them simpler and more readily available for usage; 2) to search for other parameters which are related to blood pressure and can be used for assessing continuous blood pressure and its variability.

Blood volume pulse arrival time (PAT) is one of the parameters which are related to blood pressure and the cardiovascular system (Smith et al., 1999). It is a time interval during which a pulse wave travels from the heart to a certain place in the body. PAT is used to estimate continuous beat-to-beat blood pressure (Chen et al., 2000; Heard et al., 2000; Poon, Zhang, 2005; Zong et al., 1998; Cattivelli, Garudadri, 2009; Gesche et al, 2012; Zheng et al., 2014), baroreflex sensitivity (Liu et al., 2012), cardiac output (Sugo et al., 2010), respiratory rate (Wu et al., 2012; Johansson et al., 2006), arterial stiffness (Liu et al., 2009), monitor psycho-physiological stress (Hey et al., 2009), and others.

The photoplethysmography (PPG) signal shows the changes in blood volume in the microvascular tissue bed. The PPG signal depends on the heart rate and other physiological properties (Murakami, Yoshioka, 2015) and is related to the cardiovascular system as well (Allen, 2007). The PPG signal is still not fully exploited for estimating cardiovascular parameters, therefore it has a lot of potential. All these facts raise scientific-technological problems and a working hypothesis.

Scientific-technological problem and working hypothesis

This thesis covers two main clinically relevant scientific-technological problems:

1. The algorithms for estimating the pulse arrival time of the existing blood volume are unreliable when photoplethysmogram signal is noisy, thus new noise-resistant algorithms are needed;
2. Currently there are no methods and algorithms which could evaluate short-term (beat-to-beat) blood pressure variability from a photoplethysmography signal.

The devices currently used for non-invasive continuous (beat-to-beat) blood pressure and its variability measurement and evaluation are expensive, uncomfortable to wear and use, and are based on cuff usage or calibration (arm or finger cuff). Only a few physiological parameters related to BP are measured using these methods. Measuring more parameters could provide more comprehensive information about blood pressure, its change, and variability. For these reasons, simpler signal measurement (for example, PPG), novel evaluation algorithms, and new parameters (and characteristics) related to blood pressure changes are needed and are highly desirable.

The working hypothesis of this thesis: blood volume pulse arrival time and instantaneous photoplethysmogram signal frequencies can be used for short-term blood pressure and heart rate variability evaluation.

Research object

An analysis of physiological signals to estimate short-term blood pressure and heart rate variability.

The aim of the research

The aim of the research is to develop and investigate noise-resistant algorithms for short-term blood pressure and heart rate variability estimation.

The objectives of the research

1. To develop and investigate a noise-resistant algorithm for blood volume pulse arrival time estimation.
2. To develop and investigate an algorithm which allows to extract characteristics (parameters) from a photoplethysmogram signal which is related to physiological processes (blood pressure and heart rate).
3. To evaluate the performance of the proposed algorithms to assess the short-term (beat-to-beat) blood pressure variability during rest and in non-stationary conditions.
4. To evaluate the performance of the proposed algorithms to assess the short-term (beat-to-beat) heart rate variability during rest and in non-stationary conditions.

Scientific novelty

In this doctoral thesis, a noise-resistant pulse arrival time estimation algorithm was developed. The proposed algorithm solves the parameter estimation problem associated with noisy physiological signals (electrocardiogram and photoplethysmogram) which mostly occurs in non-stationary conditions.

An algorithm for extracting instantaneous frequencies from a photoplethysmogram signal was developed. The proposed algorithm allows extracting characteristics which are related to the autonomic nervous system and the function of cardiovascular system from a photoplethysmogram signal recorded during rest and non-stationary conditions, for example, during exercise or thermal stress test.

Practical significance

The developed solutions and algorithms for estimating pulse arrival time and extracting instantaneous frequency can be used in the following clinical applications:

- The algorithm developed for estimating the pulse arrival time can be used for reliable PAT calculation when physiological signals are recorded in all conditions.
- The algorithm developed for instantaneous frequency extraction can be used for short-term blood pressure and heart rate variability assessment when physiological signals are recorded at rest or in non-stationary conditions.

- The algorithm developed for instantaneous frequency extraction allows long-term monitoring of instantaneous frequencies and variability of blood pressure and heart rate.
- The algorithms developed for extracting the instantaneous frequency and estimating the pulse arrival time can work together as a system for evaluating short-term blood pressure and heart rate variability or can be used separately.

The results of this research were presented in the project "Intellectual wearable sensors system for human wellness monitoring". No.: VP1-3.1-SMM-10-V-02-004, work sponsored by the European Social Fund, 2013-2015.

The statements presented for defense

1. The noise-resistant algorithm for estimating blood volume pulse arrival time was developed. The proposed algorithm is more accurate compared with the classical and diastole-patching pulse arrival time estimation algorithms when the photoplethysmogram signal is noisy.
2. The algorithm for extracting instantaneous frequencies from the photoplethysmogram signal was developed. The characteristics extracted using the proposed algorithm (instantaneous frequencies) are related to cardiovascular processes.
3. Characteristics estimated using the proposed algorithms can be used for evaluating short-term blood pressure variability during rest and in non-stationary conditions.
4. Characteristics estimated using the proposed algorithms can be used to evaluate short-term heart rate variability during rest and in non-stationary conditions.

Approval of the results

The results of this doctoral thesis were published in 7 publications: 2 papers in the international scientific journals referred in the Thomson Reuters Web of Science database. The results were presented at 6 scientific conferences.

Structure of the doctoral thesis

The thesis is organized as shown in Figure 0.1. Chapter 1 describes the physiology of the cardiovascular system, heart rate and blood pressure variability analysis, and currently used algorithms for pulse arrival time estimation. Chapter 2 presents the developed algorithms: pulse arrival time estimation and instantaneous photoplethysmogram signal frequency extraction. Chapter 3 describes the database of signals (simulated and experimental) used in this thesis. Chapter 4 describes the results obtained for each study. The doctoral thesis finishes with general conclusions (Chapter 5).

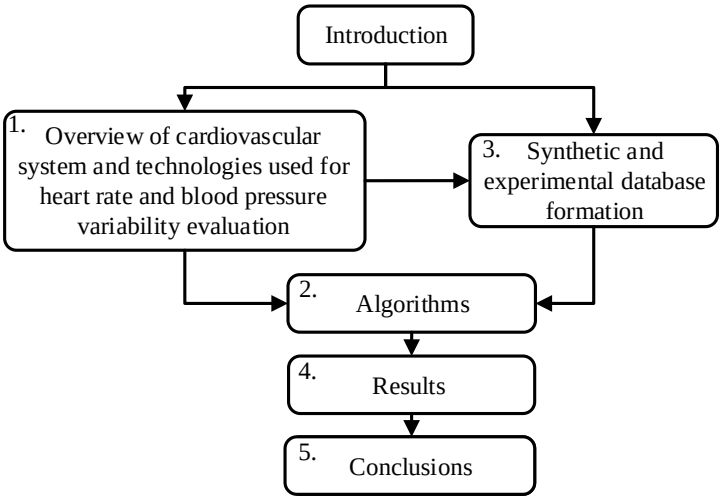

Figure 0.1. The structure of the doctoral thesis

The thesis consists of 133 pages, 64 figures, 26 tables, 39 formulas, and 180 references.

1. AN OVERVIEW OF THE CARDIOVASCULAR SYSTEM AND TECHNOLOGIES USED FOR HEART RATE AND BLOOD PRESSURE VARIABILITY EVALUATION

This chapter consists of nine parts. Section 1.1 describes the cardiovascular system (the anatomy and description of the heart and blood vessels) and the cardiac hemodynamic activity (blood circulation in the body). Section 1.2 illustrates the cardiac electrical activity (spread of action potentials) and the connection with the mechanical and hemodynamic activity (relations between mechanical events and electrical activity of the heart during a complete cardiac cycle). Section 1.3 depicts the autonomic nervous system (sympathetic and parasympathetic systems). Section 1.4 describes physiological signals (electrocardiography and photoplethysmography) whereas Section 1.5 characterizes pulse waves which travel through blood vessels, the conception of blood volume pulse arrival time and its relation to the cardiovascular and autoregulation systems, as well as blood pressure. Section 1.6 explains the conception of autonomic nervous system (ANS), how it changes, what determines the change, and the main parameters for heart rate variability evaluation (time-domain and frequency-domain). Section 0 defines the conception of blood pressure variability, how it changes, what factors influence the changes, along with the main parameters of short-term BPV evaluation. Section 1.8 describes the algorithms (time-domain and time-frequency) for pulse arrival time estimation. Finally, the chapter presents the conclusions (Section 1.9).

1.1. The cardiovascular system and cardiac hemodynamic activity

The cardiovascular system consists of two main parts: the heart and the network of blood vessels. The heart consists of four chambers: right atrium, right ventricle, left atrium, and left ventricle (Figure 1.1). Functionally, the heart is like two pumps and the pulmonary and systemic circulations are situated between these pumps.

Pulmonary circulation is blood flow through the lungs where the blood and alveoli exchange gasses. From the lungs blood returns to the heart (to the left atrium) through four pulmonary veins. Blood pressure in the left atrium is low (8–12 mmHg), thus the blood passively flows from the left atrium through the mitral valve (left atrioventricular valve) into the left ventricle. The left ventricle has a thick muscular wall, thus during contraction it can generate high pressure (100–140 mmHg). The left ventricle contracts and ejects blood through the aortic valve into the aorta and into the systemic circulation.

The systemic circulation consists of all blood vessels in the body except the vessels in the lungs. The circulation system consists of arteries (from heart to organs) and veins (from organs to heart) (Table 1.1). Arteries include the aorta, the large arteries, the small arteries, and capillaries. The aorta is the main vessel; blood flows through it from the heart into the systemic circulation. The main functions of the aorta are to distribute blood to the body and to damp the pulsatile pressure which appears because blood from the left ventricle is ejected not

continuously but intermittently. The aorta branches into the large arteries, for example, mesenteric, carotid, renal arteries; the function of these large arteries is to distribute blood to specific organs or regions. These large arteries can constrict and dilate but do not regulate pressure and blood flow under normal physiological conditions. When the large artery reaches the organs, it branches into smaller arteries which function is to distribute blood inside the organs. The smaller arteries branch into smaller and smaller vessels and when the diameters of vessels reach less than 200 μm and the number of layers of vascular smooth muscle reduces to just a few, they are called arterioles. The small arteries and arterioles regulate arterial blood pressure and blood flow within the organs. When the diameters of arterioles become smaller than 10 μm, the vessels lose smooth muscle and are termed capillaries. The capillaries consist only of endothelial cells and the basement membrane and are the smallest vessels in the body. The number of capillaries in the body is very large. When the capillaries join together, they form post-capillary venules; these venules have high permeability and can serve and exchange fluids and macromolecules. The post-capillary venules merge into larger venules with smooth muscle; they can constrict and dilate and, therefore, regulate the capillary pressure and volume of venous blood. The venules merge to larger veins; the largest systemic veins are the superior and inferior vena cava through which blood returns to the right atrium (Table 1.1).

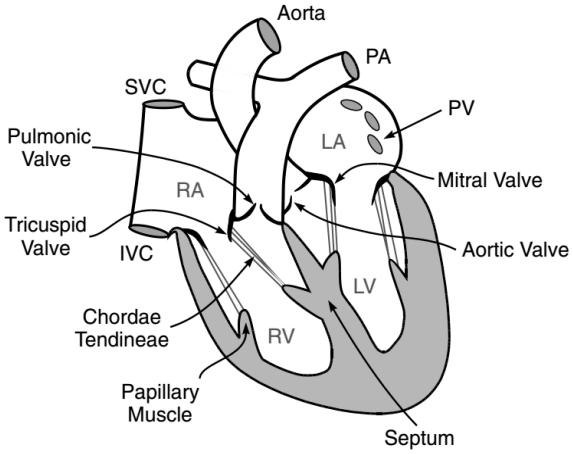

Figure 1.1. Anatomy of the heart: SVC – superior vena cava; PA – pulmonary artery; IVC – Inferior vena cava; RA – right atrium; LA – left atrium; RV – right ventricle; LV – left ventricle (adopted from Klabunde, 2011)

The right atrium receives returning venous blood from the superior and inferior vena cava (from the systemic circulation), and is very distensible because it should easily expand to accommodate the venous blood which returns at very low pressure (0–4 mmHg). Afterwards, the right atrium contracts and blood flows from the right atrium through the tricuspid valve (also called right atrioventricular valve) into the right ventricle. The contraction of the right ventricular ejects blood from the right ventricle through the pulmonic valve into the pulmonary artery (into

the pulmonary circulation). The systolic pressure during contraction is about 20–30 mmHg in a pulmonary artery. Right and left side of the heart (pulmonary and systemic circulations) have almost the same blood output which means that there is a minor shift in blood volume of pulmonary and systemic circulations.

Table 1.1. The size and function of blood vessels in systemic circulation (Klabunde, 2011)

Vessel	Diameter, mm	Function
Aorta	25	Pulse dampening and distribution
Large arteries	1.0–4.0	Distribution
Small arteries	0.2–1.0	Distribution and resistance
Arterioles	0.01–0.20	Resistance (pressure/flow regulation)
Capillaries	0.006–0.010	Exchange
Venules	0.01–0.02	Exchange, collection, and capacitance
Veins	0.2–5.0	Capacitance function (blood volume)
Vena cava	35	Collection

1.2. Cardiac electrical activity and the connection with mechanical and hemodynamic activity

The sinoatrial node generates the action potentials and they primarily spread through cell-to-cell conduction and propagate throughout the atria. The conduction velocity of action potentials in the atrial muscle is about 0.5 m/s and it is similar to the speed of action potentials in the ventricular muscle (Figure 1.2).

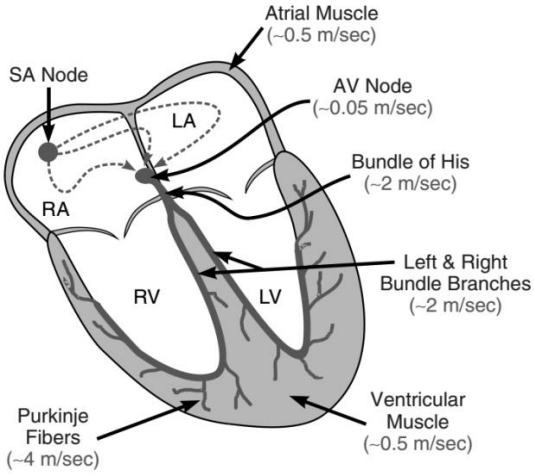

Figure 1.2. The conduction system of different heart regions and velocities of potentials. SA Node – sinoatrial node; RA – right atrium; LA – left atrium; RV – right ventricle; LV – left ventricle (adopter from Klabunde, 2011)

Atria and ventricles are separated by non-conducting connective tissue. In normal conditions the action potential can enter the ventricles only through a specialized region of cells (the atrioventricular node). The atrioventricular node is a specialized conducting tissue of the heart which slows the velocity of action

potentials about ten times, from about 0.5 m/s (in atrial muscle) to about 0.05 m/s. The delay of conduction between the atria and ventricles in the atrioventricular node is important because it gives time to complete the depolarization and contraction of the atria. A decreased conduction velocity decreases the frequency of impulses and activates the ventricle. After the atrioventricular node, the action potential enters the base of the ventricle and continues to left and right bundle branches at high velocity (about 2 m/s) along the interventricular septum. The bundle branches consist of Purkinje fibers which connect to the ventricular myocytes and become the final pathway to cell-to-cell conduction. The velocity of conduction in Purkinje fibers is very high (about 4 m/s).

Mechanical events of the heart during a complete cardiac cycle are related to the electrical activity of the heart. The diagram of a cardiac cycle (Figure 1.3) shows changes in the left side of the heart. Volume changes and timing of mechanical events in the right and left side of the heart are qualitatively similar. The difference is that the pressures in the left side are much higher.

The P wave is the first wave of the electrocardiogram (ECG) and a complete cardiac cycle is defined as the cardiac events from the current P wave to next P wave. A cardiac cycle consists of systole and diastole. Systole is associated with the contraction of the ventricle and blood ejection, while diastole relates to the relaxation of the ventricle and blood filling. The cardiac cycle consists of seven phases (beginning point – appearance of the P wave) (Figure 1.3):

- Phase No. 1: atrial systole. During this phase, the atrioventricular valves are open and the aortic and pulmonic valves are closed. Atrial contraction increases pressure in the atria chamber. This force opens the atrioventricular valves and blood flows from the atria into ventricles. Ventricular blood filling is mostly passive and depends on venous blood return. When the atrial contraction is completed, the atrial pressure begins to fall and atrioventricular valves float upward before closing. At the end of this phase, the volume of the left ventricle is about 120 ml (maximum), end-diastolic pressures – about 8–12 mmHg.
- Phase No. 2: isovolumetric contraction. During this phase, all valves are closed. Pressure in the ventricle increases suddenly and exceeds the atrial pressure, therefore, the atrioventricular valves close. Subsequently, pressure in the ventricle rises rapidly; chamber geometry changes and the shape of the heart becomes more spheroid.
- Phase No. 3: rapid ejection. During this phase, the aortic and pulmonic valves are open, atrioventricular valves remain closed. When pressure in the ventricles exceed (only a few mmHg) the pressure in the aorta and pulmonary artery, the valves (aortic and pulmonic) open and blood is ejected out from the ventricles. Maximum blood outflow velocity is in the beginning of the phase. While blood is ejected, volumes of ventricles decrease but the atria continue filling with blood.
- Phase No. 4: reduced ejection. During this phase, aortic and pulmonic valves are open, atrioventricular valves remain closed. Approximately after

150–200 ms from the ventricular contraction, the ventricular repolarization begins. For this reason, the ventricular activity decreases and rate of blood ejection starts to fall. Pressure in ventricles falls below the pressure of outflow tract. During this phase, the pressure in atria gradually rise because venous blood continues to return to the atrial chambers.

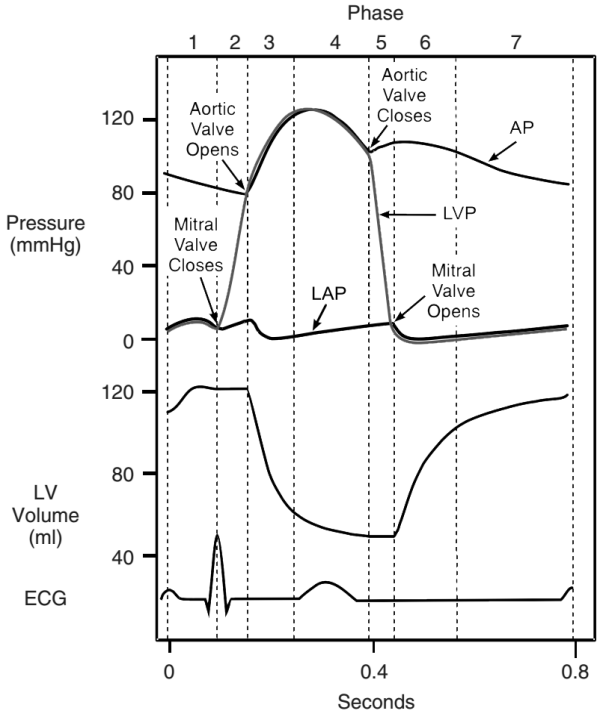

Figure 1.3. The diagram of a cardiac cycle. LV – left ventricle; AP – aortic pressure; LVP – left ventricular pressure; LAP – left atrial pressure (adopted from Klabunde, 2011)

- Phase No. 5: isovolumetric relaxation. During this phase, all valves are closed. When the ventricles continue to relax and pressure in ventricles is falling, a point is reached when the total energy in the outflow tract is greater than in ventricles and the pressure gradient causes aortic and pulmonic valves to close. During isovolumetric relaxation, pressure in the ventricles rapidly falls but volume does not change because all valves are closed. Meanwhile, volumes and pressures of the atria continue to increase because venous blood is returning.
- Phase No. 6: rapid filling. During this phase, the atrioventricular valves are open, while the aortic and pulmonic valves are closed. When pressures in the atria rise above the pressures in ventricles, atrioventricular valves open and ventricular filling phase begins. During this phase, the ventricle relaxation interval is short but it causes pressures in the ventricles to fall by several mmHg; ventricles passively fill quickly because the atria are maximally filled and have pressure before the atrioventricular valve opens.

- Phase No. 7: reduced filling. During this phase, atrioventricular valves are open and the aortic and pulmonic valves are closed. When the ventricles continue filling, they expand and the pressure starts to rise. Increased pressure in the ventricles reduces the pressure gradient between the atrial and ventricles (pressure across the atrioventricular valve). The filling rate declines, even though pressure in the atria continues to increase because venous blood continues to flow into the atria, meanwhile, the pressure in the aorta and the pulmonary artery continue to fall.

1.3. Sympathetic and parasympathetic systems and their interface with cardiac electrical and hemodynamic activity

The central nervous system controls the autonomic regulation of the cardiovascular function. The medulla oblongata is located in the brainstem, the hypothalamus and the cortical regions regulate the autonomic function. Regions within the medulla contain cell bodies for the parasympathetic (vagal) and sympathetic efferent nerves. The hypothalamus modulates medullary neuronal activity, for example, during exercise or when the body needs to regulate body temperature and blood flow to the skin. Higher centers are connected with the hypothalamus and medulla and can change the cardiovascular function in presence of an emotional stress, for example, when fear or anxiety are increased. The central nervous system receives sensory input from sensors which are in the brain and periphery. Afferent fibers from baroreceptors and chemoreceptors which are in periphery enter the medulla at the nucleus tractus solitarius (Figure 1.4) and from there interneurons project to other regions of medulla.

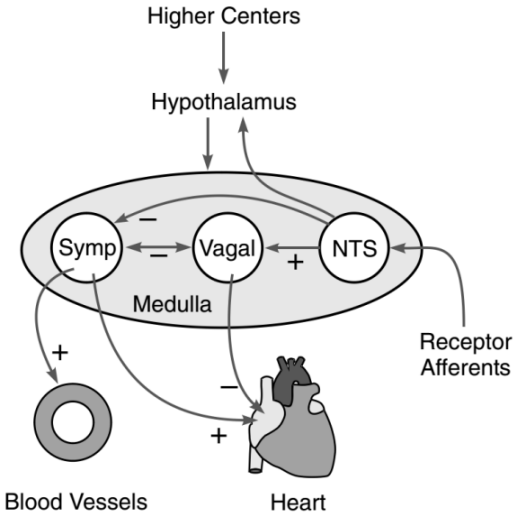

Figure 1.4. A schematic of the autonomic sympathetic and vagal interconnections with the central nervous system. Symp – sympathetic; NTS – nucleus tractus solitarius (adopted from Klabunde, 2011)

Inhibitory interneurons are related to regions which consist of sympathetic nerve cell bodies, while excitatory interneurons relate to regions composed of parasympathetic (vagal) nerves. The nucleus tractus solitarius send fibers to the hypothalamus, where sensors monitor, for example, blood temperature (thermoreceptors) and send fibers to medulla regions in order to modulate the sympathetic outflow to the cutaneous circulation.

1.3.1. Parasympathetic innervation

The parasympathetic vagal fibers are cell bodies which are located in the medulla (Figure 1.4). These cell bodies (the dorsal vagal nucleus and nucleus ambiguous) are in the collections of neurons. These neurons are active in normal (rest) conditions and produce vagal tone on the heart, therefore heart rate at rest is significantly lower than the intrinsic firing rate of the sinoatrial pacemaker. Afferent nerves (especially the peripheral baroreceptors) enter the medulla and modulate the activity of vagal neurons; the activity of baroreceptors normally activates the excitatory interneurons from the nucleus tractus solitarius and they stimulate the vagal activity. Efferent fibers which are in the hypothalamus modulate the vagal neurons as well. Efferent vagal fibers from the medulla travel to the heart within the left and right vagus nerves, branch and innervate specific regions of the heart. The preganglionic efferent fibers innervate specific tissue sites and the activation of these postganglionic fibers causes the release of the neurotransmitter acetylcholine. This neurotransmitter binds to the muscarinic receptors (M2) and decreases the chronotropy, dromotropy, and inotropy (more in the atria than in ventricles), and dilate the coronary vasculature (Table 1.2. and Figure 1.5).

Table 1.2. The effects of parasympathetic and sympathetic stimulation on the cardiovascular function (Klabunde, 2011)

	Sympathetic	**Parasympathetic**
Heart		
Chronotropy (rate)	+++	---
Inotropy (contractility)	+++	-[1]
Dromotropy (conduction velocity)	++	---
Vessels (vasoconstriction)		
Resistance (arteries, arterioles)	+++	-[2]
Capacitance (veins, venules)	+++	0

Relative magnitude of response ("+" – increase; "-" – decrease; "0" – no response) indicated by number of "+" or "-" signs.
[1]More pronounced in atria than ventricles; [2]Vasodilator effects only in specific organs.

The right and left vagus innervate different nodes or systems; the right vagus nerve innervates the sinoatrial node, the left – atrioventricular node and the ventricular conduction system. Some efferent parasympathetic fibers innervate the blood vessels in specific organs and directly or indirectly cause vasodilation. Direct vasodilation occurs due to parasympathetic activation in some tissues, for example, the genitalia, and seeks to control the release of acetylcholine which binds to the muscarinic receptors on the vascular endothelium and induces vasodilation.

Indirect vasodilation occurs due to parasympathetic activation in organs, for example, the gastrointestinal circulation, and seeks to stimulate non-vascular tissue to produce vasodilator substances which bind to the vascular receptors and induce vasodilation. Parasympathetic nerves primarily regulate blood flow in specific organs but do not have a significant role in regulating the systemic vascular resistance and arterial blood pressure.

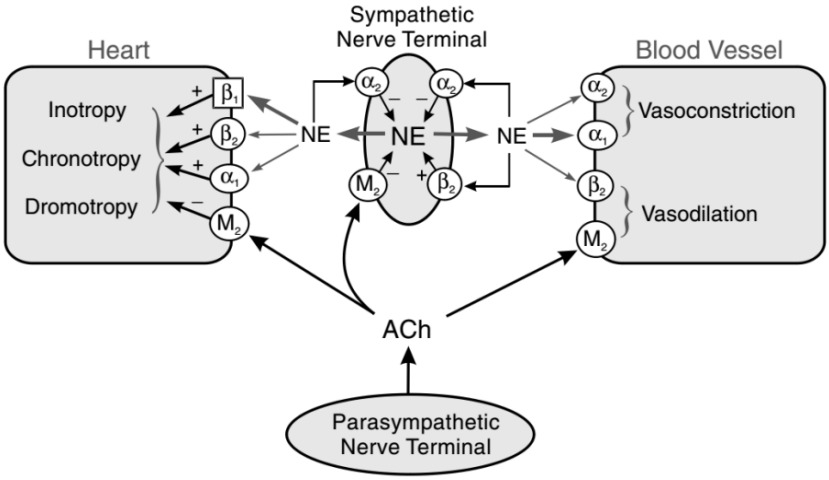

Figure 1.5. Adrenergic and muscarinic receptors in blood vessels and the heart. NE – norepinephrine; M_2 – muscarinic receptors; ACh – acetylcholine; α_1, α_2, β_1, and β_2 – adrenoceptors (adopted from Klabunde, 2011)

1.3.2. Sympathetic innervation

Neurons which are in the medulla create a highly complex system and have spontaneous action potential activity which results in tonic stimulation and sympathetic adrenergic control of the heart and vasculature. If there is an acute sympathetic denervation of the heart and systemic blood vessels, usually it causes bradycardia and systemic vasodilation. When the heart rate is low, for example, at rest, the heart is strongly influenced by the vagus nerve and the effects of sympathetic denervation are relatively small. Otherwise, if the sympathetic tone is relatively high, a sudden removal of the sympathetic tone causes significant vasodilation and hypotension. Hence, parasympathetic activity usually inhibits the sympathetic activity and vice versa. Reciprocal activation of centers in the medulla controls the vagal and sympathetic outflow, which occurs when a person stands up and arterial blood pressure falls; then the baroreceptor reflexes excite the centers in medulla to increase the sympathetic outflow to stimulate the heart (to increase heart rate, inotropy, and to constrict systemic vasculature). Sympathetic fibers are activated, the parasympathetic activity decreases and these cardiac and vascular responses help to restore a normal arterial pressure.

Preganglionic fibers travel from the medulla to the heart (Figure 1.6 A) and synapse with the cell bodies of short postganglionic fibers which can innervate the heart. Preganglionic sympathetic fibers are in the thoracic (T1–T12) and lumbar

segments of the spinal cord. Some of these fibers enter the paravertebral ganglia which are on both sides of the spinal cord and travel to the synapse above (Figure 1.6 B) or below their entry level (Figure 1.6 C). Preganglionic fibers which are in the lower thoracic and upper lumbar segments generally synapse in the prevertebral ganglia (Figure 1.6 D) and proceed to blood vessels.

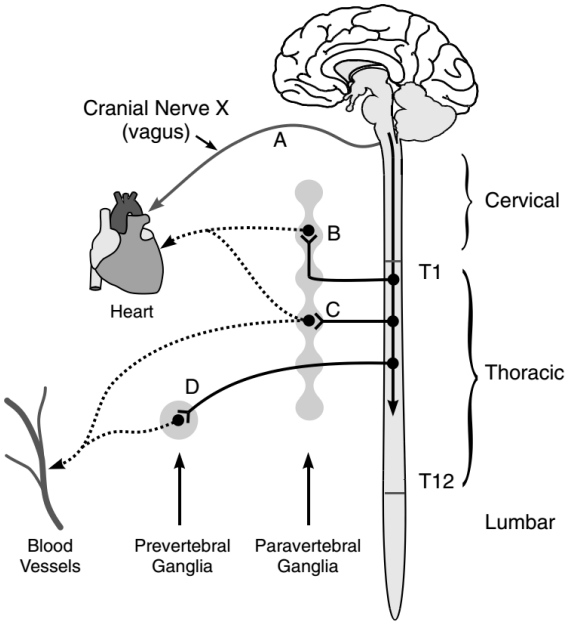

Figure 1.6. The organization of vagal and sympathetic innervation of the heart and circulation. T1–T12 – thoracic segments of the spinal cord (adopted from Klabunde, 2011)

Postganglionic fibers travel to the heart and innervate the sinoatrial and atrioventricular nodes, the conduction system, the cardiac myocytes, and the coronary vasculature. Sympathetic activation increases chronotropy, dromotropy, and inotropy (Table 1.2.), therefore, binds β_2-adrenoceptors (less important than β_1-adrenoceptors) to β_1-adrenoceptors in the heart (Figure 1.5) primarily by norepinephrine. Prejunctional β_2-adrenoceptors facilitate the release of norepinephrine, meanwhile, prejunctional α_2-adrenoceptors inhibit it. Sympathetic activation constricts the resistance and capacitance vessels, therefore, increases the systemic vascular resistance and arterial blood pressure and decreases venous capacitance which increases the venous pressure (Table 1.2.). Sympathetic adrenergic nerves release norepinephrine and preferentially bind α_1-adrenoceptors to induce a contraction and vasoconstriction of the smooth muscle (Figure 1.5) when norepinephrine binds to the postjunctional α_2-adrenoreceptors which are primarily on the small arteries and arterioles. Blood vessels have postjunctional β_2-adrenoceptors and their activation by norepinephrine causes vasodilation. The sympathetic activation of resistance vessels contributes significantly to the vascular tone in organs but the vascular response is different among organs; circulations of the skeletal muscle, the cutaneous, gastrointestinal, and renal systems

are strongly influenced by the sympathetic activity. Meanwhile, coronary and cerebral circulations have weak responses to sympathetic stimulation.

1.4. Physiological signals

This section describes physiological signals (electrocardiogram and photoplethysmogram) which are commonly used to monitor the status of the cardiovascular system.

1.4.1. Electrocardiography

As was described in section 1.2, cardiac cells can depolarize and repolarize, which is followed by the spread of electrical currents through the conductive tissues throughout the body. Using electrodes at specific locations on the surface of a body allows measuring the electrical currents and obtain an electrocardiogram (ECG) signal (Figure 1.7). ECG waves represent the sequence of depolarization and repolarization of the atria and ventricles.

The P wave of an ECG is typically the first wave. It represents depolarization and the electrical wave which spreads from the sinoatrial node throughout the atria. The duration of P wave usually is 0.08–0.1 seconds (Table 1.3). The P wave should be succeeded by a wave which represents atrial repolarization but it occurs during depolarization of ventricles and is relatively small in amplitude, therefore, this wave is not visible in the ECG. For this reason, the P wave is followed by a short isoelectric (zero voltage) period. The period from the beginning of the P wave (the onset of atrial depolarization) to the beginning of the QRS complex (the onset of ventricular depolarization) is known as the P-R interval, and it normally takes 0.12–0.20 seconds. If the duration of the P-R interval is greater than 0.2 seconds, there is a conduction defect, usually within the atrioventricular node.

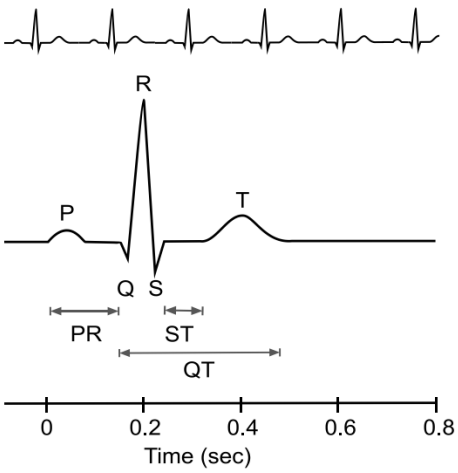

Figure 1.7. An ECG signal and its components (adopted from Klabunde, 2011)

The QRS complex of the ECG represents ventricular depolarization and the duration normally is 0.06–0.1 seconds. If the duration of the QRS complex is

longer than 0.1 seconds, it means that the conduction in ventricles is impaired. The R wave is best expressed and the most commonly used wave of the ECG; it represents early ventricular depolarization.

Table 1.3. A summary of ECG waves, intervals, and segments (Klabunde, 2011)

Component	Represents	Normal duration, s
P wave	Atrial depolarization	0.08–0.10
QRS complex	Ventricular depolarization	0.06–0.10
T wave	Ventricular repolarization	[1]
P-R interval	Atrial depolarization and atrioventricular nodal delay	0.12–0.20
ST segment	Isoelectric period of depolarized ventricles	[1]
Q-T interval	Length of depolarization and repolarization – corresponds to action potential duration	0.20–0.40[2]

[1]Duration not normally measured; [2]High heart rates reduce the action potential duration and the Q-T interval.

The QRS complex is superseded by an isoelectric period known as the ST segment. It is the time period during which the entire ventricle is depolarized. The ST segment of an ECG is important for diagnosing ventricular ischemia; it can become depressed or elevated and indicate that non-uniform membrane potentials are present in the ventricular cells. The T wave of an ECG represents the ventricular repolarization and its duration is longer than depolarization.

The Q-T interval represents ventricular depolarization and repolarization; it is possible to approximately estimate the duration of ventricular action potentials from this interval. The interval of Q-T depends on the heart rate and is about 0.2–0.4 seconds. Higher HR reduces the Q-T intervals because ventricular action potentials are shorter. Q-T intervals can be used to diagnose certain types of arrhythmias.

1.4.2. Photoplethysmography

Photoplethysmography (PPG) is an optical measurement technique which can be used to detect blood volume changes in the microvascular tissue bed. PPG is widely applied in clinical practice and medical devices, for example, in pulse oximeters, beat-to-beat blood pressure measurement systems, respiration, heart rate, and cardiac output monitoring (Allen, 2007). PPG is a non-invasive technique which requires only a few electronic components: a light source (to illuminate skin) and a photodetector (to measure tiny variations of light intensity). Most frequently used wavelengths of light are red and near infrared. The waveform of a PPG consists of two components: a) direct current – varies slowly for respiration, thermoregulation, vasoconstrictor waves, for example, the Traube Hering Mayer waves, and activity of vasomotor, b) alternating current (most commonly used) – pulsatile component which depends on the heart rate and relates to the blood volume of tissues. Light interaction with biological tissue is complex; it includes multiple optical processes, for example, absorption, scattering, reflection, fluorescence, and transmission. For this reason, a PPG waveform can provide valuable information about

thermoregulation, blood flow in capillaries, and about the cardiovascular system as well (Allen, 2007).

The quality of a photoplethysmogram signal depends on several factors, such as probe location on skin, skin properties (individual structure), skin temperatures, blood flow rate, blood oxygen saturation, measuring environment, and tissue movement (Elgendi, 2012). All these factors generate several types of artifact which may occur in a PPG signal. Common artifacts of a PPG signal (Allen, 2007; Elgendi, 2012) include:

- Power-line interference – a high frequency (50 or 60 Hz) sinusoidal artifact which occurs in a PPG signal due to the main power sources. However, this artifact can be effectively removed using a low-pass or notch filter.
- Baseline drift – a low frequency artefact which disrupts a PPG signal due to temperature variation, bias in instrumentation amplifiers or respiration. This artifact can be effectively removed using a high-pass filter.
- Motion artifact – an artifact in a PPG signal due to the movements of the PPG probe (poor PPG probe contact to skin) or subject's tissues (vibration) (Figure 1.8 a–c). Accelerometers and adaptive filters are used for motion artifact removal. However, it is a difficult task and not always successful.
- Sudden PPG signal amplitude change – often reflect physiological changes of an organism (deep gasp, yawn, etc.) (Figure 1.8 d).
- Premature ventricular contraction – interrupts regular heart rhythm and causes irregular heart rhythm, therefore, certain parameters of the PPG signal can be assessed inaccurately.

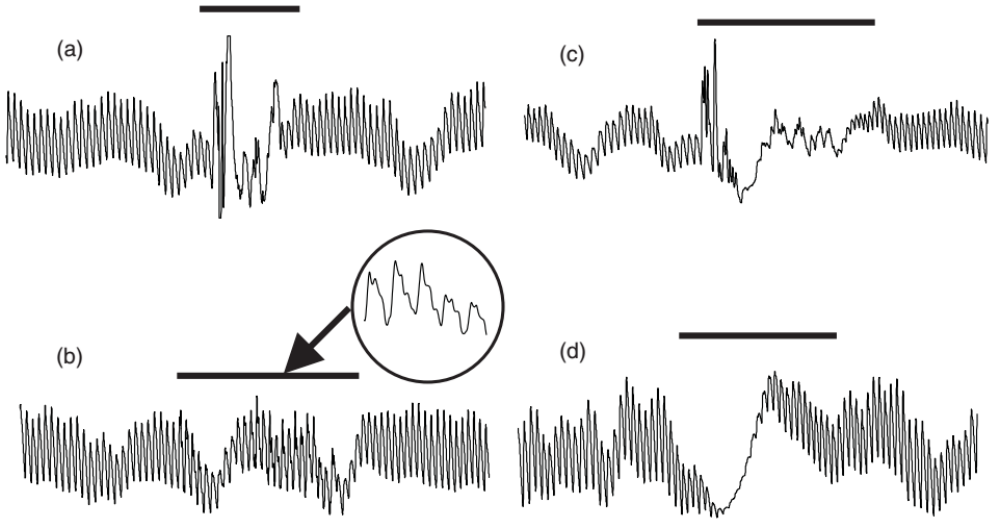

Figure 1.8. Examples of PPG measurement artefacts and extremes (artefact/physiological events are marked): gross movement artefact or twitching of the PPG probe cable a); finger and hand tremor b); coughing c); deep gasp or yawn d) (adopted from Allen, 2007)

1.5. Pulse waves and pulse arrival time

Each cardiac contraction generates a blood volume pulse wave which travels from the heart to the vascular system. A pulse wave traveling through blood vessels faces various obstacles, such as a variation in vessel diameter, branches, meanders (turns), plaque, and others. These obstructions create multiple tiny reflection waves which travel backwards from the original location, usually at points of bifurcations or abrupt changes in vascular resistance or diameter. These reflection waves add up to a composite reflection wave. The aortic pressure wave is a sum of the forward and backward waves. The reflection wave mostly affects the systolic wave and the systolic components of a pulse wave vary between individuals and depend on their sex, height, heart rate, age, physical fitness, food, and exercise (Figure 1.9) (O'Rourke et al., 2001; McEniery et al., 2008) when the pulse wave travels through major arteries, for example, the aorta.

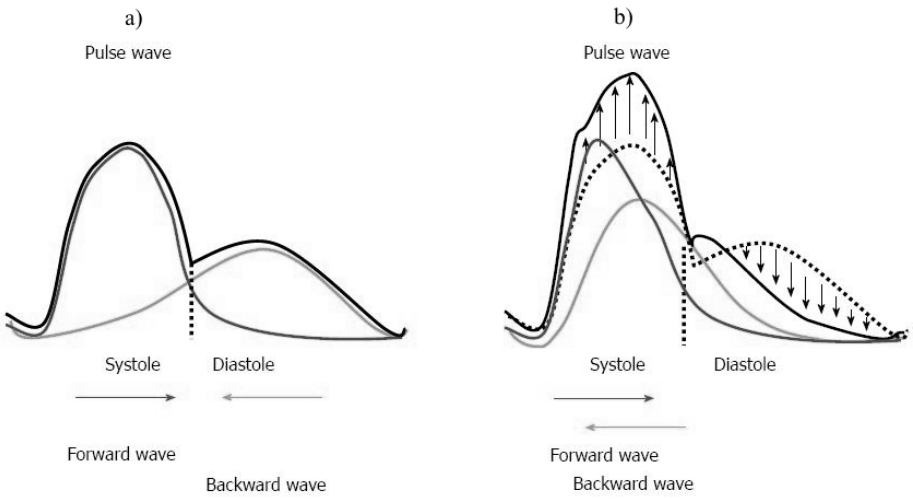

Figure 1.9. A pulse wave with normal arterial stiffness a) and with increased arterial stiffness b) (adopted from Zanoli et al., 2015)

Blood volume pulse arrival time consists of two time intervals (Figure 1.10): the pre-ejection period (PEP) and the vascular transit time, otherwise known as the pulse transit time. Pulse transit time (PTT) is the time duration or an interval during which a pulse wave propagates a segment of an artery. In other words, PTT is a time interval which is needed for a pulse wave to travel the distance from the heart to a certain place in the body (Allen, 2007). Usually PEP is evaluated using the ECG (shows electrical activity of the heart) and impedance cardiography signals (shows a mechanical activity of the heart). PEP is related to ventricular the electromechanical delay and isovolumetric contraction period. In other words, PEP is a time interval from the beginning of ventricular depolarization (Q wave of ECG) to the beginning of blood ejection to the aorta, when the aortic valve opens (B point of impedance cardiography signals).

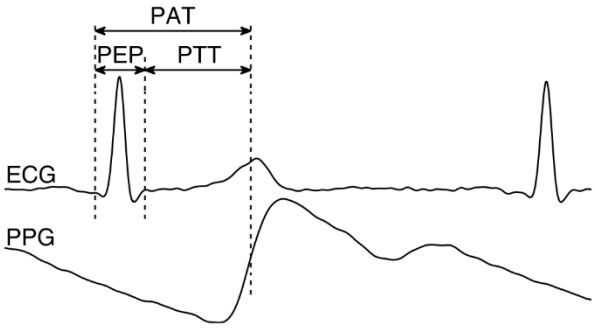

Figure 1.10. Pulse arrival time and its components

The pre-ejection period corresponds with the electro-mechanical delay and the period of isovolumetric contraction in the left ventricle (Wong et al., 2011; Cloutier et al., 2013; Mukkamala et al., 2015). PEP depends on the time development of intraventricular pressure and it is widely used as an index of myocardial contractility. Sympathetic beta-adrenergic influences modulate the variations in contractility, therefore PEP is often used as a specific and sensitive parameter for non-invasive measurement of sympathetic cardiac control (Cloutier et al., 2013). PEP also is an important part of PAT and comprises from 10 to 35% of PAT (Mukkamala et al., 2015). PAT interval duration (from ECG R wave to PPG foot point) at rest typically takes 180–260 ms (finger) and 125–155 ms (ear) (Mukkamala et al., 2015). However, the duration of a PAT interval depends on blood pressure, heart rate, peripheral resistance, arterial stiffness, venous return, and other physiological properties (Murakami, Yoshioka, 2015).

Pulse arrival time is often used in practice. PAT could provide continuous information about the cardiovascular system (Smith et al., 1999). The speed of arterial pressure wave is directly proportional to blood pressure. A strong rise of blood pressure increases the vascular tone, therefore, the arterial wall becomes stiffer and PAT becomes shorter and conversely, when blood pressure decreases – PAT increases (Smith et al., 1999). A significant number of research studies have shown that pulse arrival time is related to the arterial blood pressure (Allen et al., 1981; Lane et al., 1983; Muehlsteff et al., 2006; Obrist et al., 1978; Gribbin et al, 1976; Lutter et al., 1996). Measurements of PAT have several applications. The main application is non-invasive continuous (beat-to-beat) blood pressure monitoring because PAT is highly related to BP (Chen et al., 2000; Heard et al., 2000; Poon, Zhang, 2005; Zong et al., 1998; Cattivelli, Garudadri, 2009; Gesche et al., 2012; Zheng et al., 2014). The Moens-Korteweg equation describes a relationship between the pulse wave velocity (PWV) and the elastic properties of arteries – elastic modulus (Remington, 1963; Chen et al., 2000). Hughes' equation connects BP with the elastic modulus (Hughes et al., 1979) which exponentially increases when blood pressure increases. Using the Moens-Korteweg and Hughes' equations, a new equation is obtained which is used for blood pressure estimation (Chen et al., 2000; Rapalis, Marozas, 2012):

$$BP_e = BP_c - \frac{2}{\gamma t_{PATc}} \Delta t_{PAT} \quad (1.1)$$

where, BP_e – estimated arterial blood pressure [mmHg]; Δt_{PAT} – difference between current estimated PAT and PAT during calibration moment [s]; t_{PATc} – PAT during calibration moment [s]; BP_c – BP during calibration moment [mmHg]; γ – specific blood vessel coefficient (0,016–0,018) [$mmHg^{-1}$].

This equation shows that the approximate value of BP consists of two components: the base level of BP (BP_c) and its change, which can be evaluated using the changes of PAT. BP_c and t_{PATc} are measured or estimated during the calibration process. When BP and PAT (BP_c and t_{PATc}) values are measured or estimated (during calibration process), arterial blood pressure without re-calibration may be estimated as long as the modulus of elasticity of blood vessel walls is constant. Therefore, if the elasticity of blood vessels is changing slowly, calibration should be performed at certain time intervals (Chen et al., 2000; Rapalis, Marozas, 2012). The absolute PAT values cannot be declared as absolute blood pressure values but PAT can predict a change in blood pressure over a short period (Smith et al., 1999). Other PAT applications include the estimation of baroreflex sensitivity (Liu et al., 2012), cardiac output (Sugo et al., 2010), respiratory rate (Wu et al., 2012; Johansson et al., 2006), arterial stiffness (Liu et al., 2009), psycho-physiological stress monitoring (Hey et al., 2009), and others.

PAT should be measured as the time interval from QRS complex of ECG (Q wave) to reference the point of the photoplethysmogram signal in the same cardiac cycle. The QRS complex of ECG is a reference which indicates the initialization of ventricular depolarization. After depolarization of the ventricles, the aortic and atrioventricular valves close. The left ventricular pressure rises fast without changing the ventricular volume (isovolumetric contraction). The ventricular pressure continuously increases and the aortic valve opens when this pressure exceeds the pressure in the aorta. Then blood is ejected from the left ventricle to the aorta and pressure pulse is generated to travel along the arteries. The location of R wave of ECG is most widely used to define the beginning point of PAT because the R wave is well-known and can be easily detected. However, using the R wave as a starting point of PAT produces a small inaccuracy because the R wave is almost in the middle of PEP and there is a short delay between the R and Q waves, and between the R wave and the opening of the aortic valve (isometric contraction time) (Smith et al., 1999; Wong et al., 2011; Mukkamala et al., 2015). On the other hand, detecting the R wave is easier than the Q wave, the delay between the R and Q waves is ignored and the R wave is regarded as the starting point of PAT. The most commonly used algorithm for R wave detection is the Pan-Tompkins algorithm (Pan, Tompkins, 1985) or its modification (Hamilton, Tompkins, 1986). However, there are other points in the ECG signal which are used as the beginning point of PAT, for example, the maximum peak of ECG derivative (Wong et al., 2009b). The peripheral pressure pulse can be detected

by a photoelectric sensor which is placed on the skin surface near the arteries (Wong et al., 2011).

1.6. Autonomic nervous system evaluation

The evaluation of autonomic nervous system attracts more and more attention. The most popular method for evaluating the ANS is an analysis of heart rate variability (HRV). HRV is a continuous fluctuation of the RR interval (RRI) duration. Extremely complex neural mechanisms create these fluctuations; the activity of ANS continuously varies because it is mainly based on the interactions between the sympathetic and parasympathetic nervous systems. Actually, HRV mainly depends on the external regulation of the heart rate and describes the heart's ability to adapt and respond to changing circumstances (different types and cases stimulations). HRV analysis evaluates the health conditions and the ANS status (mainly the charge regulation of cardiac activity). Vagal activity dominates at rest and is mainly responsible for HRV. For this reason, sinus arrhythmia is most noticeable in HRV. Parasympathetic activation is fast but transient, the effects of parasympathetic neuron excitation can be visible as soon as the next cycle after the stimulus, therefore, the parasympathetic nervous system is responsible for quick changes in HR (Zygmunt, Stanczyk, 2010). Meanwhile, sympathetic stimulation evolves slowly and its effects in rhythm are visible after 2–3 s, hence sympathetic stimulation is responsible for slower but higher amplitude oscillations (Malik et al., 1996). The calculated HRV values are not direct values of the tonic activity of sympathetic and parasympathetic nervous systems, rather, HRV is a result of the influence of two systems on the sinus node cell receptors.

Heart rate variability has physiological relevance and shows a dominant ANS effect. Some health disorders reflect significant fluctuations of HR and affect the HRV. The basic and most common factors are age (Kaplan et al., 1991; Pikkujämsä et al., 1999; Stein et al., 1997; Sinnreich et al., 1998; Zhang, 2007; Carter et al, 2003), gender (Zhang, 2007; Carter et al., 2003; Huikuri et al., 1996; Ramaekers et al., 1998), heart disease (De La Cruz Torres, 2008), neurological disease (Bernardi et al., 1992; Guzzetti et al., 1994; Koh et al., 1994), and exercise (Carter et al., 2003; De La Cruz Torres, 2008; Aubert et al., 2003; Aubert et al., 2000). HRV relates to:

- **Blood Pressure.** HRV significantly decreases when cardiovascular abnormalities, such as left ventricular hypertrophy, aortic valve disease, and hypertension, are present. A strong correlation between the HRV and arterial baroreflex was found as well (De Boer et al., 1985).
- **Diabetes.** Diabetes can cause autonomic dysfunction, thus beat-to-beat variability decreases and causes lower HRV. It was also concluded that the activity of parasympathetic nervous system is reduced in diabetic patients (Pfeifer et al., 1982; Singh et al., 2000; Wheeler, Watkins, 1973).

- **Renal Failure.** HRV studies on patients with chronic renal failure have shown that after hemodialysis there is a negative correlation between the concentration of calcium ions and the mean of RR intervals. HRV also reduces in renal failure cases (Forsström et al., 1986; Zoccali et al., 1982; Lerma et al., 2004; Ewing, Winney, 1975).
- **Gender and Age.** Studies have shown that HRV depends on age and gender. A study with newborns has revealed that HRV is lower for boys than girls (Nagy et al., 2000). Another study with healthy subjects (20–70 years) has shown that HRV decreases with age and it is higher for females (Spallone et al., 1993). The maturation of sympathetic and parasympathetic (vagal) nerves increases HRV in the early stages of life, which decreases with age (van Ravenswaaij-Arts et al., 1991).
- **Drugs/Medications.** Drugs and medications affect HRV and allow to evaluate the effect of drugs on the ANS as well as to assist in quantifying the amounts of drugs/medications which should be administered (Bekheit et al., 1990; Coumel et al., 1991; Guzzetti et al., 1988).
- **Smoking.** Smoking reduces vagal activity, increases sympathetic activity, and reduces HRV (Lucini et al., 1996; Hayano et al., 1990) because the exposure to tobacco outlets, or smoking, affects the ANS control activity (Zeskind, Gingras, 2006).

There are various methodologies for analysing HRV, which include the time-domain analysis, statistical methods, geometric methods, non-linear analysis, and frequency-domain analysis (Malik et al., 1996; Oweis, Al-Tabbaa, 2014). The time-domain analysis is the simplest for HRV, usually time- and frequency-domains are used in combination.

1.6.1. Methods of time-domain analysis

To evaluate the HRV, all QRS complexes of an ECG and the intervals between QRS complexes should be detected. These intervals are also called normal-to-normal (NN) intervals (Figure 1.11).

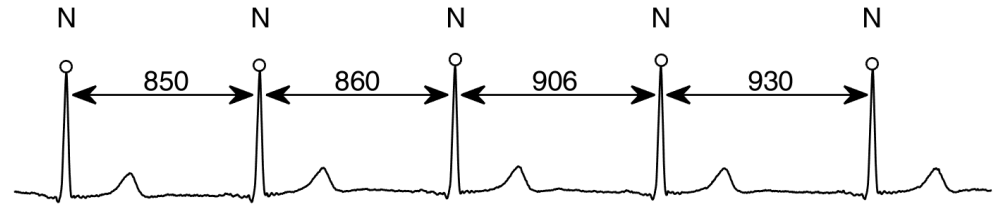

Figure 1.11. Variation of beat-to-beat NN intervals

The simplest HRV evaluation methods are time-domain measures; statistical time-domain parameters can be calculated from the evaluated NN intervals (usually from a 24-hour ECG). The time-domain parameters may be divided into groups: parameters which can be derived from direct measurements of the NN intervals and those derived from the differences between NN intervals. Time-domain parameters used for HRV analysis are:

- **SDNN** – the simplest time-domain parameter; it is a standard deviation of NN intervals or a total variability of the NN intervals. In other words, SDNN is the square root of variance:

$$SDNN = \sqrt{\frac{1}{N-1}\sum_{j=1}^{N}\left(RR_j - \overline{RR}\right)^2} \tag{1.2}$$

  where RR_j – value of j^{th} RR interval; N – total number of successive intervals.

  SDNN reflects all variability components of an assessment period. Low SDNN values indicate that there is practically no HRV and vice versa.
- **SDANN** – parameter calculated from segments of the total monitoring period. SDANN is a standard deviation of mean of short period (5 min) intervals:

$$SDANN = \sqrt{\frac{1}{N-1}\sum_{j=1}^{N}\left(RR_{5_j} - \overline{RR_5}\right)^2} \tag{1.3}$$

  Where $\overline{RR_5}$ – average of all 5 min RR intervals averages, RR_{5_j} – value of j^{th} 5 min RR interval average; N – total number of successive 5 min RR intervals.

  This parameter usually is used only for long-term HRV measurements (usually for 24 hours) (Lagi et al., 1997; Lazzeri et al., 2000; Malik et al., 1999; Osterhues et al., 1997; Wennerblom et al., 2000; Umetani et al., 1998).
- **SDNN index** – the mean of 5 min standard deviation of NN interval (calculated over 24 hours):

$$SDNN_{index} = \frac{1}{N}\sum_{j=1}^{N} SDNN_{5_j} \tag{1.4}$$

  Where $SDNN_{5_j}$ – standard deviation of j^{th} 5 min RR interval; N – total number of successive 5 min RR intervals.
- **RMSSD** – square root of mean squared differences of NN intervals:

$$RMSSD = \sqrt{\frac{1}{N-1}\sum_{j=1}^{N-1}\left(RR_{j+1} - RR_j\right)^2} \tag{1.5}$$

RMSSD is the most commonly used time-domain parameter for short-term HRV analysis (Kautzner, Camm, 1997; Lagi et al., 1997; Akinci et al., 1993; Cowan, 1995; Guzmán et al, 1999; Hilz et al., 1999; Uehara et al., 1999). RMSSD reflects the activity of the parasympathetic system.

- **NN50** – number of interval differences of successive NN intervals which are greater than 50 ms. NN50 is usually used for short-term HRV analysis and highly correlates to RMSSD, therefore, reflects the activity of the parasympathetic system.
- **pNN50** – NN50 divided by the total number of NN intervals:

$$pNN50 = \frac{NN50}{N-1} \times 100\% \tag{1.6}$$

pNN50 is also used for short-term HRV analysis, very highly correlates to RMSSD, and also reflects the activity of the parasympathetic system.

Time-domain parameters are simply and easily calculated but are not sufficiently informative when used alone, therefore other HRV analysis methods, for example, frequency-domain is used in conjunction. The main disadvantage and limitation of time-domain parameters is their inability to clearly distinguish the effects between sympathetic and parasympathetic autonomic nervous systems. SDNN and RMSSD are the most commonly used time-domain parameters for short-term HRV evaluation (Malik et al., 1996).

1.6.2. Methods for frequency-domain analysis

The main idea of frequency-domain analysis of HRV is the observation of certain rhythms which are related to different regulatory mechanisms of cardiovascular control. Spectral analysis expresses heart rate as a function of frequency and focuses on the hidden cyclical nature in a series of changing RR intervals. The measured magnitude and frequency of these oscillations allows to calculate the power spectral density (PSD). Then it is divided into three main spectral components (Figure 1.12) and the power of each band is calculated by integrating the PSD within the limits of the band which were standardized by the American Heart Association and the European Society of Cardiology in 1996. The recordings should be at least 5 min long for frequency-domain HRV calculation (Malik et al., 1996).

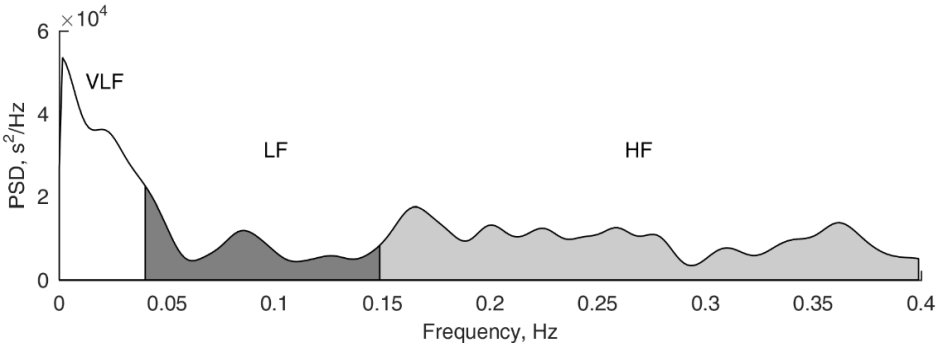

Figure 1.12. PSD and its main spectral components

There are three main spectral components used for HRV analysis but only two have physiological importance in short-term HRV (low frequency and high frequency) (Sayers, 1973; Hirsh, Bishop, 1981; Akselrod et al., 1985; Pagani et al., 1986; Akselrod et al., 1981; Malliani et al., 1991):

- **VLF Power** – very low frequency power in a range of 0–0.04 Hz. The physiological explanation of VLF is not defined and specific physiological processes attributable to it are not clearly known. In other words, VLF does not correlate with any known physiological rhythms (Malik et al., 1996; Oweis, Al-Tabbaa, 2014). Basically, the VLF band is defined as noise and VLF calculation for short-term recordings is questionable (Malik et al., 1996).
- **LF Power** – low frequency power in a range of 0.04–0.15 Hz. LF component reflects the sympathetic activity (Akselrod et al., 1985; Sands et al., 1989); however, there are statements that the LF component reflects both (sympathetic and parasympathetic) systems (Akselrod et al., 1981; Montano et al., 1994). For a normal subject, vasomotor oscillations cause a peak in the LF band at about 0.1 Hz.
- **HF Power** – high frequency power in a range of 0.15–0.4 Hz. HF component reflects the parasympathetic activity (Akselrod et al., 1985; Pomeranz et al., 1985; Kamen et al., 1996) and is related to changes in respiration and blood pressure. For a normal subject, respiration causes a peak in HF band at about 0.3 Hz.

Other frequency-domain parameters can be calculated using the following parameters (VLF, LF, and HF):

- **TP** – the total power in a range of 0–0.4 Hz is a sum of VLF, LF, and HF:

$$TP = VLF + LF + HF \tag{1.7}$$

  5 min TP mainly reflects the overall autonomic activity (both sympathetic and parasympathetic). The clinical meaning of TP is similar to SDNN.

- **LF/HF ratio** – the ratio between power in LF and HF bands:

$$LF / HF\ ratio = \frac{LF}{HF} \tag{1.8}$$

LF/HF ratio reflects the interactions of sympathetic and parasympathetic systems, in other words, shows which part of ANS dominates (Pagani et al., 1986; Malliani et al., 1991; Sloan et al., 1994).

- **LF norm and HF norm** – normalized low and high frequency is a ratio of the absolute LF and HF values and the difference between TP and VLF:

$$LF\ norm = \frac{LF}{TP - VLF} \times 100\% \tag{1.9}$$

$$HF\ norm = \frac{HF}{TP - VLF} \times 100\% \tag{1.10}$$

LF norm and HF norm are interdependent and LF norm can be calculated as 1-HF norm and vice versa. The normalization of LF and HF minimizes the effects of noise (effect of changes in VLF) and emphasizes the changes in sympathetic regulation (LF norm) and parasympathetic regulation (HF norm). LF norm and HF norm can be calculated in percentage as well. The parameters LF norm and HF norm are useful when the effects of different interventions are evaluated for the same subjects or when subjects with major differences are compared in TP (Montano et al., 1994).

Previous studies have shown that there exists an approximate correlation between the time-domain and frequency-domain parameters (Malik et al., 1996; Oweis, Al-Tabbaa, 2014) and both of these measures can contribute to a more accurate evaluation of HRV (Table 1.4).

Table 1.4. Approximate correspondence of time-domain and frequency-domain methods used in HRV evaluation (Malik et al., 1996; Oweis, Al-Tabbaa, 2014)

Time-domain	Frequency-domain
SDNN	TP
RMSSD	HF
NN50	HF
pNN50	HF

1.7. Blood pressure variability analysis

Blood pressure is one more hemodynamic parameter whose variability is used in clinical practice as well (Table 1.5). A few types of changes in BP fluctuations within a short term (24-hour) period are noteworthy (Table 1.6) (Mancia, 2012).

Table 1.5. Methods of measurement, prognostic relevance, and proposed mechanisms of very short term BPV (Parati et al., 2013a)

Characteristic	Very short term BPV (beat-to-beat)
Method of BP measurement	Continuous BP recordings in a laboratory setting or under ambulatory conditions
Time intervals	Beat-to-beat over various recording periods (1 min to 24 hours)
Advantages	Assessment of indices of autonomic cardiovascular modulation
Disadvantages	Stability of measurements might not be guaranteed outside controlled environment
Indices of BPV	SD Indices of autonomic modulation can be calculated (via spectral analysis)
Proposed mechanisms	Increased central sympathetic drive Reduced arterial / cardiopulmonary reflex Humoral and rheological factors Behavioural / emotional factors Activity / sleep Ventilation
Prognostic relevance of Cardiac and renal outcomes	Subclinical organ damage* Cardiovascular events and mortality? ** Renal outcomes? **

*cardiac, vascular, and renal subclinical organ damage

**BPV on a beat-to-beat basis has not been routinely measured in population studies

Table 1.6. Blood pressure fluctuation intervals (Mancia, 2012)

Short-term BPV	Long-term BPV
Beat-to-beat	Days
Minute-to-minute	Weeks
Hour-to-hour	Months
Day-to-night	Seasons
	Years

Variations in BP are not random, rather, they are a result of complex interactions between the intrinsic mechanisms of cardiovascular regulation, behavior factors, and extrinsic environment. It is thought that hypertension largely depends on mean BP, however, previous studies showed that the results might depend on BPV; the results also showed that the increment of BPV in short-term and long-term are related to the severity, development, and progression of cardiac, vascular, and renal damage, as well as with an increased incidence of cardiovascular events and

mortality. A large study in 2010 showed that visit-to-visit BPV is related to cardiovascular morbidity and can be used for prediction (Rothwell et al., 2010). Several studies showed that the contribution of humoral, neural, and environmental factors are related to BPV (Mancia et al., 1986; Conway et al., 1984; Schillaci et al., 2012; Mancia, Grassi, 2000) and these factors are inseparably intertwined. The variations of BP variations in very short (beat-to-beat) and short (within a 24-hour period) term mainly reflect:

- Influences of autonomic (central and reflex) modulation, (an increase of central sympathetic drive and decrease of arterial and cardiopulmonary reflexes) (Mancia et al., 1986; Conway et al., 1984; Parati et al., 1995);
- The elastic properties of arteries (a decrease of arterial compliance) (Parati et al., 2006; Kotsis et al., 2011; Fukui et al., 2013);
- The diverse nature and duration effects of humoral (bradykinin, insulin, angiotensin II, endothelin-1, nitric oxide), rheological (blood viscosity), and emotional factors (psychological stress) (Parati et al., 2013a).

Behavioral influences, such as changes in posture, sleep, and physical activity can cause significant variations of BP over a 24-hour period (beat-to-beat and day-to-night) (Mancia et al., 1983; Parati et al., 1987; Parati et al., 1998). Spontaneous and rhythmic fluctuations of BP appear as well, regardless of behavior impacts throughout the day and night because the influencers of BP originate in the central nervous system and various factors act, for example, Mayer waves (10-second period waves) (Parati et al., 1995; Parati et al., 1990). Fluctuations in blood pressure also occur in response to mechanical forces which are generated by ventilation. All types of BP variation (induced by behavior, changes in body position or movements of the thorax due to ventilation) are modulated by arterial and cardiopulmonary reflexes, and reduced efficacy can cause increases in BPV (Figure 1.13). The detection of beat-to-beat BP fluctuations (BPV) can help to select antihypertensive drugs for hypertensive patients because the low frequency spectral component of the elevated BPV can show an increased modulation of the sympathetic vascular tone and the response to sympatholytic drugs (Stauss, 2007).

For the general population, blood pressure falls during sleep by about 10–20% of day-time values (Friedman, Logan, 2009); this is also referred to as “dipping”. However, there are some other cases in changes of blood pressure during night, for example, “risers” or “inverted dippers”, when the BP increases during sleep, “extreme dippers”, when the BP falls by more than 20% of the day-time BP (Pickering et al., 2005), “non-dippers”, when the BP does not change significantly during sleep but the mean BP is higher (Pickering et al., 2005). The aforementioned changes in blood pressure occur because:

- Activity of the sympathetic nervous system increases during the night (Narkiewicz et al., 2002);
- Ability of the renal sodium excretion decreases (Fujii et al., 1999);

- Salt sensitivity (Verdecchia et al., 1993);
- Leptin and insulin resistance;
- Changes in breathing patterns during sleep, for example, sleep apnea (Haynes, 2005);
- Endothelial dysfunction (Quinaglia et al., 2011);
- Glucocorticoid use (Holt-Lunstad, Steffen, 2007).

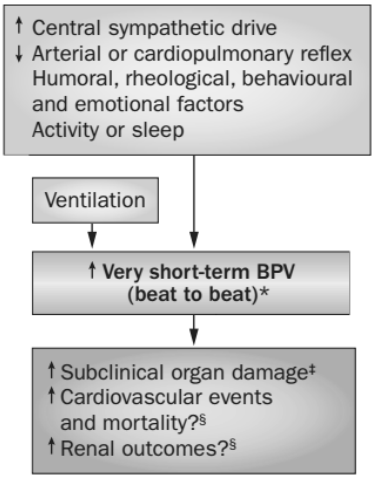

Figure 1.13. Short-term BPV: determinants, and prognostic relevance for cardiovascular and renal outcomes. *Assessed in laboratory conditions; ‡vascular, cardiac, and renal subclinical organ damage; §beat-to-beat BPV has not been routinely measured in population studies (adopted from Parati et al., 2013a)

The factors which are possibly responsible for 24-hour BPV are shown in Figure 1.14.

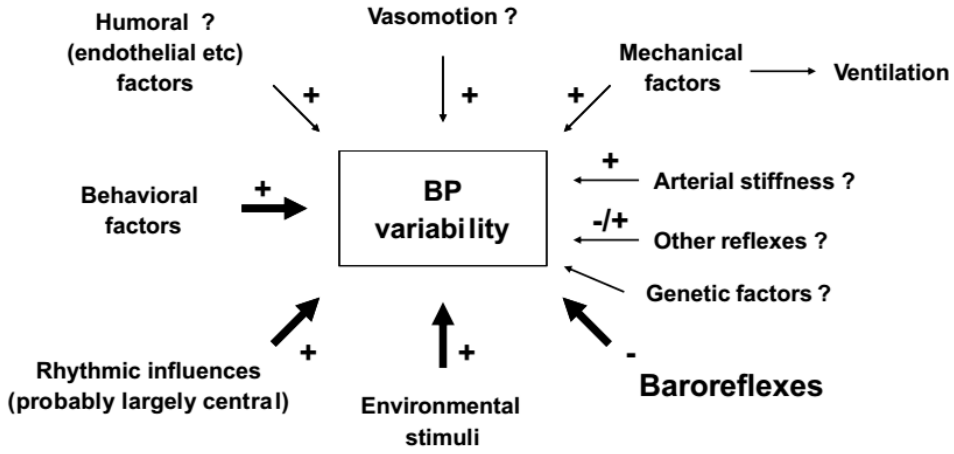

Figure 1.14. Factors related to the 24-hour BPV. "+" – stimulating factors of BPV; "-" – inhibiting factors; "?" – indicates that there is no compelling evidence (adopted from Mancia, 2012)

Continuous BP recording is needed to accurately assess the short-term BPV within a 24-hour period, and using these recordings calculate the standard deviation (SD) of the mean systolic, diastolic, and arterial blood pressure values over 24 hours (Mancia et al., 1993). The day-time and night-time recordings can be analyzed separately (Mancia et al., 1993), using the SD parameter for excluding day-to-night BP changes (Bilo et al., 2007). The coefficient of variation (normalized measure of BPV) can be calculated as well (Parati et al., 2013a):

$$CV = \frac{SD_{BP}}{mean_{BP}} \tag{1.11}$$

where CV – coefficient of variation; SD_{BP} – standard deviation of BP.

Another parameter which focuses on short-term (beat-to-beat) BPV is spectral analysis, which allows to estimate the relative contribution of neurohumoral systems to BP regulation (Stauss, 2007). These spectral parameters are not intended for the "dipping" phenomenon, however, it has been demonstrated that these parameters are better predictors of cardiovascular risk and organ damage than the 24-hour SD of blood pressure (Bilo et al, 2007; Mena et al., 2005; Stolarz-Skrzypek et al., 2010). Slow BP level fluctuations between day and night can be used to identify daily BP variation patterns. A cardiovascular prognosis can be made based on these BP variation patterns (Verdecchia et al., 1993; Boggia et al., 2007; Hansen et al., 2011; Lurbe et al., 2002; Verdecchia et al., 2012).

1.8. Algorithms for estimating pulse arrival time

Literature describes many algorithms for estimating pulse arrival time. The majority of algorithms use the R wave of an ECG as the beginning point of PAT, meanwhile, the end point of PAT is defined ambiguously.

There are a few locations in the PPG signal wave which are used as the end point of PAT (Rapalis et al., 2014). The PPG signal is not resistant to noise and its quality depends on the conditions of measurement and on the subject (Allen, 2007; Elgendi, 2012). Usually the artifacts of a PPG signal are related to motion but there are physiologic artifacts as well, such as respiration. For this reason, band-pass filtering of the PPG signal is required, the low cut-off frequency being about 0.5 Hz and high – about 10 Hz (or lower) (Mukkamala et al., 2015). PAT estimation algorithms can be divided into two groups: time-domain and time-frequency algorithms (Figure 1.15), both of which are described in more detail in the following sections.

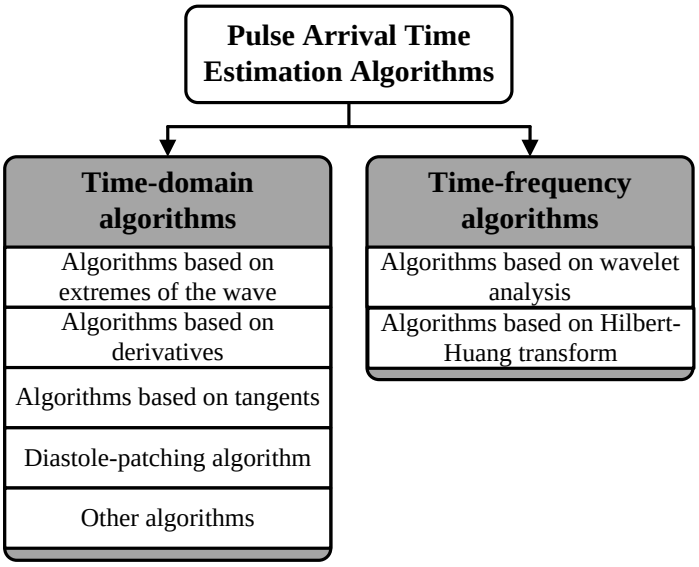

Figure 1.15. A classification of PAT estimation algorithms

1.8.1. Time-domain algorithms

Algorithms based on the extremes of the wave

PAT estimation algorithms based on the extremes of the wave calculate PAT as the time delay between the R peak of an ECG and the minimum or maximum point of PPG in the same cardiac cycle (Figure 1.16 a).

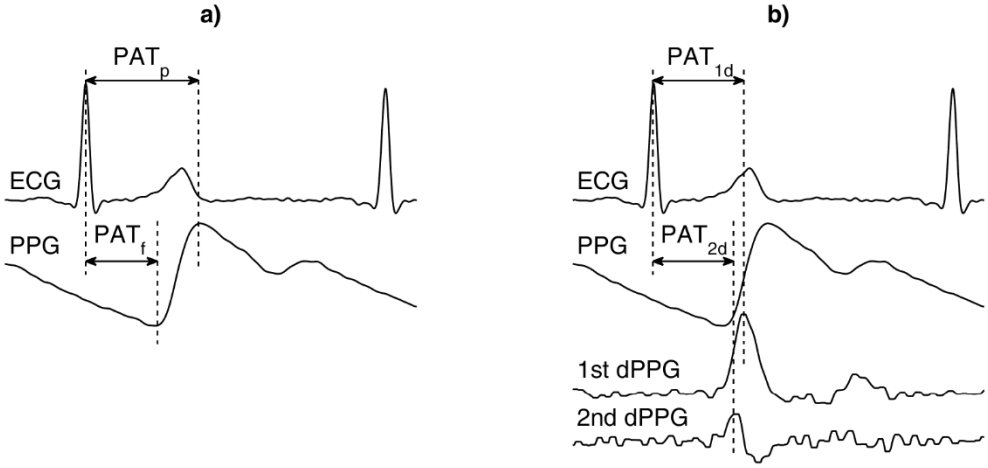

Figure 1.16. Different PAT definitions: PAT between the R peak of an ECG and the extremum point of a PPG. (PAT_f – PAT in which the end point is the minimum (foot) of PPG, PAT_p – PAT in which the end point is the maximum (peak) of PPG) a); PAT between the R peak of an ECG and the peak of the 1st or 2nd derivative of a PPG (PAT_{1d} – PAT in which the end point is the peak of 1st derivative of a PPG, PAT_{2d} – PAT in which the end point is the peak of 2nd derivative of a PPG) b)

Usually a band-pass filter is used to reduce the noise in the PPG signal, however, wavelets can be used for signal filtration as well (Sahoo et al., 2011). Then the pre-processing (noise reduction) algorithms search for the maximum (peak) or minimum (foot) point of a PPG or BP signal cycle. The PAT estimation algorithm based on the maximum point of a PPG is used rather frequently (Cattivelli, Garudadri, 2009; Wong et al., 2009a; Wu et al., 2012; Muehlsteff et al., 2012; Ma, 2014; Younessi et al., 2014; Špulák et al., 2011) as well as the algorithm based on the minimum point of a PPG (Cattivelli, Garudadri, 2009; Wong et al., 2009a; Muehlsteff et al., 2012; Chen et al., 2000; Ahlstrom et al., 2005; Špulák rt al., 2011). The maximum and minimum points of the BP signal coincide with the systolic and diastolic pressure (respectively) (Cattivelli, Garudadri, 2009; Vardoulis et al., 2013).

The algorithms based on the extremes of the wave have some modifications as well. For example, the end point of PAT in the PPG signal is where the amplitude rises 10% or 90% from the amplitude of the obtained foot point (Teng et al., 2004; Špulák et al., 2011).

Algorithms based on derivatives

PAT estimation algorithms based on derivatives calculate PAT as the time delay between the R peak of an ECG and the characteristic points of PPG derivative in the same cardiac cycle. After the pre-processing (noise reduction), algorithms search for the peak of the first or second derivative of a PPG or BP signal (Figure 1.16 b). PAT estimation algorithm based on the peak of the first PPG derivative, here called as the classical algorithm for PAT estimation, is most commonly used (Cattivelli, Garudadri, 2009; Wong et al., 2011; Teng et al., 2004; Vardoulis et al., 2013; Masè et al., 2011; Gesche et al., 2012; Wibmer et al., 2014; Špulák et al., 2011) although the algorithm based on the peak of the second PPG derivative is sometimes used as well (Kazanavicius et al., 2005; Teng et al., 2004; Ye et al., 2010). The peak of the second PPG (or BP) derivative approximately shows a location of the foot point of a PPG (or BP) signal.

PAT estimation algorithms based on derivatives have some modifications as well. In this case, the end point of PAT is the point of the PPG derivative whose amplitude rises by 30% of the PPG derivative peak amplitude (Sugo et al., 2010).

The second derivative of a PPG is very sensitive to interference. The noise can be unnoticeable in the first derivative of the PPG signal but it is obvious in the second derivative. For this reason, sometimes before locating the peak of the second derivative it is necessary to smooth the signal using the triangular moving average filter (Kazanavicius et al., 2005).

Algorithms based on tangents

PAT estimation algorithms based on tangents calculate the PAT as the time delay between the R peak of an ECG and a characteristic point of a PPG (or BP signal) which is determined by one or more tangents. After the pre-processing (noise reduction), algorithms based on tangents use two tangents on the PPG (or BP signal) wave and the end point of PAT is the characteristic point where these tangents intersect (Figure 1.17 a). The first tangent is a line which tangentially passes through

the peak of the first PPG (or BP signal) derivative. The second tangent line passes through the foot (minimum) point of a PPG (or BP signal) and is parallel to the x (time) axis (Hey et al., 2009); Vardoulis et al., 2013).

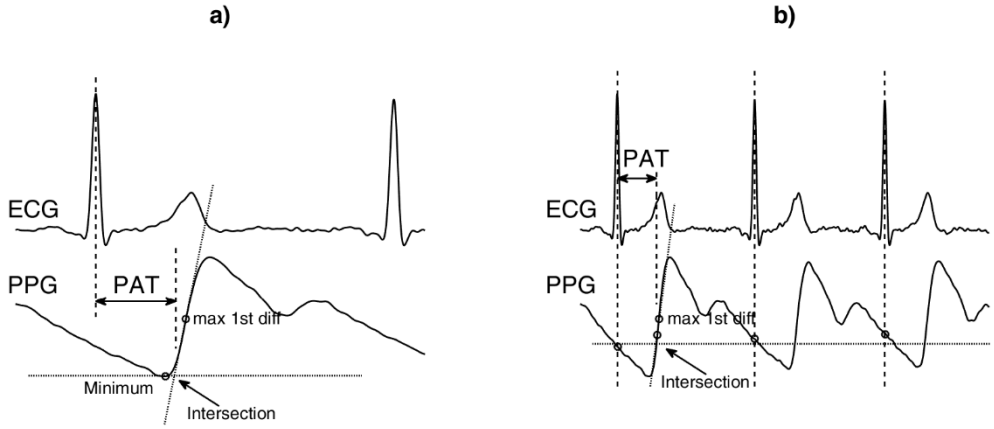

Figure 1.17. Different PAT definitions: PAT estimation between the R peak of an ECG and a characteristic point of a PPG (or BP signal) where two tangent lines intersect a); or tangent line and line intersect b)

This PAT estimation algorithm is also modified. The end point of PAT is the characteristic point where the tangent and line intersect (Figure 1.17 b). The first straight line is drawn through the maximum point of the first PPG (or BP signal) derivative and five points below it. The second straight line, using the least square method, passes through the PPG points which are at the R peaks of the ECG (Kazanavicius et al., 2005).

Diastole-patching algorithm

The diastole-patching algorithm (PATdp) is based on template fitting and calculates PAT as the time delay between the R peak of an ECG and characteristic points of a PPG (or BP signal) in which the template and PPG signal have a lower sum of square differences (SSD). These characteristic points correspond with the foot point of a PPG (or BP signal). The template size is always the same and is selected using the location of the minimum of a PPG (or BP signal) and the maximum of the first derivative of a PPG (or BP signal) (Figure 1.18 a). The template moves through the PPG (or BP) signal, SSD is calculated in each point and the foot point is considered to be where the SSD is minimized (Figure 1.18 b) (Vardoulis et al., 2013).

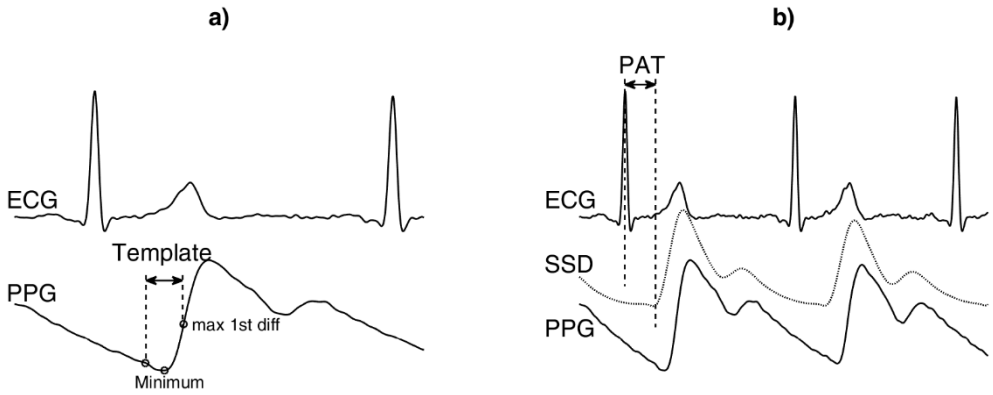

Figure 1.18. Diastole-patching PAT estimation algorithm: selection of template a); and PAT estimation between the R peak of an ECG and the foot point of a PPG (or BP signal) which is estimated using the template b) (Vardoulis et al., 2013)

Other algorithms

This PAT estimation algorithm calculates PAT as the time delay between the R peak of an ECG and a characteristic point of a PPG (or BP signal) which is determined by two intersecting straight lines. After the pre-processing (noise reduction), this algorithm uses two straight lines on the PPG (or BP signal) wave, and the end point of PAT is the characteristic point where these lines intersect. The first straight line passes through two points: the first point is the R peak in the PPG (or BP) signal, the second point is 2/5 of the whole RR interval before R peak. The second straight line passes through the peak of the first PPG (or BP signal) derivative and five points below it (Figure 1.19 a) (Kazanavicius et al., 2005).

Another algorithm is the foot approximation algorithm which calculates the PAT as the time delay between the R peak of an ECG and a characteristic point (foot point) of a PPG (or BP signal) in the same cardiac cycle. After the pre-processing (noise reduction), it is necessary to determine a search interval between the R peak of an ECG and the peak of the first PPG (or BP signal) derivative. Then the search interval is divided into ten parts; the least square method is used and straight lines are drawn through the values of these ten parts. The average of the starting point of the current and the end point of the previous straight lines is calculated. A sequence of average abscissa values is fit with a cubic polynomial and the foot point of the signal is the point of the least value (Figure 1.19 b) (Kazanavicius et al., 2005).

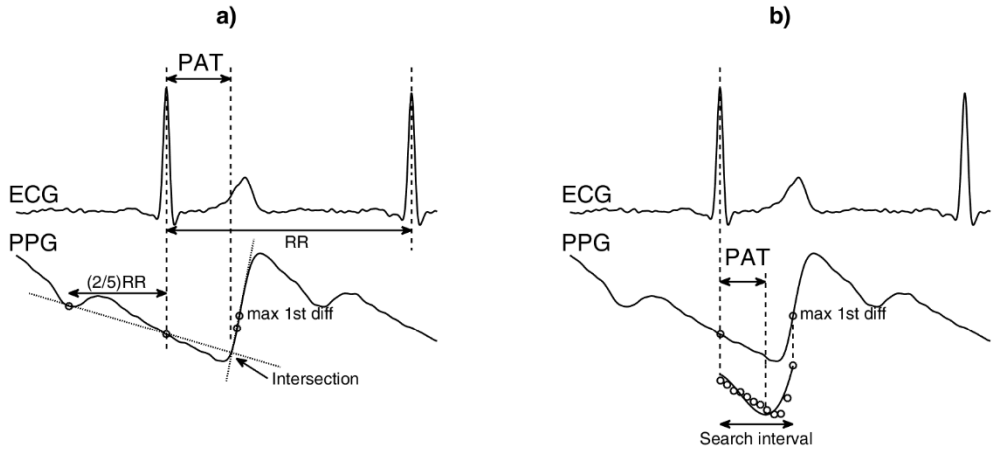

Figure 1.19. Different PAT definitions: PAT estimation between the R peak of an ECG and a characteristic point of a PPG (or BP signal) where two straight lines intersect a); and where the least value of search interval is b) (Kazanavicius et al., 2005)

1.8.2. Time-frequency algorithms

Algorithm based on wavelet analysis

PAT estimation algorithms based on wavelet analysis calculates the PAT as the time delay between the R peak of an ECG and a characteristic point (peak) of a PPG extracted using wavelet analysis in the same cardiac cycle. A function of one variable is decomposed in the 2D time-frequency space using continuous wavelet transformation. The complex Morlet wavelet is used in this algorithm because it allows to calculate the modulus and phase of wavelet decomposition. The frequency of oscillation which produces the highest energy at each time (local dominant frequency) is detected using the information from the modulus and phase. The means of correlation and phase shift of oscillations between two signals are calculated as well. After the wavelet analysis, the pulse arrival time is calculated from the phase shift between the ECG and PPG signals at the dominant frequency (which corresponds to the heart rate) (Allen et al., 2013):

$$PAT = \frac{\Delta\varphi(\nu_d, \tau)}{2\pi\nu_2} \tag{1.12}$$

where, $\Delta\varphi$ – phase shift; ν_d – local dominant frequency; τ – time.

Algorithm based on Hilbert-Huang transform

PAT estimation algorithm based on the Hilbert-Huang transform calculates PAT as the time delay between the R peak of an ECG and a characteristic point (peak) of a PPG in the same cardiac cycle. The Hilbert-Huang transform (HHT) is used to process ECG and PPG signals to obtain the intrinsic mode functions (IMF) and to determine the R peaks of an ECG signal and the peaks of a PPG signal. The IMFs are obtained using the empirical mode decomposition (EMD). A new ECG signal (without noise) is reconstructed by ignoring the IMFs, which are related

to noise, and the R peaks can be easily detected. In order to improve peak detection, each IMF of the PPG signal is compared with the rebuilt signal and it has been noticed that the third IMF of a PPG shows better performance. Pulse arrival time can be estimated after the peaks have been detected (Figure 1.20) (Zhang et al., 2009).

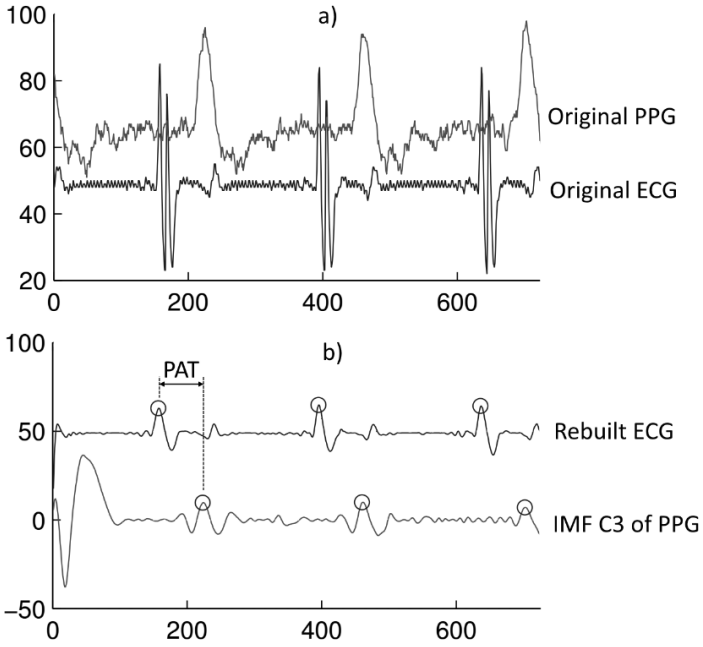

Figure 1.20. PAT estimation algorithm based on the Hilbert-Huang transform where PAT is between the R peak of an ECG and the peak of the rebuilt PPG: original ECG and PPG signals a); rebuilt ECG and IMF C3 of PPG b) (adopted from Zhang et al., 2009)

1.8.3. A comparison of PAT estimation algorithms

2000 proximal and distal pressure waveforms were simulated and distorted with white noise (five different levels of SD white noise) and the baseline wander artifact (generated using linear positive offset). The time-domain algorithms (based on the minimum of the wave, the maximum of the first and second derivatives, the tangents, and the diastole-patching algorithm) were tested (Vardoulis et al., 2013). The investigation shows that the diastole-patching algorithm is the most accurate and precise and varies the least in comparison with other time-domain PAT estimation algorithms. Pulse wave velocity estimated with diastole-patching algorithms are the most accurate and in agreement with real, analytic PWV when compared to other time-domain algorithms (Table 1.7.) (Vardoulis et al., 2013). PAT was estimated using unfiltered (distorted) simulated waveforms, therefore, the results might be distorted.

Table 1.7. A comparison of time-domain PAT estimation algorithms: correlation, agreement, accuracy, and precision between real (determined analytically) and estimated PWV (Vardoulis et al., 2013)

Algorithms	CD[1]	ICC[2]	MD[3], m/s	SD of MD, m/s	CV[4], %	RMSE[5], m/s	Limits of Agreement, m/s
Minimum	0.978	0.864	0.834	0.348	8.376	0.904	0.15; 1.52
Maximum 1st derivative	0.977	0.445	-1.743	0.605	21.155	1.845	-0.53; -2.95
Maximum 2nd derivative	0.982	0.666	-1.205	0.433	13.999	1.280	-0.34; -2.07
Tangential	0.997	0.786	-0.919	0.335	10.366	0.978	-0.26; -1.57
Diastole-patching	0.990	0.977	-0.261	0.176	2.844	0.315	0.09; -0.61

[1]CD – coefficient of determination; [2]ICC – intraclass correlation coefficient; [3]MD – mean difference; [4]CV – coefficient of variation; [5]RMSE – root mean square error.

Using simple (time-domain or time-frequency) algorithms to estimate PAT, values might be unreliable when the PPG signal is noisy (Mukkamala et al., 2015). For this reason, the estimation of foot and peak points of PPG or BP signals is not an easy task. Figure 1.21 shows a BP signal with and without a reflection wave (Figure 1.21 a and b, respectively); the foot region can be long and flat (Figure 1.21 c) and additional noise can be visible in the signal as well (Kazanavicius et al., 2005).

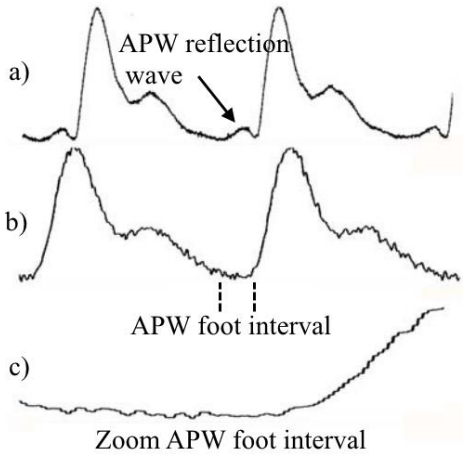

Figure 1.21. BP signal with artifacts and noise: foot interval with a reflection wave a); foot interval without a reflection wave b); foot interval close-up c) (adopted from Kazanavicius et al., 2005)

Almost all definitions of PAT are high quality PPG signal with clearly visible fiducial points on the waveform. However, there are cases when PPG signals are noisy under certain conditions, which is especially visible when the subject or the PPG probe moves. Also in some non-stationary cases, the amplitude of a PPG

signal changes considerably, for example, during a deep inspiratory gasp (Figure 1.22 a) (Allen et al., 2013) or an orthostatic test (Figure 1.22 b) (Rapalis et al., 2014).

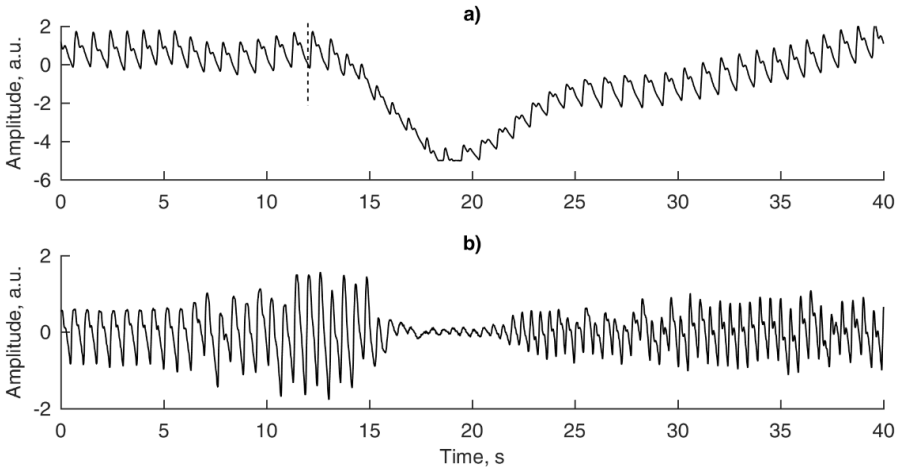

Figure 1.22. A PPG signal in non-stationary cases: deep inspiratory gasp (the beginning of a gasp is marked by a vertical dashed line) a), and orthostatic test b)

1.9. Conclusions of the chapter

1. Pulse arrival time is an important physiological parameter which relates to the cardiovascular system (blood pressure and other parameters). There are a lot of algorithms for estimating pulse arrival time but a noise resistant algorithm does not yet exist, although is especially needed when research is carried out in non-stationary conditions.
2. An ECG (R waves) recording is needed to evaluate the HRV and this technique requires to stick electrodes on the body, as opposed to PPG recording, where electrodes are not necessary. Therefore, the PPG technique is more convenient for evaluating the ANS status.
3. For short-term BPV evaluation, a continuous (beat-to-beat) BP recording is needed but this technique is used only in laboratories or under ambulatory conditions. The devices currently in use for continuous BP measurement require a doctor's care (invasive continuous BP devices), are uncomfortable to wear and use (non-invasive continuous BP devices) because they are based on cuff calibration. Therefore, new methods, estimators, and parameters which are related to BP and its variability are necessary.
4. Multimodal physiological signals (ECG and PPG) are strongly associated with physiological processes of the body and are used for its evaluation.
5. Heart rate and blood pressure variability are influenced by many factors (age, gender, heart disease, neurological disease, drugs/medications, bad habits, exercise, and other). HRV and BPV are related to an increased risk of cardiovascular events and can be used for assessing the state of the cardiovascular system.

2. PROPOSED ALGORITHMS AND SOLUTIONS FOR ESTIMATING PULSE ARRIVAL TIME AND EXTRACTING INSTANTANEOUS FREQUENCY

This chapter describes the conception of short-term heart rate and blood pressure variability estimation (section 2.1). The proposed system consists of solutions and algorithms for estimating pulse arrival time (section 2.2) and extracting instantaneous frequencies (section 2.3). The conclusions of the chapter are provided in section 2.4.

2.1. Conception of the system

This section describes the conception of short-term heart rate and blood pressure variability evaluation system. A block scheme of the proposed system is presented in Figure 2.1. The system consists of:

- Data (physiological signals – BP, ECG, and PPG);
- Parameter estimation algorithms: blood pressure (systolic and diastolic) estimation algorithm, R-R interval estimation algorithm, pulse arrival time estimation algorithm (Rapalis et al., 2014), and instantaneous PPG frequency extraction algorithm (Rapalis et al., 2016);
- Statistical analysis (variability analysis and variability comparison).

Each algorithm can be used separately or combined into a system which can evaluate short-term heart rate and blood pressure variability. This section also describes additional algorithms and statistical analysis.

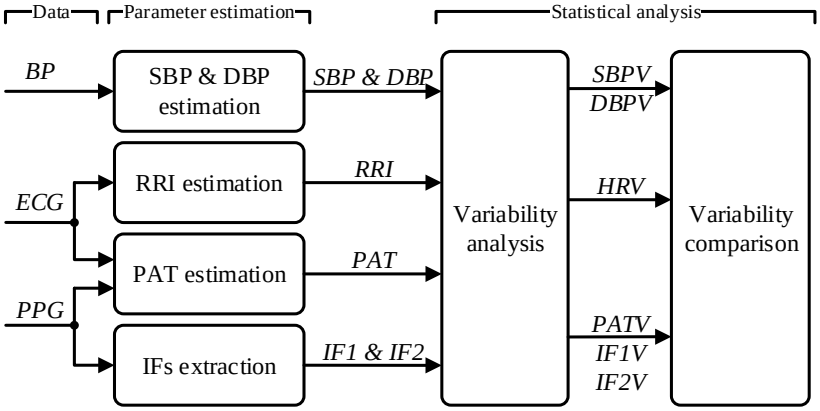

Figure 2.1. The conception of the proposed HR and BP variability evaluation system

The proposed algorithm for estimating pulse arrival time (PATht) is based on the narrowband band-pass filtration, Hilbert transform, and instantaneous phase shift estimation. The PPG signal is not resistant to noise, therefore, narrowband band-pass filtration and other steps allow to minimize noise in the PPG signal and estimate

the PAT more accurately. The proposed PAT estimation algorithm is noise-resistant and can be used not only at rest but also in non-stationary conditions.

The algorithm for extracting instantaneous PPG frequencies (IFe) is based on ensemble empirical mode decomposition and direct quadrature. Two instantaneous frequencies from two intrinsic mode functions (which have the highest correlation to PPG waveform) are extracted from the PPG signal (Janušauskas et al., 2013).

The proposed PATht algorithm requires two synchronously recorded physiological signals (ECG and PPG), meanwhile the IFe algorithm requires only the PPG signal. Any ECG lead can be used to estimate R waves, however, they should be estimated accurately. The intervals between successive R waves of the ECG (RRI) were detected using a modified Pan-Thompkins algorithm (Hamilton, Tompkins, 1986). The PPG signal can be recorded from any standard places on the body, such as the finger or forehead. PATht and IFe algorithms allow to evaluate the processes of an organism, for example, the body's condition and the possibilities of adaptation to external impacts. Each of the proposed algorithms and solutions are described in more detail in the following sections.

Systolic and diastolic BP of each cardiac cycle were defined by the values of the frontal foot and the first peak of the BP signal. The variability was analysed using the variability techniques and parameters described in sections 1.6 and 0. Variability comparison is presented with the results in Chapter 4.

2.2. The algorithm for estimating Pulse Arrival Time

The proposed algorithm for estimating pulse arrival time (PATht) is based on narrowband band-pass filtration, auxiliary ECG signal creation, amplitude normalization, Hilbert transform, and instantaneous phase shift estimation. A block diagram of the PAT estimation algorithm is shown in Figure 2.2. Each of the processing blocks is described below.

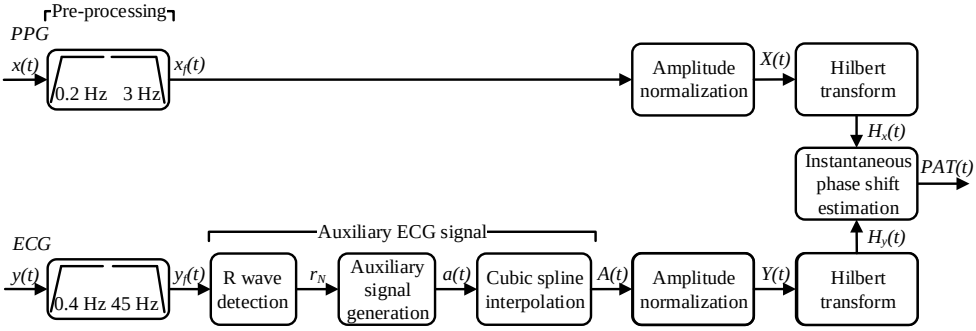

Figure 2.2. A block diagram of the PATht pulse arrival time estimation algorithm

2.2.1. Pre-processing and auxiliary ECG signal

In order to eliminate high-frequency components from the PPG signal and minimize the number of peaks in a PPG cycle, raw PPG signal *x(t)* was filtered with a narrowband Butterworth band-pass filter (order 4, cut-off frequencies of 0.2 and

3 Hz). The PPG signal after filtration $x_f(t)$ is almost a monocomponent signal (Figure 2.3).

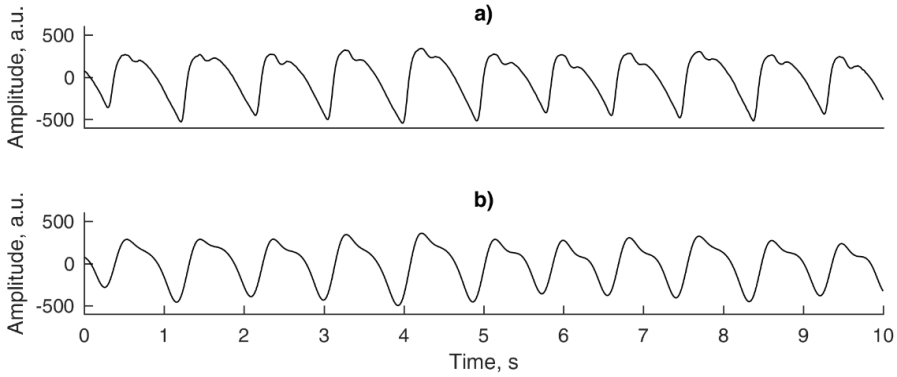

Figure 2.3. Processing of PPG signals: PPG signals after classical Butterworth band-pass filter (0.4–27 Hz) a), and after narrowband Butterworth band-pass filter (0.2–3 Hz) b)

The processing of an ECG signal $y(t)$ started with the removal of noise and artifacts (muscle activity, baseline drift and other) by using the Butterworth band-pass filter (order 4, cut-off frequencies of 0.4 and 45 Hz). In the next stage, R waves r_N were detected using a modified Pan-Thompkins algorithm with an adaptive threshold (Hamilton, Tompkins, 1986). An auxiliary signal $a(t)$ was generated by assigning 1 to time indices of the detected R waves r_N, -1 in the middle of RR interval, and 0 to the rest of the samples:

$$a(t) = \begin{cases} 1, t = r_N \\ -1, t = (r_N + r_{N+1})/2 \\ 0, t \neq r_N \ \& t \neq (r_N + r_{N+1})/2 \end{cases} \quad (2.1)$$

where r_N are the locations of ECG R waves.

A harmonic ECG signal was synthesized using a cubic spline interpolation through unit pulses:

$$A(t) = a_0 + a_1 t + a_2 t^2 + a_3 t^3 \quad (2.2)$$

where a_0, a_1, a_2, a_3 are coefficients.

The generated monocomponent ECG signal $A(t)$ produces an instantaneous frequency equal to the instantaneous heart rate (Figure 2.4).

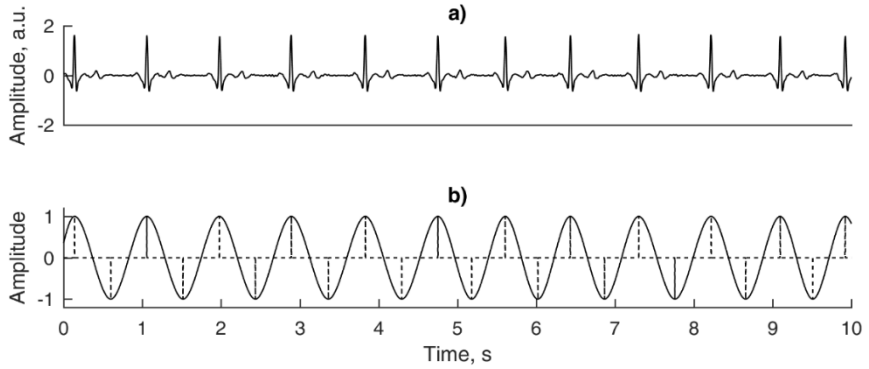

Figure 2.4. The processing of ECG signals: ECG signals a), an auxiliary ECG signal (dotted line) and an auxiliary ECG signal after cubic spline interpolation (line) b)

2.2.2. Amplitude normalization of the extracted monocomponent signals

The amplitude normalization was implemented for both extracted monocomponent PPG $x_f(t)$ and ECG $A(t)$ signals. The normalization consists of an iterative process of Hilbert transform (signal envelope calculation) and the cubic spline interpolation between the peaks (defined in 2.2). The Hilbert transform is a convolution of signals $x_f(t)$ and $A(t)$ with signal $1/\pi t$ and defined by:

$$H\left[x_f(t)\right] = x_f(t) * \frac{1}{\pi t} = \frac{1}{\pi}\int_{-\infty}^{\infty} \frac{x_f(\tau)}{t-\tau} d\tau \tag{2.3}$$

$$H\left[A(t)\right] = A(t) * \frac{1}{\pi t} = \frac{1}{\pi}\int_{-\infty}^{\infty} \frac{A(\tau)}{t-\tau} d\tau \tag{2.4}$$

Signals $X_n(t)$ and $Y_n(t)$ after cubic spine interpolation were divided by the input signal $x_f(t)$ and the process was repeated until all peak amplitudes of the normalized signal were either 1 or -1. The result of this processing is normalized "quasi" monocomponent PPG $X(t)$ and ECG $Y(t)$ signals with a frequency equal to the instantaneous heart rate (Figure 2.5).

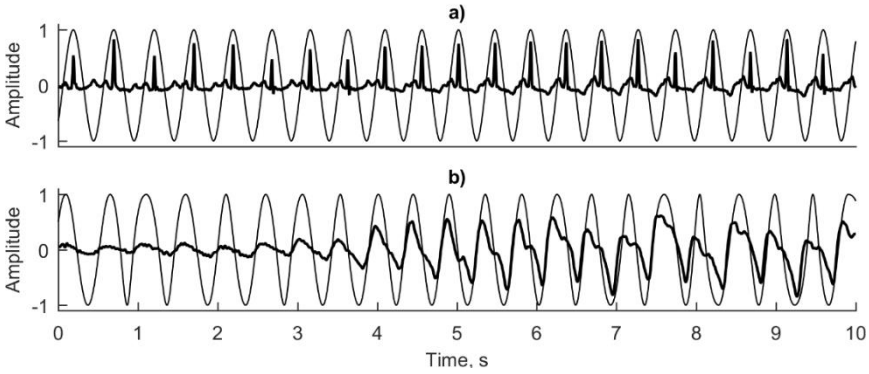

Figure 2.5. Filtered ECG a) and PPG b) signals (bold line) and their fundamental frequency components: $X(t)$ and $Y(t)$ (thin line)

2.2.3. Hilbert transform and instantaneous phase shift estimation

Hilbert transform is a convolution of signals *X(t)* and *Y(t)* with signal $1/\pi t$ in which the phase angle of all signal components is shifted by ±90° (defined in eq. 2.3). Therefore, using the Hilbert transform both ECG and PPG monocomponent signals were transformed to analytic signals:

$$H_{yj}(t) = v_{ECGj}(t) + iu_{ECGj}(t) \tag{2.5}$$

$$H_{xj}(t) = v_{PPGj}(t) + iu_{PPGj}(t) \tag{2.6}$$

The instantaneous phase shifts between ECG $H_y(t)$ and PPG $H_x(t)$ components which are equivalent to PAT evolution in time were calculated by the following relation (Zielinski, 1996):

$$PAT(t) = \frac{\Delta\varphi(t)}{2\pi} = arctg\left(\frac{\Im\left[v_{ECG}(t)\cdot v^{*}_{PPG}(t)\right]}{\Re\left[v_{ECG}(t)\cdot v^{*}_{PPG}(t)\right]}\right)\Big/ 2\pi \tag{2.7}$$

where $\varphi(t)$ is instantaneous phase shift; $v_{ECG}(t)$ and $v_{PPG}(t)$ – components of ECG and PPG analytic representation after Hilbert transform.

2.3. The instantaneous PPG frequency extraction algorithm

The proposed algorithm for instantaneous PPG frequency extraction (IFe) is based on the ensemble empirical mode decomposition (EEMD) and direct quadrature. The hypothesis of this algorithm is that the extracted instantaneous PPG frequencies reflect the speed of PPG signal change and can be used to estimate heart rate and blood pressure variability. A block diagram of the IF extraction algorithm is shown in Figure 2.6. Each of the processing blocks is described below.

Figure 2.6. A structural scheme of instantaneous PPG frequency extraction algorithm

2.3.1. Pre-processing

In order to remove physiological artefacts and reduce measurement errors which occur for conditions of measurement, band-pass filtering of the PPG signal is required. Band-pass filtering also reduces EEMD performance time because less components (modes) are extracted when the PPG signal has less noise thus the first (higher) modes (noise modes) are extracted faster. Raw PPG signal *x(t)* was filtered using the Butterworth band-pass filter (order 4); low and high cut-off frequencies (0.5 and 14 Hz, respectively) were chosen based on literature (Mukkamala et al., 2015).

2.3.2. Ensemble empirical mode decomposition

The empirical mode decomposition decomposes a signal into locally narrow band oscillating components called intrinsic mode functions (IMFs) (Huang et al., 1998). A block diagram of the EMD algorithm is shown in Figure 2.7.

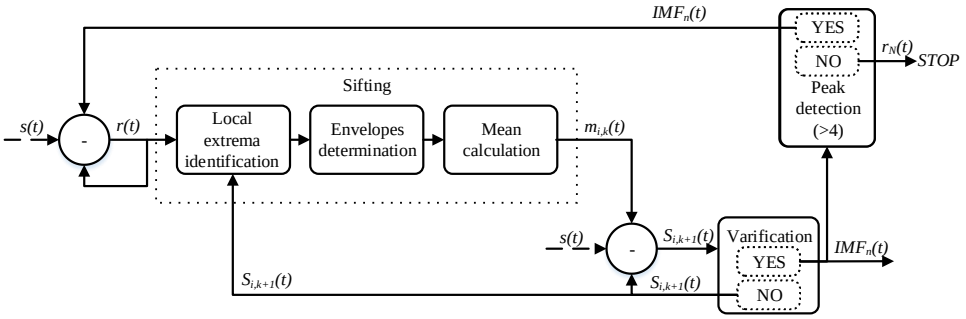

Figure 2.7. A structural scheme of empirical mode decomposition. *s(t)* is input signal (dashed line); $IMF_n(t)$ – output signal – instantaneous frequency

The IMFs are monocomponent signals which are needed to extract instantaneous frequencies. The IMFs result from an iterative procedure consisting of extrema identification and "sifting". The observed signal *s(t)* constitutes the input to sifting, and $s_{i,k}(t)$ defines a component of the sifting process (*i* denotes iteration number, *k* – sifting component). The procedure is initialized with $s_{1,1}(t) = s(t)$. The following steps define sifting:

1. The local minima and maxima of $s_{i,k}(t)$ are determined.
2. The lower and upper envelopes are determined by interpolation of $s_{i,k}(t)$ between the local maxima and minima, respectively.
3. The mean value $m_{i,k}(t)$ of the resulting upper and lower envelopes is computed and subtracted from $s_{i,k}(t)$ so that the next component of sifting is defined by:

$$S_{i,k+1}(t) = s_{i,k}(t) - m_{i,k}(t) \tag{2.8}$$

4. The component $S_{i,k+1}(t)$ is checked against the following IMF conditions and if they are not met, sifting continues (steps 1 through 3 are repeated with $k=k+1$). Condition No. 1: an IMF, by definition, is symmetric in time and has a number of extrema and zero crossings which must be equal or, at most, differ by one. Condition No. 2: the mean value of the envelopes defined by the local maxima and the local minima must be zero at all times.
5. The steps above are repeated until the two conditions are met; the resulting IMF is denoted as $IMF_n(t)$. To quicken the procedure, certain stop criteria could be used, for example, by relaxing the second IMF condition allowing certain deviation from zero or by limiting the number of sifting steps. It is obvious that in both cases the sifting result will differ to a certain extent

from the "true" IMF and should be used with caution. The next sifting process starts after the subtraction of $IMF_n(t)$ from the signal $s_{i,1}(t)$ so the resulting signal $r_i(t)$ is the input to the successive sifting process:

$$r_i(t) = s_{i,1}(t) - IMF_n(t) \tag{2.9}$$

$$S_{i+1,1}(t) = r_{i,1}(t) \tag{2.10}$$

This process is repeated until the residual $r_N(t)$ has less than 3 extrema, which means that all IMFs have been extracted. The observed signal $s(t)$ can be expressed as a sum of IMFs and the residual $r_N(t)$,

$$S(t) = \sum_{i=1}^{n} IMF_n(t) + r_N(t) \tag{2.11}$$

The EMD process can be understood as a step-by-step extraction of the locally highest frequency oscillation of the signal, progressively forming the low-pass intrinsic mode functions.

The empirical mode decomposition often has a specific shortcoming called mode mixing when very different momentary frequencies are present at the same scale or very close frequencies are present in a few scales. The modification of EMD called ensemble empirical mode decomposition method has been proposed to overcome the problem of mode mixing (Figure 2.8) (Wu, Huang, 2009); Yen et al., 2010; Tsui et al., 2010).

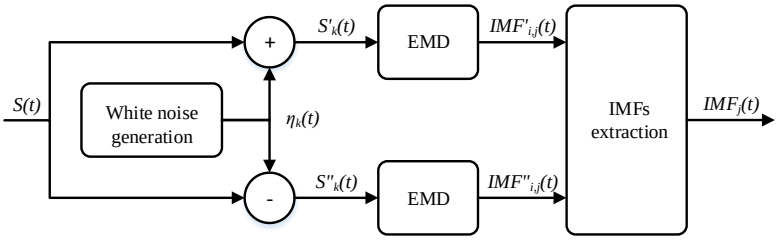

Figure 2.8. A structural scheme of ensemble empirical mode decomposition. k – number of realizations, $k = 1...N/2$; i – number of IMFs realizations, $i = 1...N$; j – number of modes, $j = 1...N$

EEMD defines the true IMF components as the mean of ensemble of trials, each consisting of the signal $S(t)$ plus white noise $\eta(t)$ of a finite amplitude. According to this approach, the realization of artificial white noise is added to the analyzed signal and then the EMD method is applied on the noisy data ($S'(t)$ and $S''(t)$):

$$S'(t) = S(t) + \eta_k(t) \tag{2.12}$$

$$S''(t) = S(t) - \eta_k(t) \tag{2.13}$$

These operations are repeated for a certain number of times, each time adding a new white noise realization to the same signal. Each individual trial produces noisy IMFs (*IMF'(t)* and *IMF''(t)*) because each input to the decomposition consists of the analyzed signal and added white noise. The output is a set of an ensemble of data decompositions with added white noise. Since the noise in each trial is different, it is cancelled out by averaging all realizations of each IMF. The final average of the corresponding IMFs is treated as the result of EEMD:

$$IMF_j(t) = \frac{1}{N}\sum_{i=1}^{N/2}\left(IMF'_{i,j}(t) + IMF''_{i,j}(t)\right) \tag{2.14}$$

Where N – number of realizations, N = *1…n*; i – number of IMFs realizations, $i = 1 \ldots N$; j – number of modes, $j = 1 \ldots N$.

Added noise forces a uniform scale distribution in each trial and the mean of IMFs stays within the natural dyadic filter windows, significantly reducing the chance of mode mixing and preserving the dyadic property (Wu, Huang, 2009). IMFs obtained from a real PPG signal are shown in Figure 2.9.

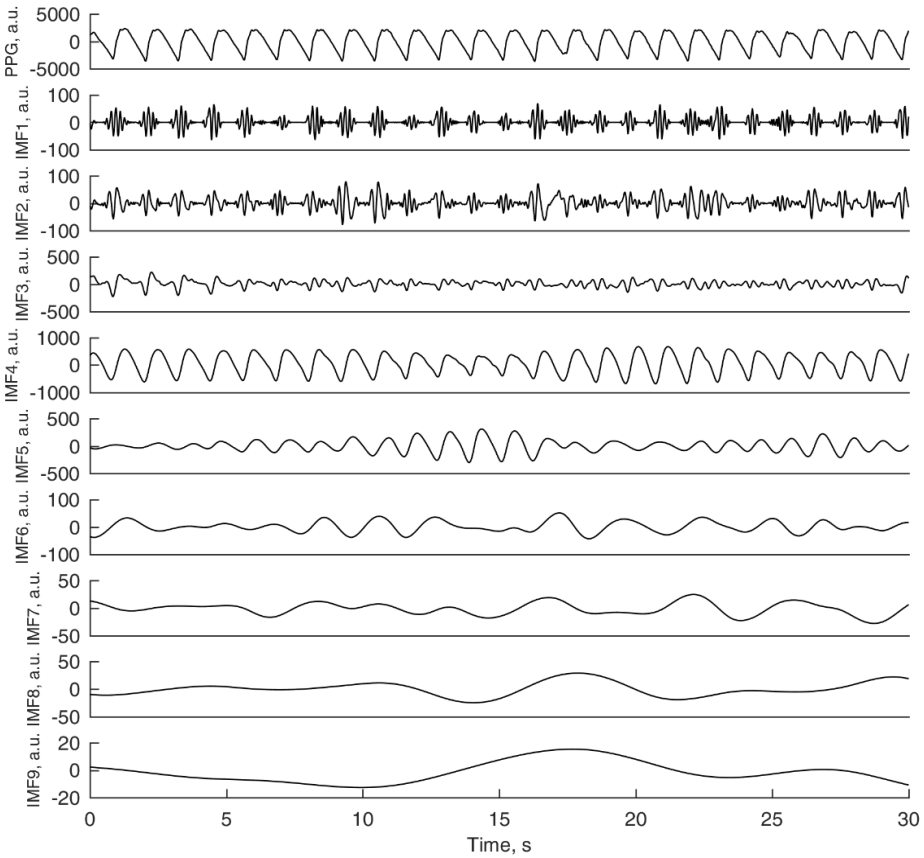

Figure 2.9. A filtered PPG signal and IMFs obtained using EEMD

2.3.3. Selection of IMFs

After EEMD, several IMFs were obtained (the number of decomposed IMFs depends on the waveform of the PPG signal). The cross-correlation coefficient *r* was calculated between the original PPG signal $x_f(t)$ and each extracted IMF using a technique similar to the method presented in Janušauskas et al., 2013. Cross-correlation is a standard measure of similarity of two series, for example, cross-correlation between two series ($x_f(t)$ and $IMF_j(t)$, t = *0, 1, 2 ... N-1*) can be defined by:

$$r = \frac{\sum_t \left(x_f(t) - \overline{x_f}\right) * \left(IMF_j(t-d) - \overline{IMF_j}\right)}{\sqrt{\sum_t \left(x_f(t) - \overline{x_f}\right)^2} \sqrt{\sum_i \left(IMF_j(t-d) - \overline{IMF_j}\right)^2}} \tag{2.15}$$

where $\overline{x_f}$ and $\overline{IMF_j}$ are the means of series; *d* – delay (*d = 0, 1, 2 ... N-1*).

Two or three IMFs which have a high cross-correlation coefficient *r* are extracted from the PPG signal $x_f(t)$ (the waveforms of these IMFs are the most similar to the original waveform of the PPG signal). The hypothesis is that all other IMFs are noise components. Therefore, two IMFs are selected (which provided the highest cross-correlation coefficient) and used in the following analysis (Figure 2.10 a and d) because more appropriate IMFs may not always be available. It is assumed that one IMF (lower frequency) better reflects the fundamental frequency, while the other (higher frequency) better represents the signal details. The frequency of selected IMFs is assessed as well, and the lower IMF is entitled as IMF1 (first IMF), while the higher IMF is named IMF2 (second IMF). Instantaneous frequencies are obtained only from these two selected IMFs.

2.3.4. Amplitude normalization

The amplitude is normalized for both decomposed and selected IMFs (IMF1 and IMF2). Normalization consists of an iterative process of the Hilbert transform (signal envelope calculation defined in eq. 2.3) and Hermite interpolation between peaks. Hermite interpolation is defined with:

$$IMF_N(t) = a_0 + a_1 t + a_2 t^2 + a_3 t^3 + a_4 t^4 \tag{2.16}$$

where a_0, a_1, a_2, a_3, a_4 are coefficients.

The normalized signal is divided by the input signal (input IMF) and the process is repeated until all amplitude peaks of the normalized IMF signal are either 1 or -1 (Figure 2.10 b and e).

2.3.5. Direct quadrature

Instantaneous frequencies can be calculated using a Hilbert transform, normalized Hilbert transform, direct quadrature (DQ), and other techniques. However, the DQ technique is the best method for IF calculation for really noisy recorded physiological signals because it is more resistant to noise (Huang et al.,

2009). For this reason, instantaneous frequencies were calculated from the selected and amplitude normalized IMFs (IMF1 and IMF2) using the DQ technique. Using this method, the correct phase functions can be obtained even for extremely complicated phase functions. According to direct quadrature, the phase from IMF $\varphi(t)$ can be calculated with (Huang et al., 2009):

$$\phi(t) = \arctan \frac{IMF_N(t)}{\sqrt{1 - IMF_N{}^2(t)}}, \tag{2.17}$$

where $IMF_N(t)$ – normalized IMF.

Smoothing of the instantaneous frequency is often applied to produce trends of the time-frequency information. IFs computed using the DQ are shown in Figure 2.10 (c and f). IFs medians between adjacent heart beats were calculated in order to get IF1 and IF2 values (Huang et al., 2009).

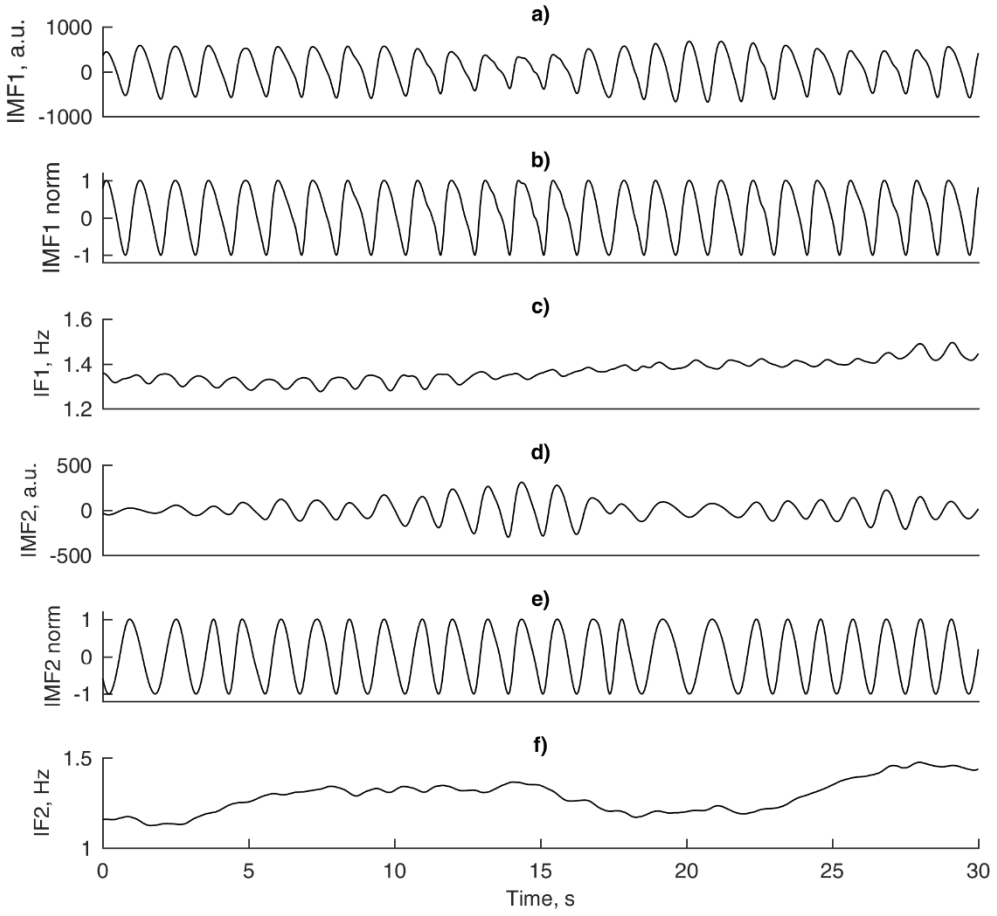

Figure 2.10. Two decomposed and selected IMFs, IMFs after amplitude normalization, and extracted IF using DQ: IMF1 a); IMF1 norm b); IF1 c); IMF2 d); IMF2 norm e), and IF2 f)

2.4. Conclusions of the chapter

1. An algorithm for estimating pulse arrival time was developed. It consists of pre-processing (narrowband band-pass filtration), Hilbert transform, and instantaneous phase shift estimation. The algorithm can be used only offline and can be a part of the system or work separately.
2. An algorithm for extracting instantaneous PPG frequencies was developed. It consists of ensemble empirical mode decomposition and direct quadrature. The IF extraction algorithm requires only a PPG signal. The algorithm can be used only offline and can be a part of the system or work separately.

3. THE FORMATION OF SYNTHETIC AND EXPERIMENTAL DATABASE

This chapter describes the database of synthetic and experimental signals used in this research. Section 3.1 describes the usage data and how the experimental tests affect the body. Section 3.2 describes the simulated data, section 3.3 – experimental data (including information about subjects, protocols, and equipment): orthostatic test (section 3.3.1) and thermal stress test (section 3.3.2). Conclusions of the chapter are presented in section 3.4.

3.1. Methodology justification

Simulated and experimental data have been used for testing the developed algorithms. Simulated signals were modelled based on observation of ECG and PPG recorded during the orthostatic test. The simulated data were used to evaluate the performance of pulse arrival time estimation algorithm when the signal-to-noise ratio (SNR) of the PPG signal varied. All information about the simulated data is provided in section 3.2.

In order to stimulate the autonomic nervous system of the body and observe its reaction (Zygmunt, Stanczyk, 2010), the experimental data was obtained from two different cardiovascular tests (the orthostatic test and thermal stress test). The orthostatic test is a cardiovascular test which is widely used for the stimulation of the autonomic nervous system. Under normal conditions, in a standing position 10–15% of blood is pooled in the legs, therefore, the venous return, cardiac output, and arterial pressure are reduced. The fall of blood pressure (by at least 20 mmHg in SBP and at least 10 mmHg in DBP) activates baroreceptors with a subsequent reflex, which increases the sympathetic outflow and parasympathetic inhibition which, in turn, leads to peripheral vasoconstriction and increased heart rate and contractility (Naschitz, Rosner, 2007). For these reasons, the orthostatic test was selected as an appropriate cardiovascular test for stimulating the autonomic nervous system.

In order to observe and monitor significant changes in physiological parameters (heart rate and blood pressure), a high stress should be caused to an organism. A Finnish sauna is one of the most common thermal therapy in the world. Many people use thermal therapy for treatment, hygiene, strengthening the immune and cardiovascular systems, rehabilitation, and physiological (muscle and nervous system) stress reduction (Kukkonen-Harjula, Kauppinen, 2006). The effects of sauna are described as relaxant of muscles and suppressive of the central nervous system (Sutkowy et al., 2014). A Finnish sauna session (ambient temperature from 80 to 90°C and relative humidity from 30 to 40%) can increase the body (rectal) temperature up to 39°C (Sohar et al., 1976). This body temperature (>39°C) is described as a high physiological thermal stress (hyperthermia) of the body (Moran et al., 1998; Moran et al., 1999; Brazaitis et al., 2012) which

worsens cognitive function (Racinais et al., 2008) and reduces central activation to working muscles (Brazaitis et al., 2012; Racinais et al., 2008; Nybo, Nielsen, 2001). Therefore, the thermal stress test was selected as a suitable high stress test.

Experimental data was used for testing both proposed (pulse arrival time estimation and instantaneous frequencies extraction) algorithms. All experimental data (subjects, protocols, and used equipment) are described in section 3.3.

3.2. Simulated data

The PPG signal *s(t)* was modeled based on direct measurement of a real PPG signal change during an orthostatic test as phase modulated two harmonic waves with a variable period and amplitude. The length of an RR interval (one heart cycle) and the period of PPG impulse was equal. The simulated signal was divided into two parts: lying (horizontal posture) and standing (vertical posture). The periods of PPG impulses (RR intervals as well) were 0.60–1.50 seconds (100–40 bpm) in horizontal posture and 0.40–0.67 seconds (150–90 bpm) in vertical posture (Figure 3.1). The length of simulated signal was 180 beats (99.00–232.65 seconds). Mathematical model of the acquired PPG signal is:

$$s(t) = A_n(t)\sin\left(2\pi f_n(t)\right) \tag{3.1}$$

where $A_n(t)$ – non-stationary amplitude of harmonic component; n – harmonic number; $n = 1…2$; $f_n(t)$ – frequency which changes randomly from 0.83 to 1.33 Hz for horizontal posture and from 1.37 to 2 Hz for vertical posture.

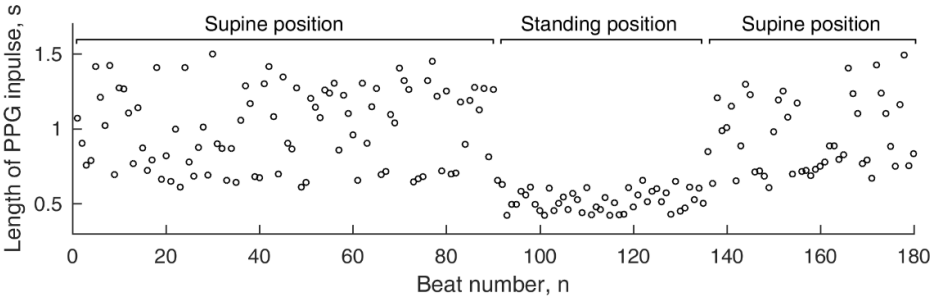

Figure 3.1. An example of simulated periods of PPG impulses

The amplitude variations of the modelled PPG signal *s(t)* (Figure 3.2) were similar to the real variations of a PPG signal amplitude during the orthostatic test (Figure 1.22 b).

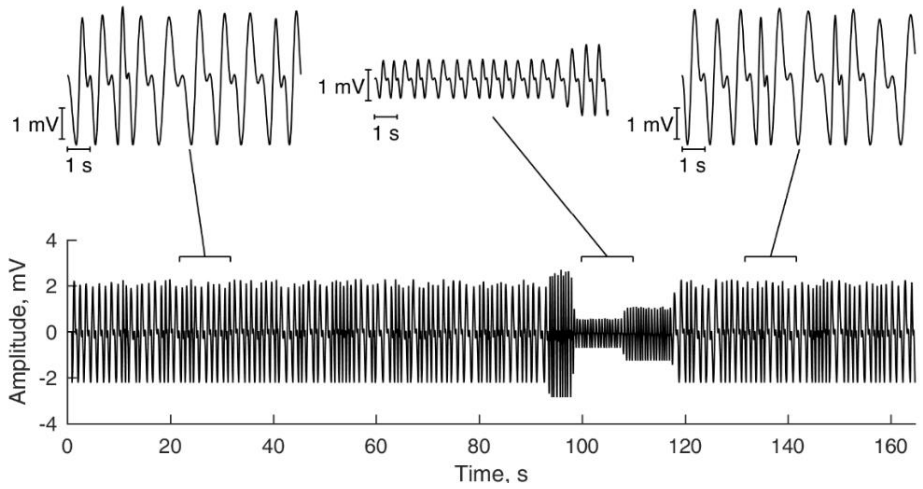

Figure 3.2. A modelled PPG signal

The ECG signal *u(t)* was modelled as a phase modulated signal with R wave peaks r_N (unit impulses). The RR interval and PPG peak-to-peak interval are almost equal. ECG R waves were modelled in the middle of PPG signal peak-to-peak intervals. PAT values are higher when the subject is lying (horizontal posture) and lower when standing (vertical posture). The modelled ECG *u(t)* signal:

$$u(t)=\begin{cases}1, & t=r_N\\ -1, & t=(r_N+r_{N+1})/2\\ 0, & t\neq r_N \;\&\; t\neq (r_N+r_{N+1})/2\end{cases} \tag{3.2}$$

where r_N represents ECG R wave locations.

The noise component *η(t)* was modelled using pink noise (also known as *1/f* noise). Pink noise has more low frequency components, therefore, has more power at low frequencies. The power spectral density of pink noise is inversely proportional to frequency and power spectrum falls of approximately 3 dB per octave.

$$S(f)=\frac{C_f}{|f|^{\alpha}} \tag{3.3}$$

where *S(f)* – power spectral density; C_f – constant; $0 < \alpha < 2$, γ is usually close to 1 ($\alpha = 0$ – white noise, $\alpha = 2$ – brown noise).

Pink noise has the same power distribution (equal energy) for each octave. For these reasons, pink noise is more similar to the artifacts of the PPG signal and is more appropriate to use than a standard white noise.

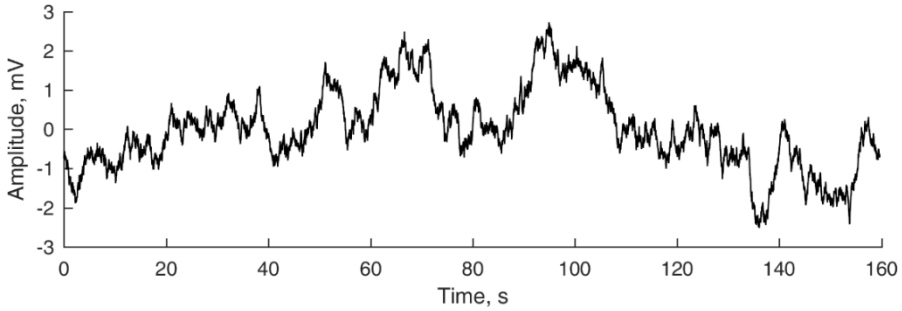

Figure 3.3. An example of simulated pink noise

The mathematical model of the acquired PPG signal and noise *sn(t)*:

$$sn(t) = s(t) + \eta(t) \tag{3.4}$$

where *s(t)* – modeled PPG signal; *η(t)* – noise component.

Five noise realizations *η(t)* (with different amplitudes) were added to the modelled PPG signal *s(t)* in order to get signal-to-noise ratios from 0 to 20 dB (Figure 3.4). 500 realizations of ECG *u(t)* and PPG *sn(t)* signals were modelled and used in the following analysis.

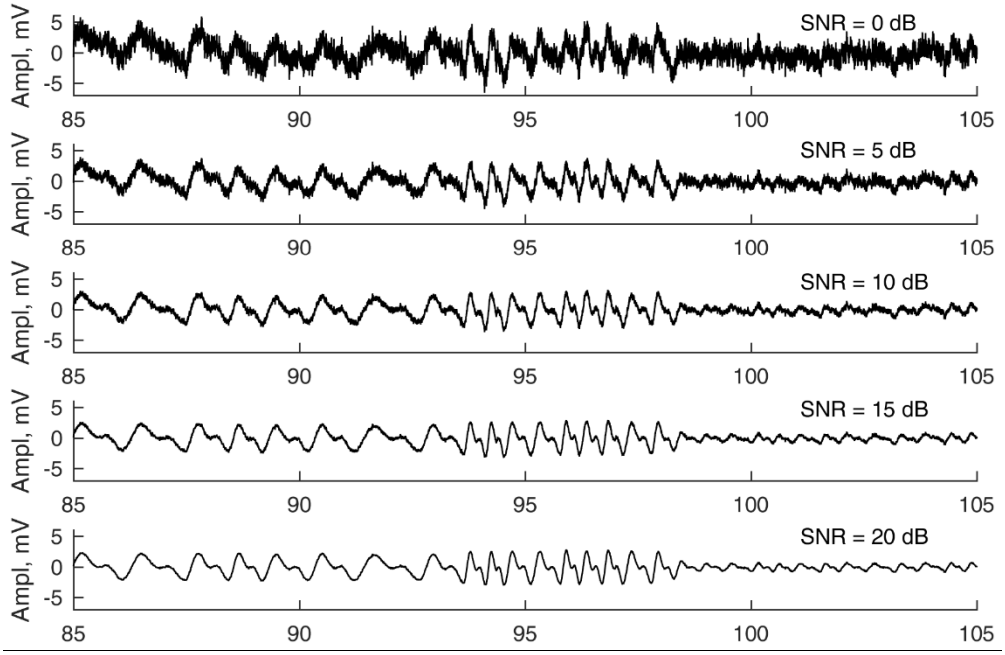

Figure 3.4. Modelled noisy PPG signals in a short range when SNR is from 0 to 20 dB

3.3. Experimental data

The experimental data consist of two different cardiovascular tests: body's position change – orthostatic test (Study No. 1) and thermal effect – thermal stress test (Study No. 2).

3.3.1. Study No. 1: orthostatic test

Subjects

The data was obtained from 14 healthy volunteers (6 females, 8 males) aged 20–29 years (Table 3.1). The subjects were instructed to avoid smoking and substances influencing the activity of the cardiovascular system (alcohol, caffeine, etc.) for 6 hours before the examination. The subjects were normotensive, non-obese, and were taking no medication for the duration of the study.

Table 3.1. Characteristics of the subjects

Subjects (n = 14)	
Age (year)	24.93 ± 2.81
Height (cm)	173.64 ± 8.82
Weight (kg)	68.36 ± 11.10
BMI* (kg/m^2)	22.55 ± 2.35

Values are mean ± standard deviation

*BMI – body mass index

Protocol

The database was recorded during an orthostatic test, according to the following protocol: 10 min in a stabilization period (resting in a supine position); 10 min in an early supine position; 5 min in a standing position; 5 min in a later supine position (Figure 3.5). Synchronous ECG, PPG, accelerometer (ACC), and BP signals were recorded in the early supine, standing, and later supine positions. The subjects changed body position (stand up and lie down) slowly (about 10 s) and the (stand up and lie down) intervals of moving were cut out and were not used for the following analysis.

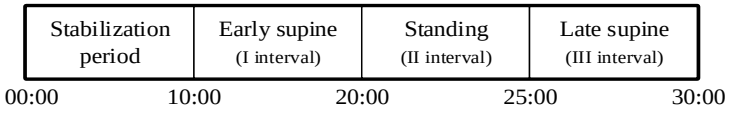

Figure 3.5. The protocol of the orthostatic test

Equipment

Data was acquired by using two synchronized physiological signal recording systems. ECG, PPG, and ACC signals were acquired by using the Cardioholter 6.2-8E78 (BMII, Lithuania) (Gargasas et al., 2012). Cardioholter 6.2-8E78 recorded the standard Einthoven leads of ECG (I, II, and III leads), the PPG signal from the right hand, left hand, and forehead (two channels in each sensor – red and near infrared), and ACC signals from three PPG sensors and from the device base. The sampling frequency of ECG was 500 Hz, PPG – 250 Hz, and

ACC – 50 Hz. Continuous arterial blood pressure was measured by using a non-invasive continuous finger blood pressure measurement and recording system Portapres Model-2 (Finapres Medical Systems B. V., Netherlands) (Finapres Medical Systems | Portapres, 2015). The sampling frequency of BP was 100 Hz.

3.3.2. Study No. 2: thermal stress test

A large study was carried out in conjunction with partners from the Lithuanian Sports University. The aim of the study was to determine how thermal stress (hyperthermia) caused in the evening using a sauna affects the mental activity at night and the functional efficiency of cognitive and neuro-muscular system as well as the change of stress hormones in the morning. The thermal stress test was a part of this large study and the total duration of the study was 2 years. Each subject conducted three experiments: experiment1, experiment2, and control1, each lasted about 54 hours and each experiment consisted of two parts, therefore, six experiments were done in total: experiment1 day1 (E1D1), experiment1 day2 (E1D2), experiment2 day1 (E2D1), experiment2 day2 (E2D2), control1 day1 (C1D1), and control1 day2 (C1D2). The time between experiments was not shorter than one week. In order to explore subjects in various conditions, all three experiments were carried out in different conditions; the protocols of experiments are shown in Figure 3.6. The main parts of experiments were:

- Detailed specialized testing – detailed specialized studies were carried out (blood sampling, performed testing of neuromuscular, potential of higher nerve centers and cognitive functions). These data were needed for the researchers from the Lithuanian Sports University and a detailed description will not be given.
- ANAM4 tests – Automated Neuropsychological Assessment Metrics (C-Shop, 2007) are cognitive memory and attention tests which were used to simulate a normal working day. These tests lasted 8 hours (8 series of 45 min with 15 min break).
- Thermal stress test – a thermal experiment in a sauna (protocol is described in detail below).
- Normal work day – a normal working day is considered to be 8 hours in a usual workplace.
- Sleep – 8 hours of sleep at home.

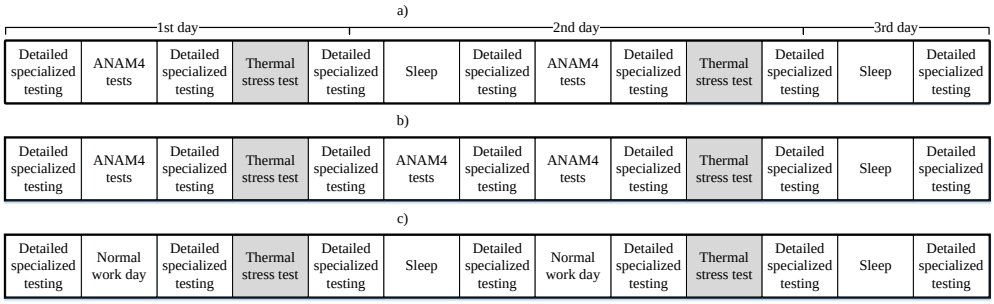

Figure 3.6. The protocols of three different thermal stress test experiments: experiment1 a); experiment2 b); and control1 c) (thermal stress test is accentuated)

The differences between the experiments: 1) the only difference between experiment1 and experiment2 is that the subject slept (8 hours) at night at home during experiment1, meanwhile, during experiment2 the subject solved ANAM4 tests all night (8 hours). 2) the only difference between experiment1 and control1 is that the subject solved ANAM4 tests all day during experiment1, meanwhile, during control1 the subject worked his usual work in the workplace (8 hours). There were no differences between the protocols of thermal stress test of different experiments.

The protocol of the study was quite long (six experiments – 54 hours each and in order to avoid additional disturbance, the study was carried out only on weekends), rigid, and complex. Moreover, the study may have caused discomfort or pain to the subjects, for example:

- Blood samples were taken seven times during one experiment;
- Subjects had to stay awake for 42 hours;
- ANAM4 tests were solved for 8 hours (it was difficult to remain vigilant at daytime and especially at night);
- Consumption of food and liquids was restricted during experiments;
- The thermal stress test in a sauna was a particularly high load and stress to the body; in some instances, after the last sauna session subjects presented with side effects, such as the contraction of limbs and facial muscles, complete physical exhaustion, or even anger.

For these reasons, it was difficult to find volunteers and only eight subjects participated in the 24 experiments (35 tests in total) of the study (detailed information is provided below). The implementation of the experiment was expensive and long, thus, each experiment could only be conducted once (it was not possible to repeat the experiment). Some experiments failed because the equipment was faulty or it was not possible to conduct the experiment for other reasons. The successfully performed experiments are presented in Table 3.2.

Table 3.2. Successfully accomplished experiments

	Experiment 1		Experiment 2		Control 1	
Subject	**Day 1**	**Day 2**	**Day 1**	**Day 2**	**Day 1**	**Day 2**
Subject No. 1	-	+	-	-	+	+
Subject No. 2	+	-	+	+	-	+
Subject No. 3	+	+	+	+	+	+
Subject No. 4	-	+	+	+	+	+
Subject No. 5	+	+	+	-	-	-
Subject No. 6	+	+	-	+	-	+
Subject No. 7	+	+	+	+	+	+
Subject No. 8	+	-	+	+	+	-
Total	6	6	6	6	5	6

"+" – successful experiments
"-" – unsuccessful experiments

Subjects

The data was obtained from 8 healthy male volunteers aged 22–35 years (Table 3.3).

Table 3.3. Characteristics of the subjects

Subject	Age (years)	Height (cm)	Weight (kg)	BMI* (kg/m^2)	BFP** (%)
Subject No. 1	28	183	69.7	20.8	12.3
Subject No. 2	35	183	82.0	24.5	14.8
Subject No. 3	26	187	80.1	22.9	13.8
Subject No. 4	22	180	93.0	28.7	21.8
Subject No. 5	23	189	78.0	21.8	10.0
Subject No. 6	24	210	128.0	29.0	22.0
Subject No. 7	24	186	79.0	22.8	13.4
Subject No. 8	23	177	71.0	22.7	11.0
Mean	25.6	186.9	85.1	24.2	14.9
SD	4.0	9.5	17.5	2.9	4.3

*BMI – body mass index
**BFP – body fat percentage

The subjects were non-smokers and were instructed to avoid strenuous exercise for 54 hours, food for 6 hours, and any stimulants (such as coffee, energy drinks, etc.) for 12 hours before the examination. The subjects were normotensive and were taking no medication for the duration of the study.

Protocol

The experiments of thermal stress were carried out at the same time of the day according the protocol shown in Figure 3.7. The ambient temperature in the sauna room was 80–90°C, relative humidity – 30%. Before and after the sauna sessions, the subjects sat (semi Fowler's position) in neutral temperature environment (25°C). Data was recorded at rest: interval I (Rest1) – before the first sauna session,

interval II (Rest2) – after the first sauna session, interval III (Rest3) – after the second sauna session, interval IV (Rest4) – after the third sauna session, interval V (Rest5) – after the fourth sauna session. Recorded intervals were 10 minutes in length.

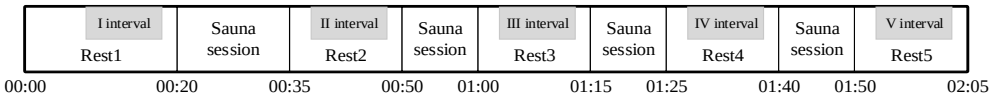

Figure 3.7. The protocol of the thermal stress test

Equipment

The data was acquired by using two synchronized physiological signal recording systems. ECG, PPG, ACC, and temperature signals were acquired by using the Nautilus1 (BMII, Lithuania). It recorded the standard Einthoven leads of ECG (I, II, and III leads), PPG from the right hand, forehead, and earlobe (two channels in each sensor – red and near infrared), ACC signals from the base of device, and temperatures of environment and chest skin. The sampling frequency of the ECG was 2 kHz, PPG – 1 kHz, ACC and temperature – 50 Hz. Continuous arterial blood pressure was acquired by using a non-invasive continuous finger blood pressure measurement and recording system Portapres Model-2 (Finapres Medical Systems B. V., Netherlands) (Finapres Medical Systems | Portapres, 2015). The sampling frequency of BP was 100 Hz.

3.4. Conclusions of the chapter

1. The modelled PPG signals are adequate for evaluating the method since they are based on direct change measurement of a real PPG waveform during orthostatic tests. Five realizations of pink noise were added to the modelled PPG signal and five signal-to-noise ratios (0–20 dB) were obtained.
2. The orthostatic test leads to many changes in the physiological process of the body and may be used to stimulate the autonomic nervous system. The orthostatic test experiment was conducted and the database (physiological signals) was collected from 14 subjects.
3. The thermal stress test causes a high physiological stress (hyperthermia) and can considerably change the physiological processes of the body, thus can be used to evaluate the behavior of the autonomic nervous system in very strong stress conditions. The thermal stress test experiment was performed and the unique database (physiological signals) was collected from 8 subjects.
4. Since the thermal stress test causes a very strong stress to the body, the study focused on young and healthy subjects. Due to the complexity of thermal stress test execution, the collected database is not large enough; the data was collected from a narrow age group and subjects of different physical training. In order to obtain more accurate data, the database must be expanded.

4. THE RESEARCH AND RESULTS

Algorithms (PAT estimation and IF extraction) described in Chapter 2 were tested using the databases (simulated and recorded signals) described in Chapter 3. Section 4.1 describes the results using simulated data, section 4.2 provides the results of experimental data: orthostatic and thermal stress tests. Conclusions of the chapter are provided in section 4.3.

4.1. Results using the simulated data

In order to evaluate the accuracy of the algorithms for estimating pulse arrival time, two statistical parameters were used: mean absolute difference (MAD) and root mean square error (RMSE):

$$MAD = \frac{1}{n}\sum_{i=1}^{n}\left|x_i - y_i\right| \tag{4.1}$$

$$RMSE = \sqrt{\frac{1}{n}\sum_{i=1}^{n}\left(x_i - y_i\right)^2} \tag{4.2}$$

where x_i are actual values; y_i – estimated values; n – sample size.

Three PAT estimation algorithms were compared:

- classical PAT estimation algorithm based on the maximum of the 1st PPG signal derivative – PATca (mostly used in literature);
- diastole-patching PAT estimation algorithm – PATdp (showed the best results in algorithm comparison, see Table 1.7);
- proposed PAT estimation algorithm – PATht, based on narrowband band-pass filtration, Hilbert transform, and instantaneous phase shift estimation.

MAD and RMSE show the accuracy of PAT estimation algorithms. All parameters were evaluated between clean and noisy (different SNR) PPG signals. The results of accuracy (MAD and RMSE) are presented in Figure 4.1. The algorithm is more accurate when the values of RMSE and MAD are lower and vice versa.

MAD and RMSE of the classical algorithm are considerably higher than the MAD and RMSE of the diastole-patching and proposed algorithm in all investigated SNR (0–20 dB). MAD and RMSE of PATdp and PATht are almost identical when SNR is from 10 to 20 dB (MAD – 6.25–13.63 ms, RMSE – 8.36–18.14 ms); however, when SNR is low (0 and 5 dB), PATht presents a lower MAD (28.52 and 18.81 ms) and RMSE (36.25 and 24.06 ms) than PATdp (MAD – 58.77 and 21.91 ms, RMSE – 114.80 and 40.14 ms).

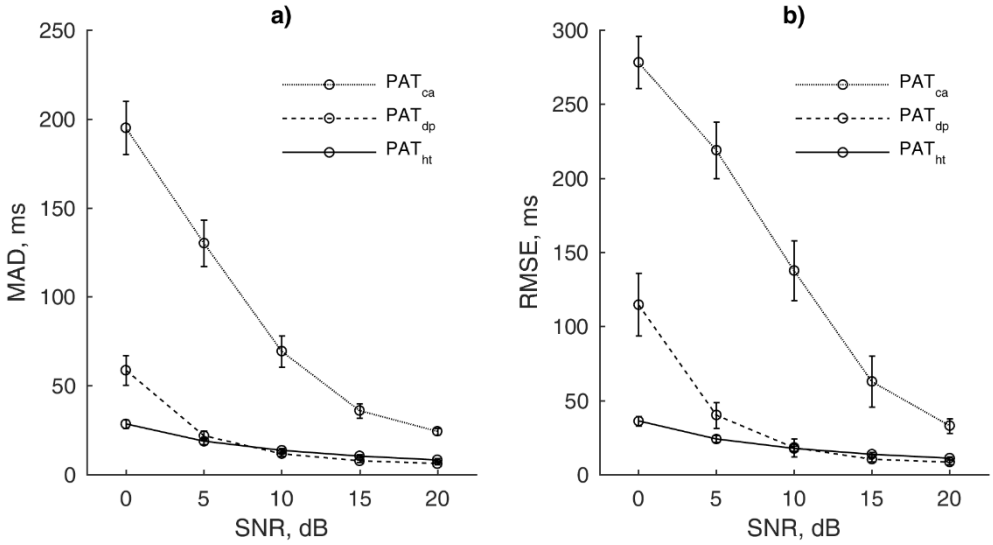

Figure 4.1. Accuracy evaluation: MAD a) and RMSE b) of the classical (PAT_{ca}) (dashed line), diastole-patching (PAT_{dp}) (dotted line), and PATht (PAT_{ht}) (line) PAT estimation algorithms

Discussion

The results indicate that the proposed algorithm for estimating pulse arrival time (PATht) is more accurate than the classical PAT estimation algorithm in all investigated SNRs (0–20 dB) as well as than the diastole-patching algorithm when SNRs are low (0–5 dB). When SNRs are 10–20 dB, the accuracy of PATht and PATdp is similar. Therefore, it can be concluded that the proposed PAT estimation algorithm (PATht) is better than the diastole-patching and classical PAT estimation algorithms when PPG signals are noisy.

4.2. Results using experimental signals

The results obtained using the experimental data consist of two parts: the results of the orthostatic test (section 4.2.1) and of the thermal stress test (section 4.2.2). Variability parameters (time-domain and frequency-domain) were used to investigate the proposed algorithms (PATht and IFe). When processing the data of the orthostatic test, the instantaneous frequency extraction algorithm first divided the physiological signals into three parts: lying (horizontal body position), standing (vertical body position), and lying. The IFe algorithm processed the signals of each interval separately and combined the IFs after extraction because the fundamental frequency is more expressed in a horizontal body position and the details of the signal are more prominent in a vertical body position. In order to avoid frequency (IF1 and IF2) switching, the frequencies of selected IMFs were assessed: the lower IMF was entitled IF1, higher IMF – IF2. For the thermal stress test, the IFe algorithm processed the entire signal (10 min in length) without dividing it into separate intervals.

4.2.1. Study No. 1: orthostatic test

The orthostatic test was carried out according to the methodology described in section 3.3.1. All parameters (R-R intervals, systolic and diastolic blood pressure, pulse arrival time, first and second instantaneous frequencies) were obtained using algorithms described in Chapter 2. Figure 4.2 shows the obtained parameter variation of one of the test subjects during the orthostatic test. It is visible that the variabilities of parameters are different in different body positions (laying and standing, or vertical and horizontal).

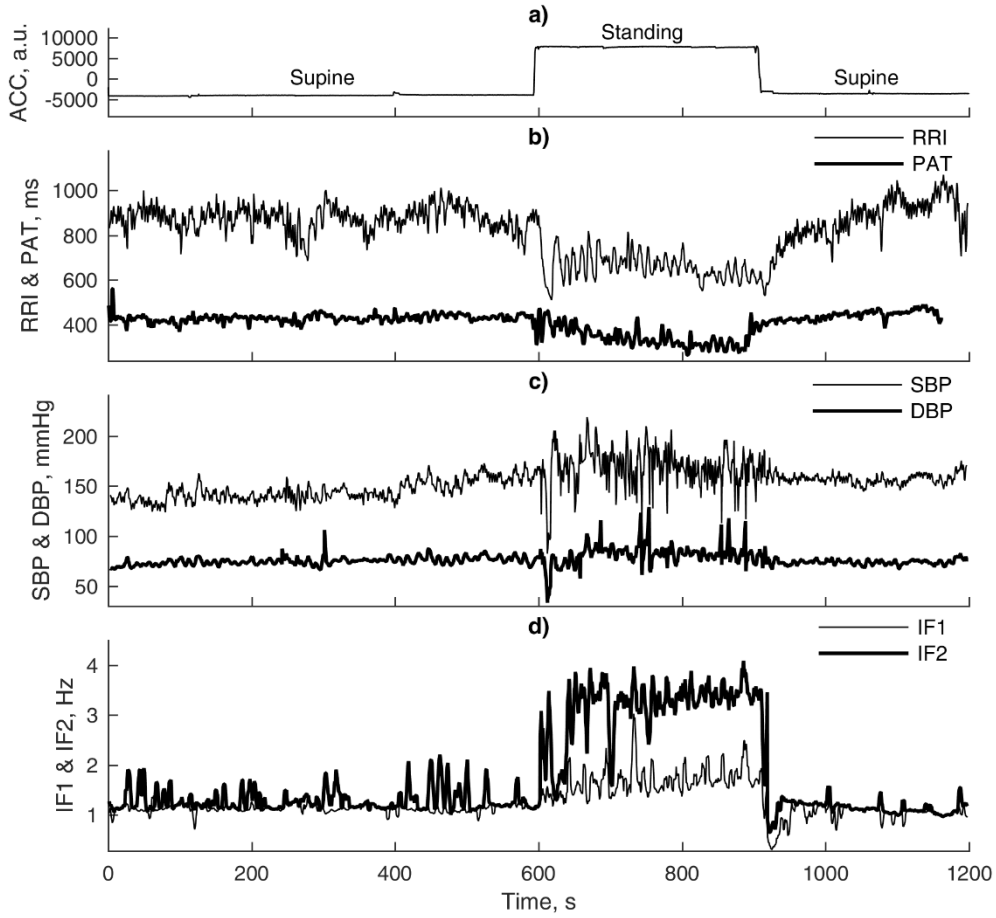

Figure 4.2. The recorded accelerometer signal and estimated parameters during the orthostatic test (one test subject): ACC a); RRI and PAT b); SBP and DBP c); IF1 and IF2 d)

Figure 4.3 shows the histograms of all detected, evaluated, estimated, or extracted parameters (R-R intervals, systolic and diastolic blood pressure, pulse arrival time, first and second instantaneous frequency) of one test subject during the orthostatic test. Figure 4.3 shows the scatter plot of RRI, SBP, DBP, PAT, and

IFs. RRI and PAT are shorter in interval II (standing) when compared with intervals I and III (laying). The opposite tendency is visible in SBP, DBP, and IF2. The values of BP and IF2 are higher in interval II (standing) than in intervals I and III (laying). The values of IF1 are more scattered than others and the intervals overlap. However, it is evident that the values of intervals I and III (laying) are lower. Figure 4.3 shows that there are differences between different body positions (laying – intervals I and III and standing – interval II) and these differences are visible in all parameters.

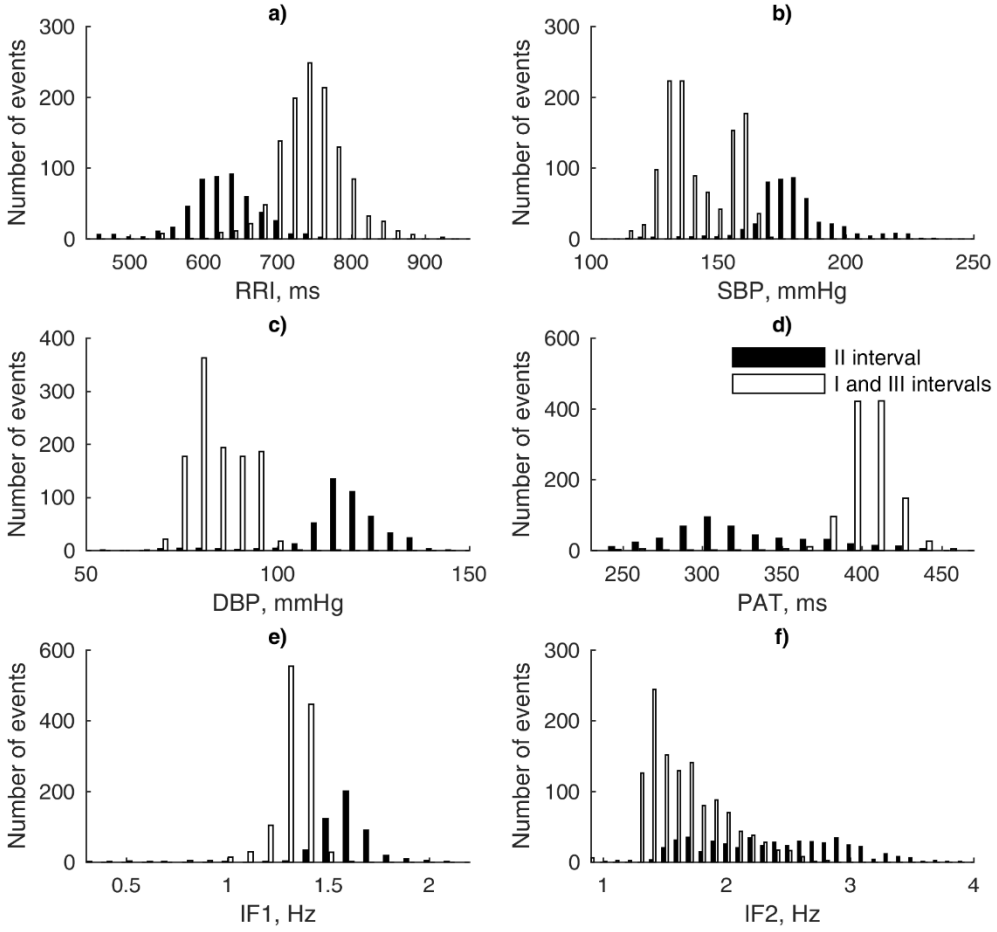

Figure 4.3. The histograms of RRI a), SBP b), DBP c), PAT d), IF1 e), and IF2 f) of intervals I, III and II of the orthostatic test (one test subject)

Time-domain analysis

The values of time-domain parameters (described in section 1.6.1) of R-R intervals, systolic and diastolic blood pressure, pulse arrival time, first and second instantaneous frequencies during the orthostatic test are presented in the appendix (Study No. 1: orthostatic test). Figure 4.4 summarizes the time-domain parameters

of RRI, SBP, DBP, PAT, IF1, and IF2 during the orthostatic test (in different body positions). The Wilcoxon statistical test shows significant differences ($p \leq 0.05$ and $p \leq 0.001$) between intervals I and II, and between II and III. SDNN of SBP, DBP, PAT, and IF1 show that the differences between supine-standing positions (interval I–II) and between standing-supine positions (interval II–III) are statistically significant ($p \leq 0.05$ or $p \leq 0.001$). SDNN of RRI is significantly different only between intervals II and III, meanwhile, the SDNN of IF2 shows significant differences between intervals I and II. RMSSD show that the differences between the supine and standing positions are statistically significant ($p \leq 0.05$ or $p \leq 0.001$) in SBP, DBP, PAT, and IF1. The changes in time-domain parameters between intervals I–II and II–III are presented in the appendix (Study No. 1: orthostatic test). All variability parameters are normalized by interval II (standing) of the orthostatic test:

$$X_{N\,\mathrm{int}} = \frac{X_{\mathrm{int}}}{X_2} \tag{4.3}$$

where X_{Nint} is normalized variability parameter of *int* interval number; *int* – an interval number of the orthostatic test (*int = 1, 2, 3*); X_{int} – variability parameter of *int* interval number; X_2 – variability parameter of the second orthostatic test interval.

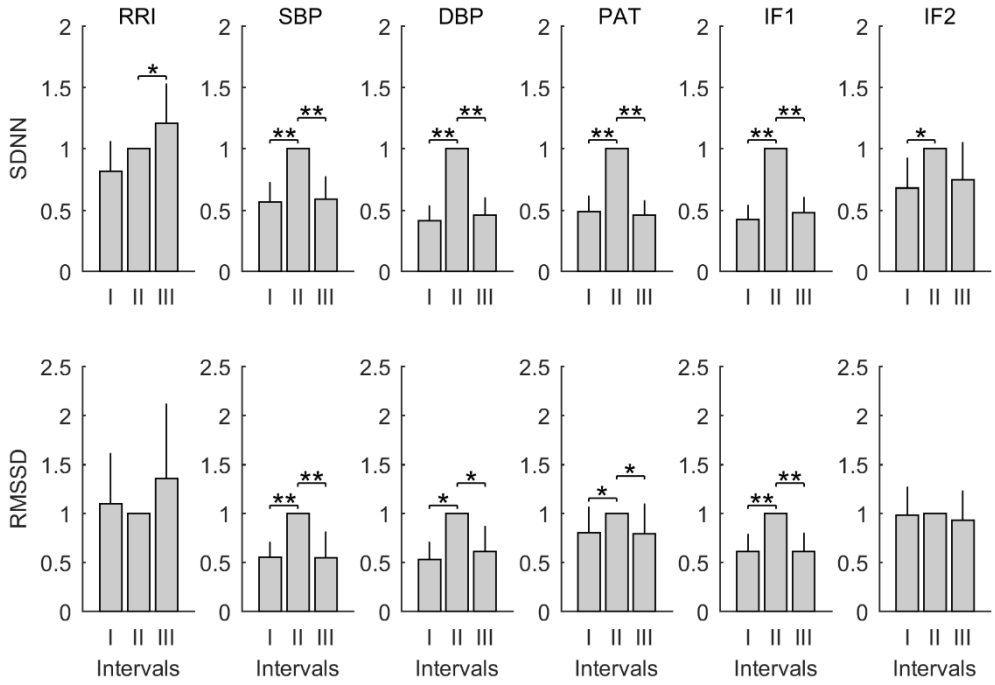

Figure 4.4. Time-domain parameters of RRI, SBP, DBP, PAT, IF1, and IF2 during the orthostatic test (data normalized by interval II). The results are presented as mean and SD. *p* – value (* – $p \leq 0.05$ and ** – $p \leq 0.001$) shows the statistically significant difference between intervals I–II and between intervals II–III

Mean absolute difference (MAD – defined in section 4.1) and Spearman correlation coefficient (r_S) between R-R intervals, systolic blood pressure, and diastolic blood pressure and pulse arrival time, first instantaneous frequency, and second instantaneous frequency of time-domain parameters (SDNN and RMSSD) are shown in Table 4.1. Two variables X_i and Y_i can be converted to ranks (rgX_i and rgY_i) and the Spearman correlation coefficient r_S is defined by:

$$r_S = \frac{\mathrm{cov}(rg_X, rg_Y)}{\sigma_{rg_X, rg_Y}} \tag{4.4}$$

where $cov(rg_X,rg_Y)$ is the covariance of the rank variables; σ_{rgx} and σ_{rgy} – the standard deviations of the rank variables.

r_S of SBP-IF1, DBP-PAT, and DBP-IF1 are high in SDNN (0.714–0.786) and RRI-IF1, RRI-IF2, SBP-PAT, SBP-IF1, and DBP-IF1 in RMSSD (0.714–0.786). High accuracy (low MAD) is present between BP and PAT, IF1, and IF2 in SDNN (0.081–0.219) and in RMSSD (0.191–0.276).

Table 4.1. Spearman correlation coefficient r_S and mean absolute difference of time-domain parameters ($r_S \geq 0.700$ and MAD ≤ 0.300 marked)

		SDNN		
		PAT	IF1	IF2
r_S	RRI	0.643±0.234	0.679±0.249	0.607±0.213
	SBP	0.679±0.249	0.750±0.259	0.571±0.182
	DBP	0.714±0.257	0.786±0.257	0.607±0.213
MAD	RRI	0.408±0.290	0.406±0.308	0.313±0.299
	SBP	0.126±0.065	0.110±0.084	0.160±0.087
	DBP	0.086±0.051	0.081±0.049	0.219±0.120
		RMSSD		
		PAT	IF1	IF2
r_S	RRI	0.643±0.234	0.750±0.259	0.786±0.259
	SBP	0.714±0.259	0.750±0.259	0.679±0.249
	DBP	0.643±0.234	0.786±0.257	0.643±0.234
MAD	RRI	0.774±0.908	0.843±1.028	0.855±0.934
	SBP	0.191±0.182	0.206±0.166	0.260±0.098
	DBP	0.231±0.197	0.276±0.175	0.239±0.122

Figure 4.5–4.7 show the scatter plots of time-domain parameters of R-R intervals, systolic and diastolic blood pressure, pulse arrival time, first and second instantaneous frequencies. Linear regression curves (between RRI-PAT, RRI-IF1, RRI-IF2, SBP-PAT, SBP-IF1, SBP-IF2, DBP-PAT, DBP-IF1, and DBP-IF2) show how one parameter depends on another.

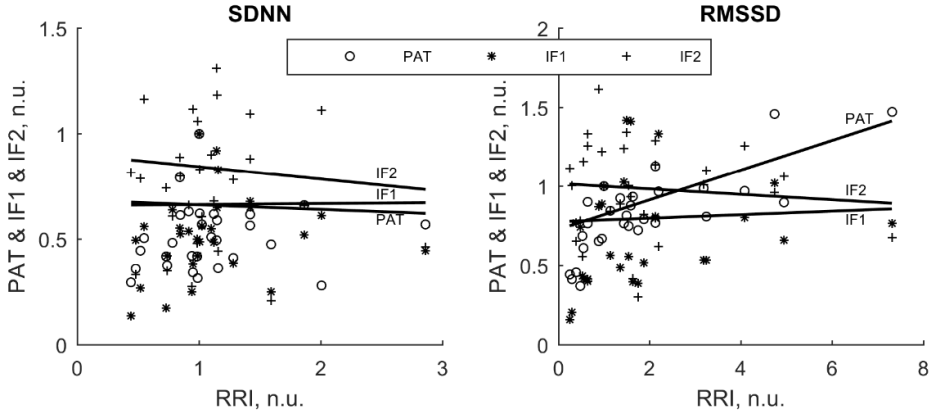

Figure 4.5. Scatter plots of time-domain parameters of RRI, PAT, IF1, and IF2. Regression lines are between RRI-PAT, RRI-IF1, and RRI-IF2

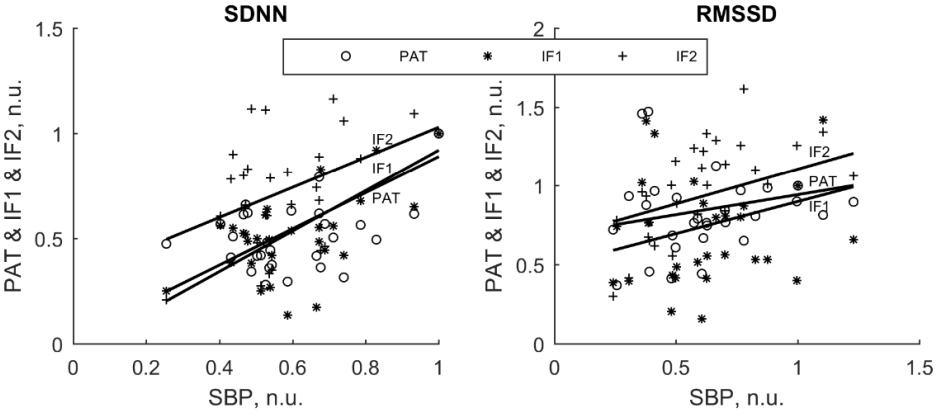

Figure 4.6. Scatter plots of time-domain parameters of SBP, PAT, IF1, and IF2. Regression lines are between SBP-PAT, SBP-IF1, and SBP-IF2

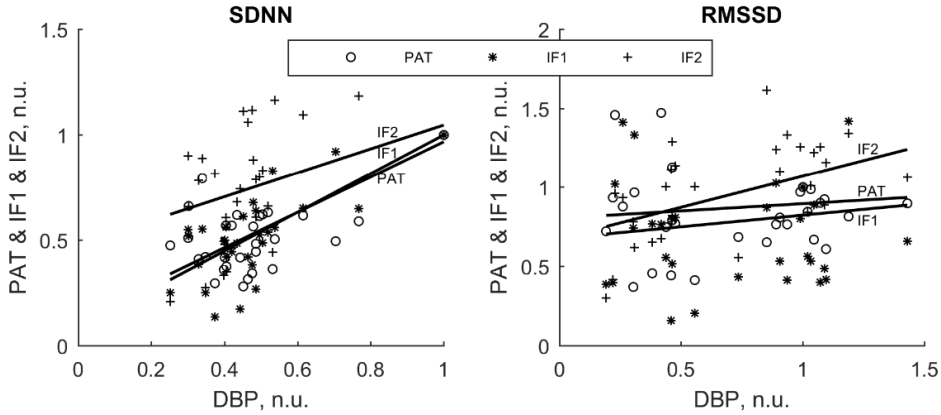

Figure 4.7. Scatter plots of time-domain parameters of DBP, PAT, IF1, and IF2. Regression lines are between DBP-PAT, DBP-IF1, and DBP-IF2

Table 4.2 shows the coefficient of determination (CD) between RRI, SBP, and DBP and PAT, IF1, and IF2 of time-domain parameters (SDNN and RMSSD). CD indicates how the changes of a dependent variable (y) are explained by the changes of an independent variable (x). Therefore, CD shows the level of linear relationship between two variables:

$$CD = r^2 \tag{4.5}$$

where r is a correlation coefficient.

SBP-IF1 and DBP-IF1 shows higher CD only in SDNN (0.613 and 0.730).

Table 4.2. The coefficient of determination of time-domain parameters (CD ≥ 0.700 marked)

	SDNN			RMSSD		
	PAT	IF1	IF2	PAT	IF1	IF2
RRI	0.022	0.048	0.012	0.146	0.031	0.009
SBP	0.466	0.613	0.369	0.239	0.186	0.152
DBP	0.546	0.730	0.388	0.039	0.016	0.165

Frequency-domain analysis

The values of frequency-domain parameters (described in section 1.6.2) of R-R intervals, systolic and diastolic blood pressure, pulse arrival time, first and second instantaneous frequency during the orthostatic test are presented in the appendix (Study No. 1: orthostatic test). Figure 4.8 summarizes the frequency-domain parameters of RRI, SBP, DBP, PAT, IF1, and IF2 during the orthostatic test (in different body positions). The Wilcoxon statistical test indicates significant differences ($p \leq 0.05$ and $p \leq 0.001$) between intervals I and II, and between intervals II and III.

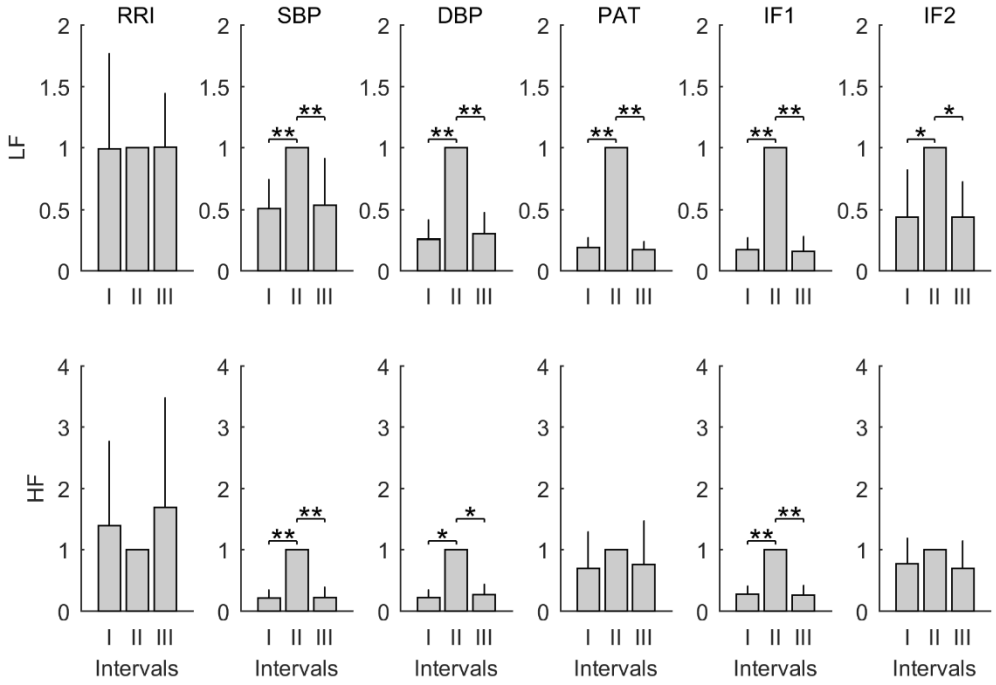

Figure 4.8. Frequency-domain parameters of RRI, SBP, DBP, PAT, IF1, and IF2 during the orthostatic test (data normalized by interval II). The results are presented as mean and SD. p – value (* – $p \leq 0.05$ and ** – $p \leq 0.001$) shows statistically significant difference between intervals I–II and between intervals II–III

The differences in the LF range of SBP, DBP, PAT, IF1, and IF1 are statistically significant between the supine and standing positions ($p \leq 0.05$ or $p \leq 0.001$). Significant differences ($p \leq 0.05$ or $p \leq 0.001$) between supine and standing positions in the HF range are in SBP, DBP, and IF1 (between intervals I–II and intervals II–III). The changes of frequency-domain parameters between intervals I–II and II–III (data normalized by interval II (standing) (defined in section 4.3) are presented in the appendix (Study No. 1: orthostatic test).

Mean absolute difference (MAD) and Spearman correlation coefficient (r_S) between RRI, SBP, and DBP and PAT, IF1, and IF2 of frequency-domain parameters (LF and HF) are shown in Table 4.5. r_S of RRI-IF2, SBP-PAT, DBP-PAT, DBP-IF1, and DBP-IF2 are high in LF (0.714–0.857) and RRI-IF1, RRI-IF2, SBP-PAT, SBP-IF1, and SBP-IF2 in HF (0.714–0.893). High accuracy (low MAD) is present between BP and PAT, IF1, and IF2 in LF (0.149–0.242) and in SBP-IF1 in HF (0.172).

Table 4.3. Spearman correlation coefficient and mean absolute difference of frequency-domain parameters ($r_S \geq 0.700$ and MAD ≤ 0.300 marked)

		LF		
		PAT	IF1	IF2
r_S	RRI	0.643±0.234	0.607±0.213	0.857±0.234
	SBP	0.750±0.259	0.679±0.247	0.643±0.234
	DBP	0.714±0.257	0.750±0.259	0.750±0.259
MAD	RRI	0.778±0.651	0.796±0.687	0.642±0.589
	SBP	0.236±0.184	0.227±0.174	0.242±0.082
	DBP	0.175±0.177	0.149±0.154	0.251±0.157
		HF		
		PAT	IF1	IF2
r_S	RRI	0.679±0.249	0.786±0.259	0.821±0.249
	SBP	0.714±0.259	0.893±0.213	0.714±0.259
	DBP	0.679±0.249	0.679±0.249	0.643±0.234
MAD	RRI	1.969±2.450	2.177±2.630	2.245±2.623
	SBP	0.429±0.333	0.172±0.225	0.395±0.339
	DBP	0.506±0.413	0.388±0.334	0.405±0.325

Figure 4.9–4.11 show the scatter plots of frequency-domain parameters of R-R intervals, systolic blood pressure, and diastolic blood pressure and pulse arrival time, first and second instantaneous frequencies. Linear regression curves (between RRI-PAT, RRI-IF1, RRI-IF2, SBP-PAT, SBP-IF1, SBP-IF2, DBP-PAT, DBP-IF1, and DBP-IF2) show how one parameter depends on another.

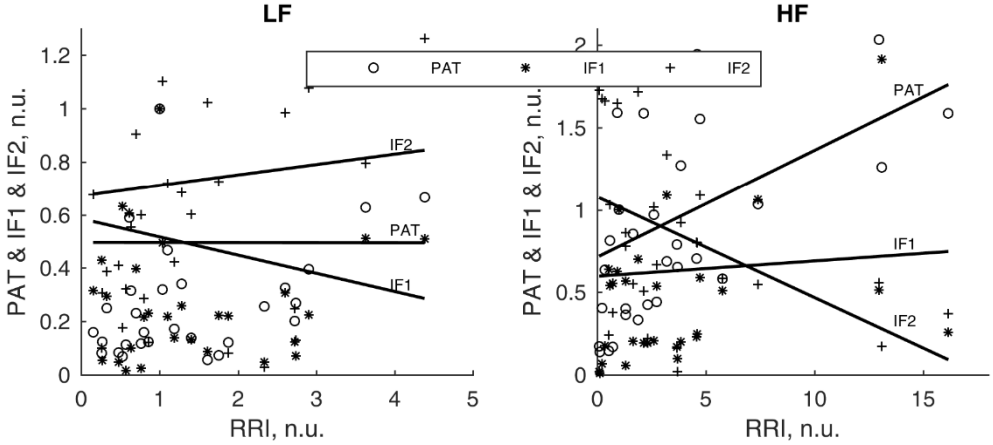

Figure 4.9. Scatter plots of frequency-domain parameters of RRI, PAT, IF1, and IF2. Regression lines are between RRI-PAT, RRI-IF1, and RRI-IF2

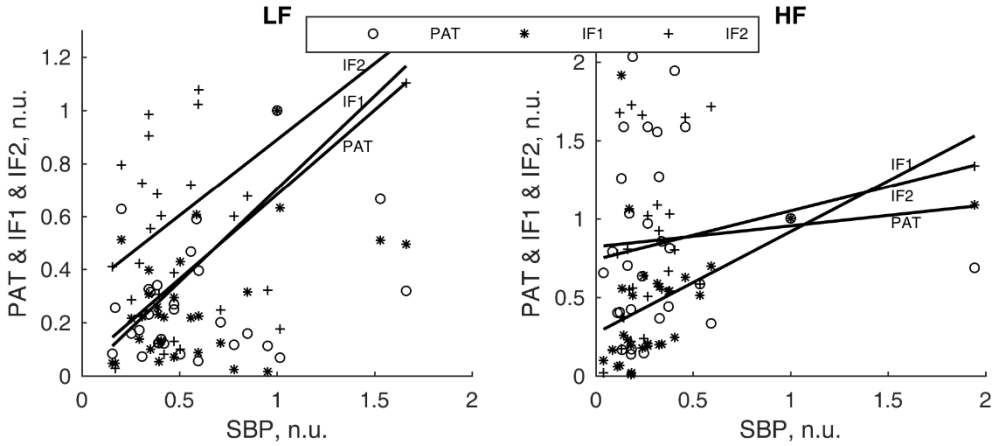

Figure 4.10. Scatter plots of time-domain parameters of SBP, PAT, IF1, and IF2. Regression lines are between SBP-PAT, SBP-IF1, and SBP-IF2

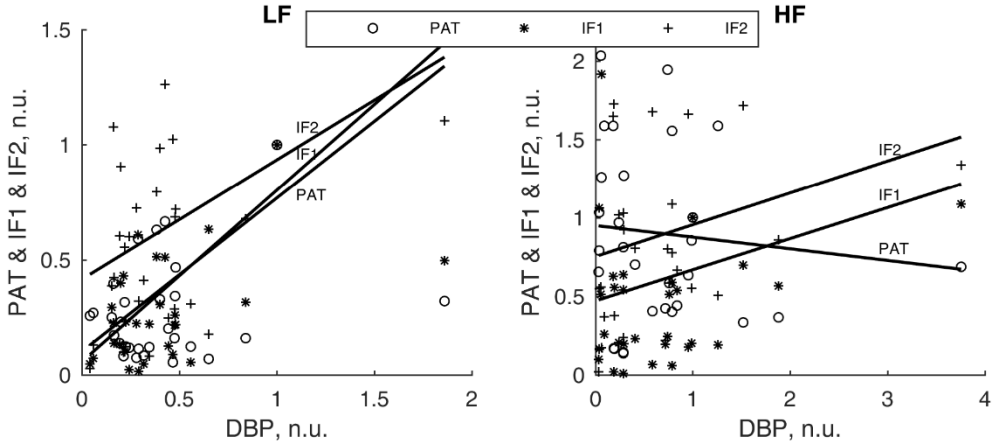

Figure 4.11. Scatter plots of time-domain parameters of DBP, PAT, IF1, and IF2. Regression lines are between DBP-PAT, DBP-IF1, and DBP-IF2

Table 4.4 shows the coefficient of determination (CD) between RRI, SBP, and DBP and PAT, IF1, and IF2 of frequency-domain parameters (LF and HF). SBP-IF1 and DBP-IF1 show an average CD in SDNN (0.472 and 0.557) and SBP-IF1 in RMSSD (0.490).

Table 4.4. Coefficients of determination of frequency-domain parameters

	LF			HF		
	PAT	IF1	IF2	PAT	IF1	IF2
RRI	0.034	0.003	0.042	0.154	0.000	0.323
SBP	0.312	0.472	0.359	0.081	0.490	0.186
DBP	0.422	0.557	0.323	0.000	0.215	0.126

Discussion

The results show that the variability of pulse arrival time as well as first and second instantaneous frequencies are related to the variability of heart rate and blood pressure (Figure 4.4–4.11 and Table 4.2–4.4). The variability of PAT, IF1, and IF2 indicate the same tendencies as the variability of SBP and DBP. This is visible when the variability decreases in intervals I and III (supine – horizontal posture) compared with interval II (standing – vertical posture) in the time-domain and frequency-domain parameters (SDNN, RMSSD, LF, and HF). The results reveal that the differences between supine and standing positions are statistically significant ($p \leq 0.05$ or $p \leq 0.001$). These findings confirm that rhythmic fluctuations in blood pressure are notable at rest, meanwhile, BPV increases in orthostasis (Mukai, Hayano, 1995; Zhang et al., 1998).

The results also show that the Spearman correlation coefficients are high between SBP-PAT, SBP-IF1, DBP-PAT, and DBP-IF1 in SDNN, RRI-IF1, RRI-IF2, SBP-IF1, and DBP-IF1 in RMSSD, RRI-IF2, SBP-PAT, DBP-IF1, and DBP-IF2 LF, RRI-IF1, RRI-IF2, and SBP-IF1 in HF. Mean absolute differences are low between SBP-PAT, SBP-IF1, DBP-PAT, and DBP-IF1 in SDNN, SBP-PAT, SBP-IF1, DBP-PAT and DBP-IF2 in RMSSD, SBP-PAT, SBP-IF1, SBP-IF2, DBP-PAT, DBP-IF1, and DBP-IF2 in LF, SBP-PAT, SBP-IF1, SBP-IF2, DBP-IF1, and DBP-IF2 in HF. Therefore, IF1 better reflects SBP and DBP (than PAT and IF2) and has a lower MAD. Meanwhile, IF2 better reflects RRI and has a lower MAD as well. The variability of RRI is higher when a person is lying (horizontal posture) and lower when standing (vertical posture). However, the variability of SBP, DBP, PAT, IF1, and IF2 is higher when a person is standing and lower when lying. This is because arterial pressure receptors (baroreceptors) send afferent impulses to the brain at a rate that depends on the instantaneous BP level and on the rate of BP change. This way, the central nervous system gets information about the actual level of arterial BP and adjusts its output along the efferent sympathetic and vagal or parasympathetic nerves accordingly. An increased output along the vagal nerves decreases HR and has therefore a depressor effect. Conversely, the primary effect of an increased sympathetic output is a rise in pressure (De Boer, 1985).

Previous studies have shown that pulse arrival time is related to blood pressure (Ochiai et al., 1999; Chen et al., 2000; Wibmer et al., 2014). The results of the study show that instantaneous frequencies extracted from a PPG signal are related to PAT, therefore, IF is related to blood pressure as well.

On the other hand, the database was limited; 14 young and healthy subjects were investigated. In order to get more accurate trends and interrelations between HR, BP, PAT, and IF more comprehensive investigation and a larger database is required. The database should be expanded by including more data from volunteers of different age groups and in various physical states. The results should be analyzed and compared with regard to sex, age, and physical state.

4.2.2. **Study No. 2: thermal stress test**

The thermal stress test was carried out according to the methodology described in section 3.3.2. All parameters (R-R intervals, systolic and diastolic blood pressure, pulse arrival time, first and second instantaneous frequencies) were obtained using algorithms described in Chapter 2.

Figure 4.12 shows an example of RRI, SBP, DBP, PAT, IF1, and IF2 at five rest intervals of experiments E1D1. The results are expressed as box plots with a median (line inside box), 25% and 75% quartiles (box), range (whiskers) and outliers (plus). The Wilcoxon statistical test reveals significant differences ($p \leq 0.05$) between interval I and other intervals (II, III, IV, and V). Other results of the experiments (E1D2, E2D1, E2D2, C1D1, and C1D2) are presented in the appendix (Study No. 2: thermal stress test).

The results show that the statistically significant differences ($p \leq 0.05$) between interval I and other intervals (intervals II, III, IV, and V) are only in RRI, SBP, and DBP. Statistically significant differences can be seen in IF1 in intervals II, III, and IV, and in IF2 in interval V.

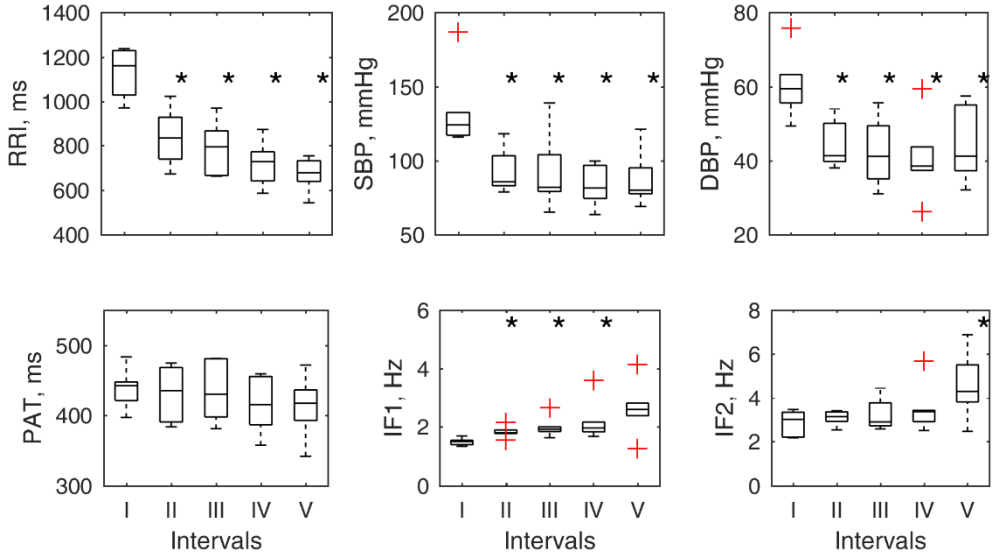

Figure 4.12. Means of RRI, SBP, DBP, PAT, IF1, and IF2 of all subjects of experiment E1D1. * – statistically significant difference ($p \leq 0.05$) between a particular interval and interval I

Time-domain analysis

The values of time-domain parameters (described in section 1.6.1) of R-R intervals, systolic and diastolic blood pressure, pulse arrival time, first and second instantaneous frequencies during thermal stress test are presented in the appendix (Study No. 2: thermal stress test). Figure 4.13–4.18 summarize the normalized curves of RRI, SBP, DBP, PAT, IF1, and IF2 of time-domain parameters (SDNN and RMSSD). The changes between the interval of thermal

stress of time-domain parameters are presented in the appendix (Study No. 2: thermal stress test).

All variability parameters are normalized by interval I of the thermal stress test:

$$X_{N\,\mathrm{int}} = \frac{X_{\mathrm{int}}}{X_1} \tag{4.6}$$

where *int* is an interval number of the thermal stress test (*int = 1, 2, 3, 4, 5*); X_{Nint} – normalized variability parameter of *int* interval number; X_{int} – variability parameter of *int* interval number; X_1 – variability parameter of the first thermal stress test interval.

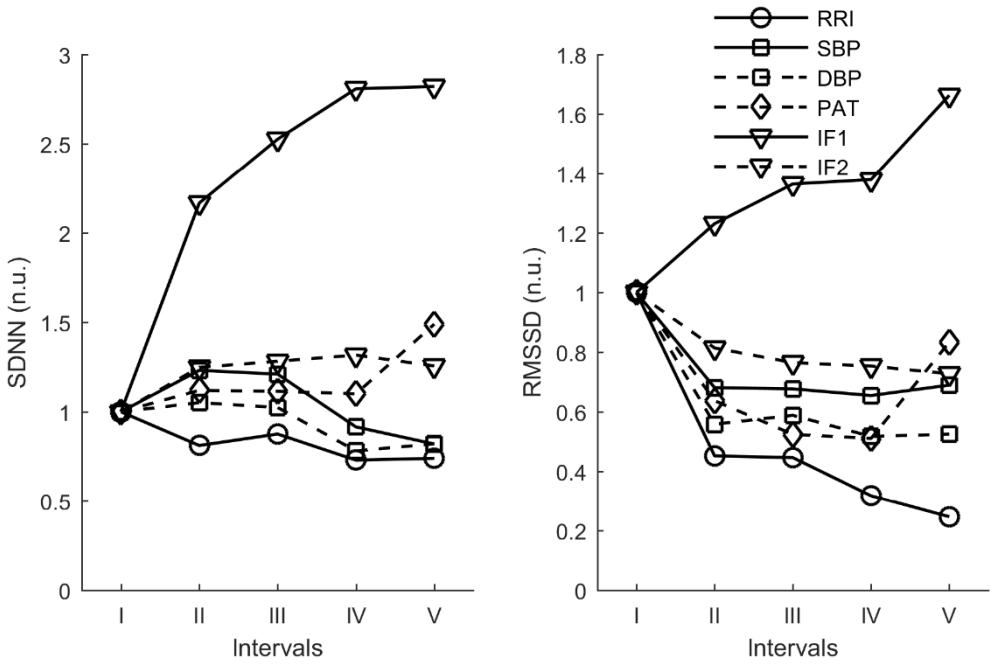

Figure 4.13. Curves of time-domain parameters of RRI, SBP, DBP, PAT, IF1, and IF2 during the thermal stress test (experiment E1D1)

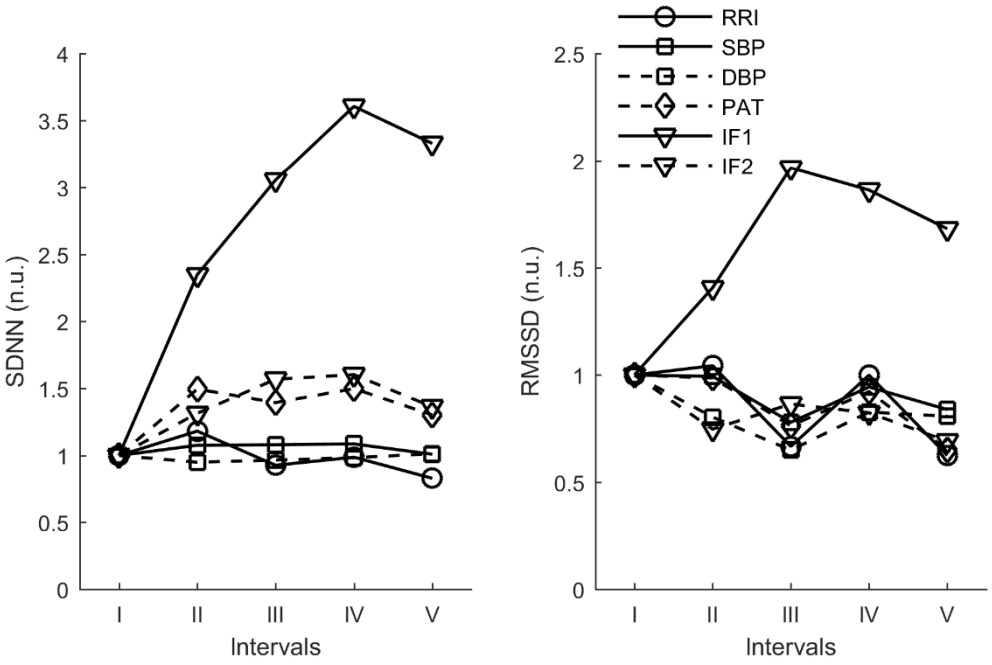

Figure 4.14. Curves of time-domain parameters of RRI, SBP, DBP, PAT, IF1, and IF2 during the thermal stress test (experiment E1D2)

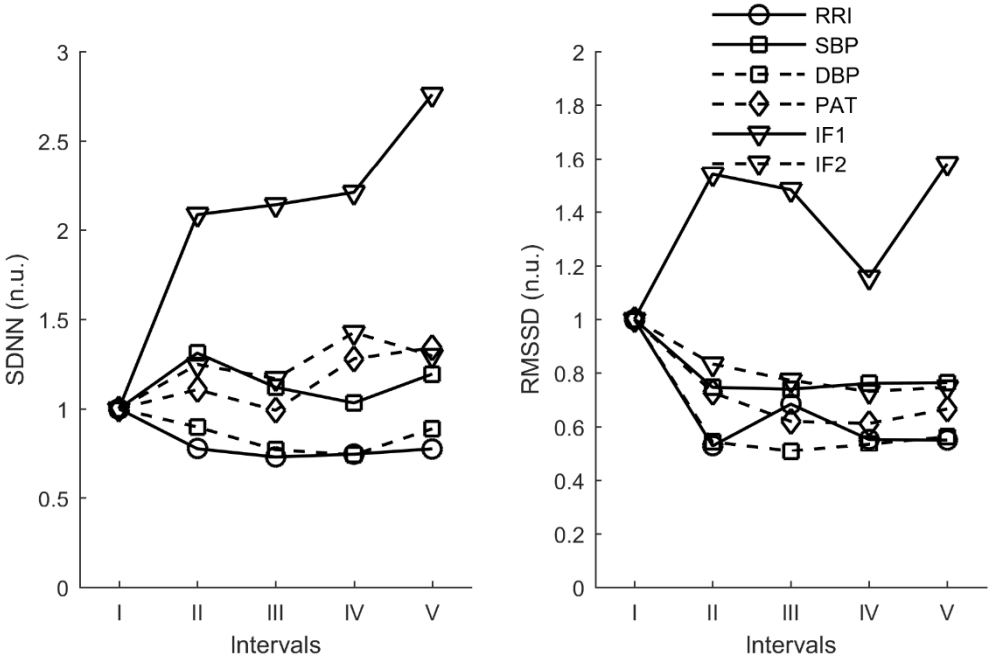

Figure 4.15. Curves of time-domain parameters of RRI, SBP, DBP, PAT, IF1, and IF2 during the thermal stress test (experiment E2D1)

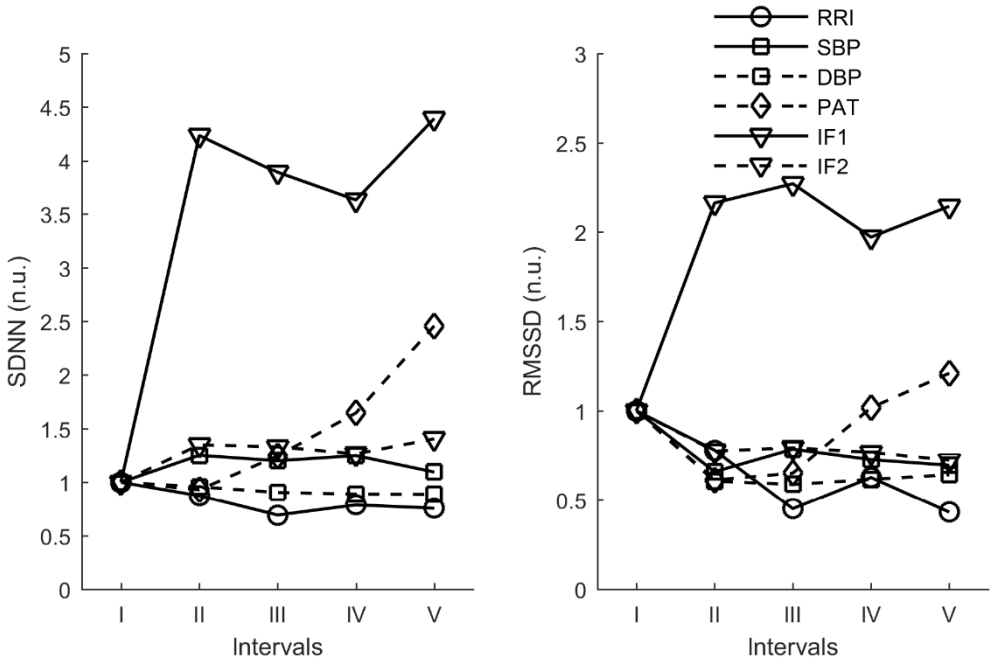

Figure 4.16. Curves of time-domain parameters of RRI, SBP, DBP, PAT, IF1, and IF2 during the thermal stress test (experiment E2D2)

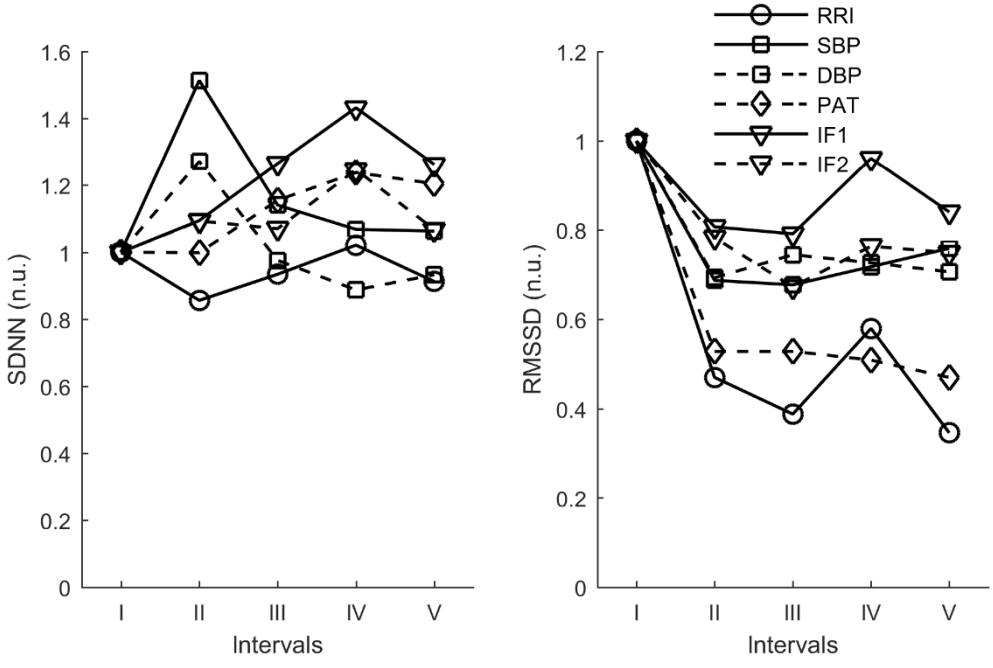

Figure 4.17. Curves of time-domain parameters of RRI, SBP, DBP, PAT, IF1, and IF2 during the thermal stress test (experiment C1D1)

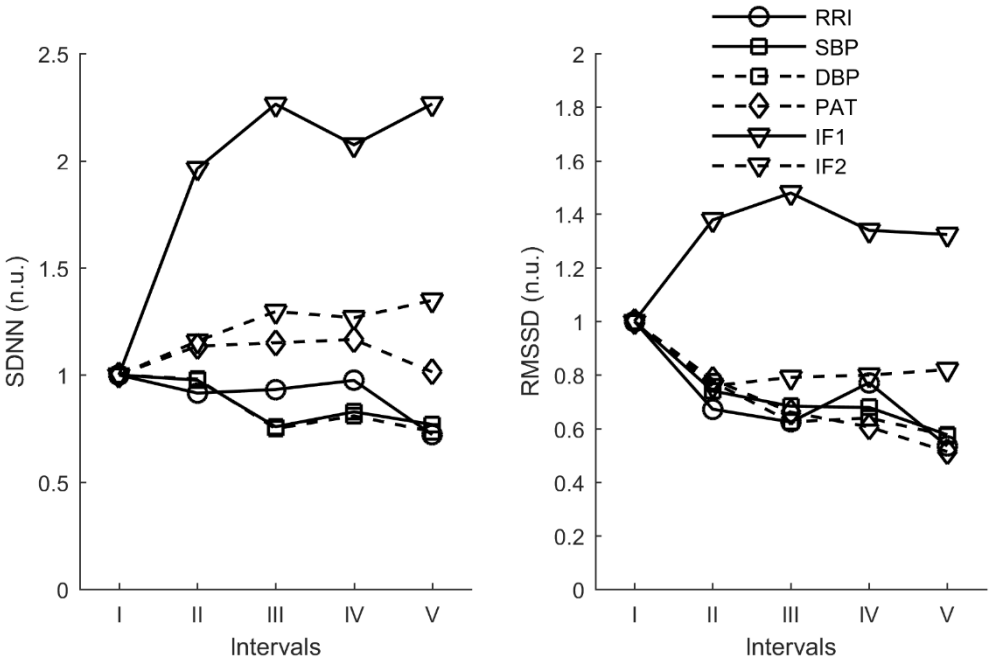

Figure 4.18. Curves of time-domain parameters of RRI, SBP, DBP, PAT, IF1, and IF2 during the thermal stress test (experiment C1D2)

Table 4.5–4.7 show the Spearman correlation coefficient of time-domain parameters between two groups of variability curves: 1) R-R intervals, systolic blood pressure, and diastolic blood pressure 2) pulse arrival time, first instantaneous frequency, and second instantaneous frequency. The results show that: PAT best reflects RRI in SDNN and RMSSD (0.563 and 0.665, respectively), PAT best reflects the SBP in SDNN and RMSSD (0.542 and 0.535 respectively), IF1 best reflects the DBP in SDNN (0.460) and PAT in RMSSD (0.622). Therefore, the Spearman correlation coefficients are poor.

Table 4.5. Spearman correlation coefficients of time-domain parameters of R-R intervals ($r_S \geq 0.700$ marked)

	SDNN			RMSSD		
	PAT	IF1	IF2	PAT	IF1	IF2
E1D1	0.650±0.197	0.533±0.320	0.517±0.343	0.767±0.266	0.200±0.126	0.450±0.302
E1D2	0.600±0.290	0.300±0.228	0.600±0.253	0.633±0.418	0.250±0.315	0.450±0.266
E2D1	0.575±0.287	0.450±0.342	0.475±0.222	0.750±0.332	0.650±0.387	0.625±0.250
E2D2	0.550±0.387	0.350±0.289	0.425±0.275	0.600±0.424	0.600±0.294	0.675±0.206
C1D1	0.520±0.402	0.400±0.255	0.280±0.268	0.740±0.305	0.440±0.378	0.400±0.381
C1D2	0.483±0.436	0.500±0.303	0.683±0.264	0.500±0.290	0.417±0.313	0.583±0.397
Mean	0.563±0.333	0.422±0.290	0.497±0.271	0.665±0.339	0.426±0.302	0.531±0.300

Table 4.6. Spearman correlation coefficients of time-domain parameters of systolic blood pressure ($r_S \geq 0.700$ marked)

	SDNN			RMSSD		
	PAT	IF1	IF2	PAT	IF1	IF2
E1D1	0.783±0.271	0.400±0.329	0.367±0.361	0.467±0.294	0.283±0.306	0.450±0.302
E1D2	0.567±0.378	0.617±0.204	0.417±0.325	0.500±0.228	0.433±0.250	0.383±0.293
E2D1	0.525±0.287	0.600±0.346	0.650±0.311	0.600±0.408	0.175±0.206	0.325±0.222
E2D2	0.650±0.100	0.475±0.386	0.375±0.310	0.425±0.222	0.550±0.173	0.450±0.311
C1D1	0.460±0.313	0.460±0.182	0.620±0.277	0.500±0.387	0.620±0.217	0.660±0.152
C1D2	0.267±0.137	0.400±0.268	0.317±0.293	0.717±0.240	0.417±0.349	0.417±0.271
Mean	0.542±0.248	0.492±0.286	0.458±0.313	0.535±0.297	0.413±0.250	0.448±0.259

Table 4.7. Spearman correlation coefficients of time-domain parameters of diastolic blood pressure ($r_S \geq 0.700$ marked)

	SDNN			RMSSD		
	PAT	IF1	IF2	PAT	IF1	IF2
E1D1	0.483±0.232	0.467±0.327	0.533±0.320	0.700±0.352	0.300±0.167	0.383±0.183
E1D2	0.600±0.369	0.583±0.194	0.467±0.350	0.667±0.121	0.433±0.280	0.417±0.366
E2D1	0.375±0.222	0.525±0.263	0.475±0.350	0.725±0.310	0.400±0.200	0.500±0.245
E2D2	0.175±0.287	0.475±0.222	0.400±0.294	0.550±0.173	0.575±0.395	0.675±0.386
C1D1	0.440±0.288	0.360±0.152	0.400±0.255	0.420±0.277	0.400±0.200	0.520±0.402
C1D2	0.600±0.276	0.350±0.243	0.267±0.186	0.667±0.314	0.300±0.261	0.233±0.242
Mean	0.446±0.279	0.460±0.234	0.424±0.293	0.622±0.258	0.401±0.251	0.455±0.304

Table 4.8–4.10 show the mean absolute difference of time-domain parameters between two groups of variability curves: 1) R-R intervals, systolic blood pressure, and diastolic blood pressure; 2) pulse arrival time, first instantaneous frequency, and second instantaneous frequency. The results show that PAT accurately reflects RRI in SDNN and RMSSD (0.430 and 0.311, respectively). Meanwhile, IF2 accurately reflects SBP and DBP in SDNN and RMSSD (SBP – 0.449 and 0.191, DBP – 0.454 and 0.221).

Table 4.8. Mean absolute difference of time-domain parameters of RRI (MAD ≤ 0.300 marked)

	SDNN			RMSSD		
	PAT	IF1	IF2	PAT	IF1	IF2
E1D1	0.421±0.332	1.496±1.129	0.508±0.325	0.269±0.291	0.860±0.463	0.336±0.114
E1D2	0.363±0.164	2.007±1.700	0.631±0.368	0.323±0.157	1.223±0.777	0.490±0.398
E2D1	0.422±0.328	1.366±0.856	0.477±0.313	0.353±0.236	0.973±0.379	0.440±0.252
E2D2	0.870±1.041	2.517±2.334	0.468±0.314	0.550±0.458	1.344±0.967	0.335±0.196
C1D1	0.266±0.235	0.605±0.536	0.512±0.388	0.156±0.118	0.365±0.385	0.278±0.233
C1D2	0.236±0.099	1.197±0.692	0.558±0.392	0.216±0.083	0.813±0.470	0.424±0.145
Mean	0.430±0.367	1.531±1.208	0.526±0.350	0.311±0.224	0.930±0.574	0.384±0.223

Table 4.9. Mean absolute difference of time-domain parameters of SBP (MAD ≤ 0.300 marked)

	SDNN			RMSSD		
	PAT	IF1	IF2	PAT	IF1	IF2
E1D1	0.607±0.482	1.500±1.230	0.562±0.236	0.394±0.311	0.663±0.492	0.256±0.106
E1D2	0.462±0.276	1.789±1.440	0.476±0.326	0.399±0.217	0.784±0.598	0.173±0.090
E2D1	0.415±0.282	0.948±0.663	0.293±0.236	0.203±0.094	0.569±0.447	0.116±0.065
E2D2	0.910±1.000	2.399±2.150	0.416±0.206	0.479±0.499	1.215±0.848	0.182±0.107
C1D1	0.334±0.094	0.629±0.369	0.502±0.371	0.183±0.082	0.284±0.246	0.165±0.146
C1D2	0.428±0.104	1.130±0.745	0.446±0.274	0.156±0.106	0.676±0.483	0.255±0.138
Mean	0.526±0.373	1.399±1.100	0.449±0.275	0.302±0.218	0.699±0.519	0.191±0.109

Table 4.10. Mean absolute difference of time-domain parameters of DBP (MAD ≤ 0.300 marked)

	SDNN			RMSSD		
	PAT	IF1	IF2	PAT	IF1	IF2
E1D1	0.427±0.362	1.449±1.164	0.472±0.236	0.229±0.254	0.711±0.426	0.228±0.043
E1D2	0.503±0.247	1.831±1.531	0.511±0.440	0.327±0.240	0.875±0.714	0.204±0.079
E2D1	0.344±0.386	1.149±0.817	0.384±0.180	0.135±0.059	0.718±0.492	0.207±0.119
E2D2	0.881±1.031	2.466±2.285	0.409±0.308	0.416±0.518	1.221±0.946	0.203±0.120
C1D1	0.348±0.121	0.496±0.409	0.369±0.181	0.209±0.047	0.259±0.173	0.137±0.104
C1D2	0.322±0.213	1.259±0.648	0.581±0.296	0.183±0.082	0.766±0.462	0.346±0.184
Mean	0.471±0.393	1.442±1.142	0.454±0.274	0.250±0.200	0.758±0.536	0.221±0.108

Scatter plots and linear regression of time-domain parameters (between RRI-PAT, RRI-IF1, RRI-IF2, SBP-PAT, SBP-IF1, SBP-IF2, DBP-PAT, DBP-IF1, and DBP-IF2) show that parameters are not depended on each other. The coefficient of determination is poor as well, therefore it is not presented.

Frequency-domain analysis

The values of frequency-domain parameters (described in section 1.6.2) of R-R intervals, systolic and diastolic blood pressure, pulse arrival time, first and second instantaneous frequencies during thermal stress test are presented in the appendix (Study No. 2: thermal stress test). Figure 4.19–4.24 summarize the normalized curves of RRI, SBP, DBP, PAT, IF1, and IF2 of frequency-domain parameters (LF and HF). The changes between the intervals of the thermal stresses of frequency-domain parameters (data normalized by interval I defined in section 4.4) are presented in the appendix (Study No. 2: thermal stress test).

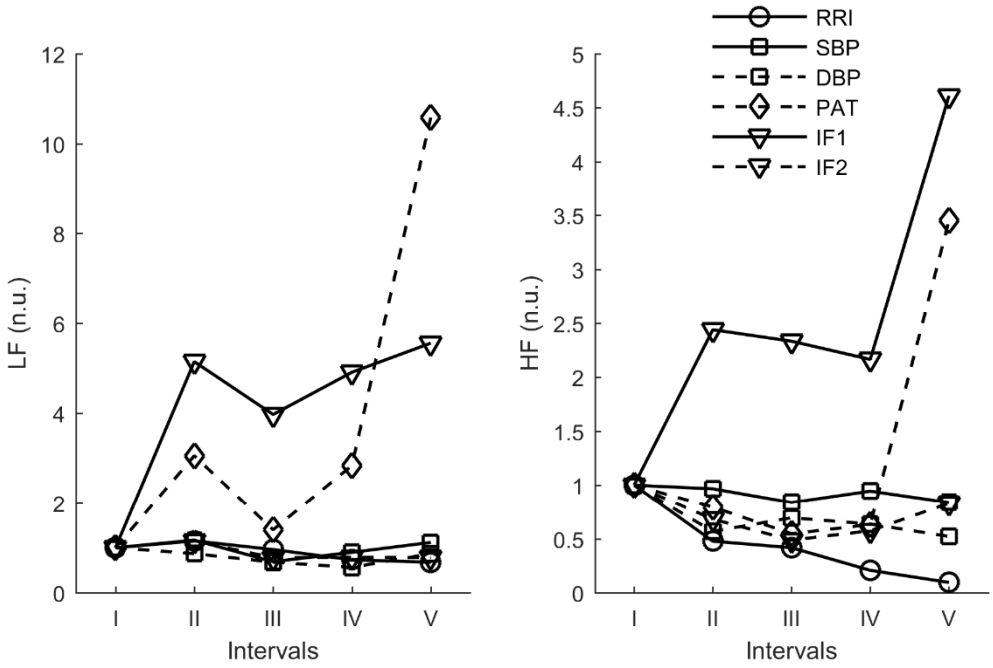

Figure 4.19. Curves of frequency-domain parameters of RRI, SBP, DBP, PAT, IF1, and IF2 during the thermal stress test (experiment E1D1)

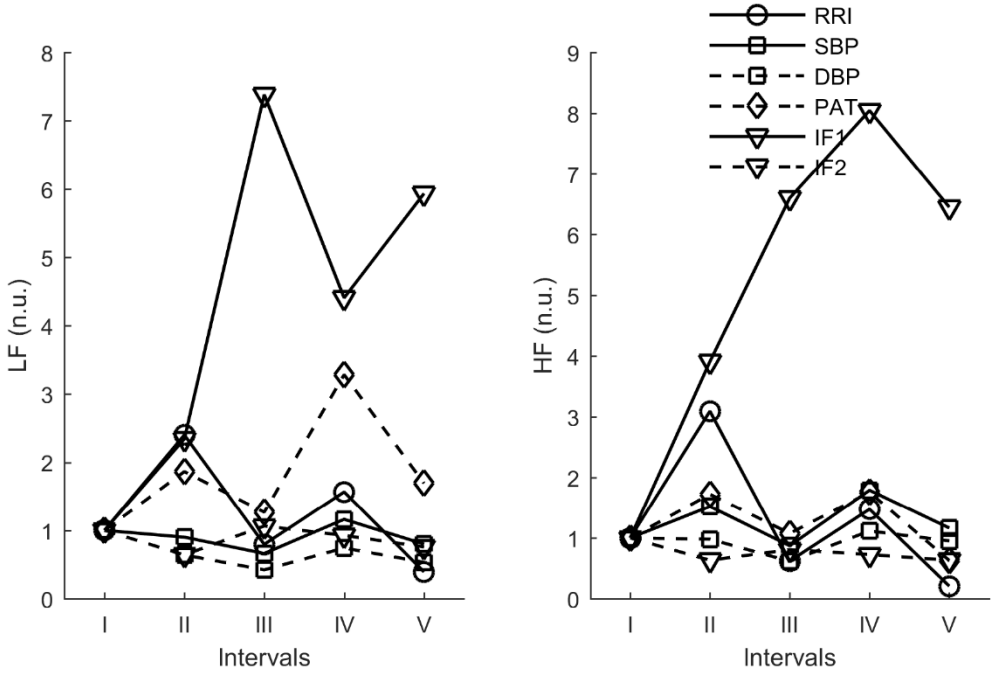

Figure 4.20. Curves of frequency-domain parameters of RRI, SBP, DBP, PAT, IF1, and IF2 during the thermal stress test (experiment E1D2)

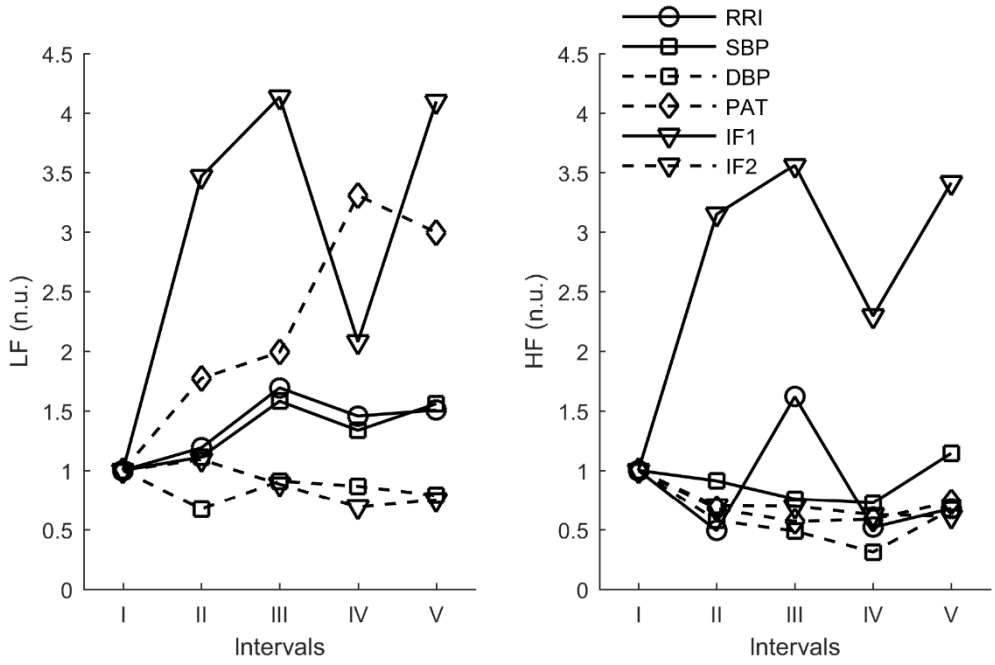

Figure 4.21. Curves of frequency-domain parameters of RRI, SBP, DBP, PAT, IF1, and IF2 during the thermal stress test (experiment E2D1)

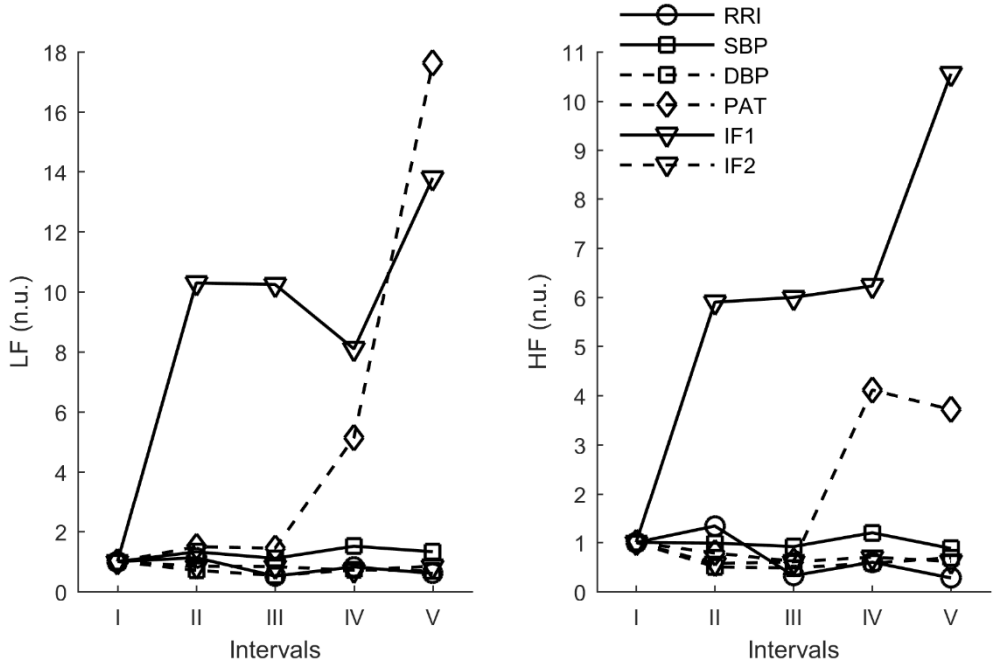

Figure 4.22. Curves of frequency-domain parameters of RRI, SBP, DBP, PAT, IF1, and IF2 during the thermal stress test (experiment E2D2)

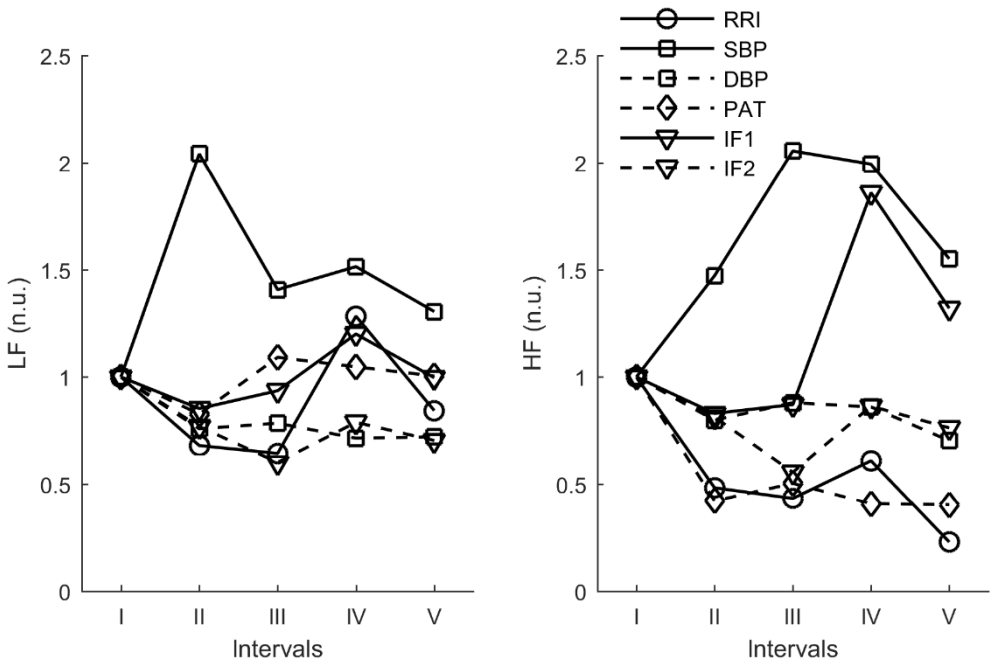

Figure 4.23. Curves of frequency-domain parameters of RRI, SBP, DBP, PAT, IF1, and IF2 during the thermal stress test (experiment C1D1)

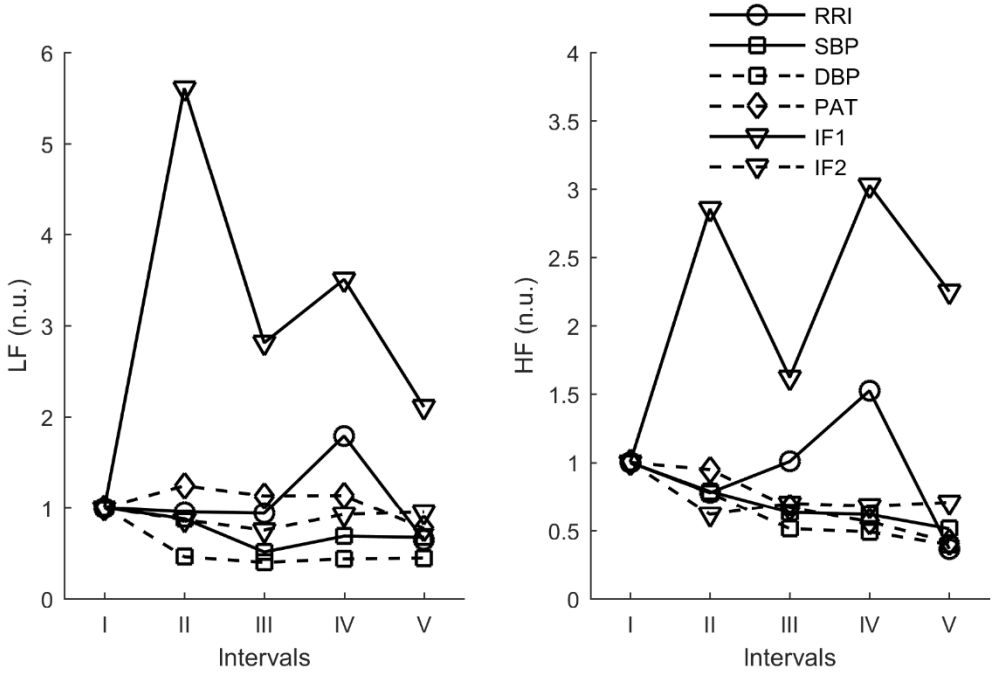

Figure 4.24. Curves of frequency-domain parameters of RRI, SBP, DBP, PAT, IF1, and IF2 during the thermal stress test (experiment C1D2)

Table 4.11–4.13 show Spearman correlation coefficients of frequency-domain parameters between two groups of variability curves: 1) R-R intervals, systolic blood pressure, and diastolic blood pressure; 2) pulse arrival time, first instantaneous frequency, and second instantaneous frequency. The results show that: PAT best reflects the RRI, SBP, and BP in SDNN and RMSSD (0.484–0.685), therefore, the Spearman correlation coefficients are poor.

Table 4.11. Spearman correlation coefficients of frequency-domain parameters of R-R intervals ($r_S \geq 0.700$ marked)

	LF			HF		
	PAT	IF1	IF2	PAT	IF1	IF2
E1D1	0.467±0.388	0.417±0.256	0.400±0.341	0.817±0.172	0.400±0.245	0.467±0.344
E1D2	0.617±0.319	0.200±0.126	0.267±0.163	0.750±0.235	0.350±0.266	0.383±0.256
E2D1	0.775±0.263	0.300±0.356	0.450±0.311	0.700±0.424	0.200±0.183	0.625±0.250
E2D2	0.375±0.320	0.475±0.275	0.475±0.236	0.525±0.330	0.650±0.332	0.375±0.171
C1D1	0.600±0.367	0.520±0.327	0.320±0.268	0.620±0.228	0.380±0.311	0.300±0.122
C1D2	0.717±0.194	0.433±0.314	0.267±0.197	0.700±0.283	0.583±0.214	0.483±0.397
Mean	0.592±0.309	0.391±0.276	0.363±0.253	0.685±0.279	0.427±0.259	0.439±0.257

Table 4.12. Spearman correlation coefficients of frequency-domain parameters of systolic blood pressure ($r_S \geq 0.700$ marked)

	LF			HF		
	PAT	IF1	IF2	PAT	IF1	IF2
E1D1	0.433±0.137	0.367±0.234	0.233±0.151	0.367±0.151	0.383±0.271	0.417±0.279
E1D2	0.700±0.228	0.433±0.294	0.350±0.164	0.467±0.258	0.417±0.223	0.483±0.299
E2D1	0.725±0.171	0.450±0.300	0.375±0.340	0.650±0.208	0.475±0.411	0.400±0.346
E2D2	0.500±0.424	0.550±0.252	0.500±0.337	0.400±0.163	0.375±0.359	0.300±0.283
C1D1	0.440±0.404	0.280±0.327	0.400±0.274	0.420±0.356	0.580±0.383	0.600±0.308
C1D2	0.350±0.235	0.267±0.186	0.383±0.279	0.600±0.297	0.500±0.369	0.350±0.339
Mean	0.525±0.267	0.391±0.266	0.374±0.258	0.484±0.239	0.455±0.336	0.425±0.309

Table 4.13. Spearman correlation coefficients of frequency-domain parameters of diastolic blood pressure ($r_S \geq 0.700$ marked)

	LF			HF		
	PAT	IF1	IF2	PAT	IF1	IF2
E1D1	0.500±0.276	0.333±0.344	0.350±0.302	0.567±0.418	0.433±0.207	0.200±0.245
E1D2	0.667±0.339	0.367±0.301	0.567±0.378	0.433±0.320	0.467±0.121	0.317±0.133
E2D1	0.675±0.250	0.425±0.320	0.200±0.200	0.500±0.424	0.275±0.126	0.450±0.465
E2D2	0.325±0.126	0.650±0.208	0.275±0.189	0.525±0.377	0.525±0.236	0.550±0.311
C1D1	0.560±0.365	0.400±0.274	0.380±0.370	0.400±0.274	0.460±0.351	0.460±0.410
C1D2	0.433±0.372	0.400±0.155	0.417±0.172	0.600±0.253	0.517±0.299	0.200±0.110
Mean	0.527±0.288	0.429±0.267	0.365±0.269	0.504±0.344	0.446±0.223	0.363±0.279

Table 4.14–4.16 show the mean absolute differences of frequency-domain parameters between two groups of variability curves: 1) R-R intervals, systolic blood pressure, and diastolic blood pressure; 2) pulse arrival time, first instantaneous frequency, and second instantaneous frequency. The results show that IF2 accurately reflects RRI, SBP, and DBP in LF and HF (RRI – 0.681 and 0.668, SBP – 0.654 and 0.636, DBP – 0.441 and 0.406).

Table 4.14. Mean absolute difference of frequency-domain parameters of R-R intervals (MAD ≤ 0.300 marked)

	LF			HF		
	PAT	IF1	IF2	PAT	IF1	IF2
E1D1	3.267±6.408	3.647±3.843	0.654±0.355	1.003±1.800	2.266±1.515	0.430±0.106
E1D2	0.930±0.812	4.042±3.490	0.896±0.999	0.868±0.920	5.333±4.447	1.096±1.517
E2D1	1.072±1.360	2.560±1.514	0.960±0.655	0.721±0.864	2.590±1.794	0.685±0.768
E2D2	5.799±11.516	7.682±6.712	0.366±0.164	2.093±3.803	5.256±4.842	0.522±0.365
C1D1	0.677±0.687	0.825±0.776	0.607±0.338	0.241±0.144	0.933±0.943	0.516±0.384
C1D2	0.434±0.286	2.417±2.310	0.603±0.482	0.514±0.686	1.930±1.507	0.756±0.758
Mean	2.030±3.512	3.529±3.108	0.681±0.499	0.907±1.370	3.051±2.508	0.668±0.650

Table 4.15. Mean absolute difference of frequency-domain parameters of systolic blood pressure (MAD ≤ 0.300 marked)

	LF			HF		
	PAT	IF1	IF2	PAT	IF1	IF2
E1D1	3.487±6.667	3.698±4.003	0.643±0.591	1.283±1.710	2.107±1.487	0.528±0.330
E1D2	0.999±1.169	3.449±3.663	0.358±0.224	0.982±0.559	4.171±4.226	0.670±0.516
E2D1	1.541±1.281	1.834±1.608	0.644±0.379	0.391±0.157	1.876±1.958	0.390±0.161
E2D2	6.092±11.538	7.965±6.121	0.816±0.576	2.332±3.706	5.462±4.539	0.537±0.403
C1D1	1.015±0.772	1.165±0.787	0.916±0.918	1.067±1.239	1.684±1.127	1.263±1.345
C1D2	0.702±0.274	2.411±2.771	0.549±0.346	0.254±0.116	1.629±1.549	0.429±0.100
Mean	2.306±3.617	3.420±3.159	0.654±0.506	1.052±1.248	2.822±2.481	0.636±0.476

Table 4.16. Mean absolute difference of frequency-domain parameters of diastolic blood pressure (MAD ≤ 0.300 marked)

	LF			HF		
	PAT	IF1	IF2	PAT	IF1	IF2
E1D1	3.096±6.424	3.489±3.912	0.567±0.333	0.944±1.708	2.039±1.518	0.324±0.096
E1D2	1.155±1.171	3.590±3.880	0.383±0.158	0.754±0.708	4.413±4.656	0.574±0.192
E2D1	1.446±1.758	2.153±1.573	0.384±0.086	0.169±0.101	2.060±1.992	0.289±0.038
E2D2	5.837±11.670	7.720±6.732	0.386±0.222	2.025±3.851	5.284±4.962	0.306±0.153
C1D1	0.614±0.436	0.688±0.565	0.448±0.176	0.358±0.159	0.957±0.645	0.523±0.271
C1D2	0.558±0.402	2.548±2.709	0.477±0.386	0.308±0.153	1.740±1.552	0.420±0.274
Mean	2.118±3.644	3.365±3.229	0.441±0.227	0.760±1.113	2.749±2.554	0.406±0.171

Scatter plots and linear regression of time-domain parameters (between RRI-PAT, RRI-IF1, RRI-IF2, SBP-PAT, SBP-IF1, SBP-IF2, DBP-PAT, DBP-IF1, and DBP-IF2) show that parameters are not depended on each other. The coefficient of determination is poor, therefore it is not presented.

Discussion

The results show that R-R intervals and blood pressure decrease (decrease of DBP is not always statistically significant) during thermal stress. During thermal stress, the core temperature increases rapidly because two large surfaces (skin and epithelium of the pulmonary alveoli) are influenced by heat. Elevated core temperature causes thermoregulatory reactions which protect the body from overheating (Pilch et al., 2014). The only effective way to reduce temperature of the body is vaporization of fluid from the skin (sweating), which reduces body

water, mass, and plasma volume (Blum, Blum, 2007). The responses of an organism to elevated temperature are dilatation of skin vessels (dilatation reduces peripheral resistance) and to 60% increased skin blood flow (Stephenson, Kolka, 1988). Increased skin blood flow may be continued because the flow in different vessels reduces, for example, blood flow is reduced in muscles and kidneys. HR increases because of increased activation of the sympathetic nervous system and secretion of noradrenalin (Hannuksela, Ellaham, 2001). Therefore, it is possible to conclude that the results of this study coincide with those described in literature.

Based on preliminary results (obtained from a limited number of healthy subjects) of time-domain and frequency-domain analysis, it is possible to conclude that PAT variability is more accurately than RRI variability in time-domain parameters, meanwhile, IF2 variability – in frequency-domain parameters. IF2 (higher instantaneous frequency) variability is more accurate than SBP and DBP variability in time-domain and frequency-domain parameters.

On the other hand, the thermal stress test is a very complex and difficult test for the human body because high temperatures affect the whole organism (cardiovascular system, nervous system, and other). Therefore, complicated processes take place in the body and it tries to adapt to stressful situations. Every human organism is different and, therefore, the adaptations to stressful situations are different, which is clearly visible in the data of each subject, hence case-to-case studies should be applied in future work.

During a thermal stress test the organism experiences higher stress than during an orthostatic test. Therefore, during the orthostatic test, slower processes occur and lower extracted instantaneous frequency (IF1) better reflects the variability of BP, meanwhile, during thermal stress test, faster processes occur and higher extracted instantaneous frequency (IF2) better reflects the variability of BP.

However, the database is limited; only 8 healthy subjects are investigated. In order to get more accurate trends and interrelations of BP, PAT and IF more comprehensive investigation and a larger database is required. The database should be expanded by collecting more data from volunteers of different age groups and in various physical shapes; more studies with different stress tests should be done.

4.3. Conclusions of the chapter

1. The noise-resistant algorithm for estimating pulse arrival time (PATht) shows better accuracy than the classical and diastole-patching pulse arrival time estimation algorithms when physiological signals are noisy (SNR 0–20 dB).
2. The variability of pulse arrival time, first and second instantaneous frequencies show the same tendency as the variability of systolic and diastolic blood pressure and the same or opposite tendency as heart rate variability during the orthostatic test. Mean absolute difference between the variability of R-R intervals and the variability of pulse arrival time, first and second instantaneous frequencies are lower in the SDNN parameter, meanwhile, mean absolute difference is high in RMSSD, LF, and

HF parameter. Mean absolute difference is lower between the variability of blood pressure and the variability of pulse arrival time and first instantaneous frequency in time-domain and frequency-domain parameters.

3. In thermal stress case, mean absolute difference between the variability of blood pressure and the variability of second instantaneous frequency is low in the time-domain and frequency-domain parameters. Meanwhile, mean absolute difference between heart rate (R-R intervals) variability and the variability of pulse arrival time is low in the time-domain parameters.
4. When slower processes occur in an organism (for example, during an orthostatic test), the variability of lower extracted instantaneous frequency (IF1) better reflects the variability of blood pressure, and vice versa; when faster processes occur in an organism (for example, during a thermal stress test), the variability of higher extracted instantaneous frequency (IF2) better reflects the variability of blood pressure.

5. CONCLUSIONS

1. A noise-resistant algorithm for estimating pulse arrival time was developed. The proposed algorithm shows better accuracy than the classical and diastole-patching pulse arrival time estimation algorithms when the photoplethysmogram signal is noisy at all investigated signal-to-noise ratios (at 0–20 dB).
2. An algorithm for extracting instantaneous frequencies from a photoplethysmogram signal was developed. The results show that the extracted characteristics (instantaneous frequencies) are related to the physiological processes: short-term blood pressure and heart rate variability.
3. Results show that the characteristics estimated using the proposed algorithms can be used to evaluate short-term blood pressure variability during rest and in non-stationary conditions. The variability of pulse arrival time, first instantaneous frequency, and second instantaneous frequency show the same tendency as the variability of systolic and diastolic blood pressure during the orthostatic test. The mean absolute difference between pulse arrival time, first instantaneous frequency variability and blood pressure (systolic and diastolic) variability is low (0.086–0.231 and 0.081–0.276, respectively) in time-domain and higher (0.175–0.506 and 0.149–0.388, respectively) in frequency-domain parameters. In thermal stress case, the mean absolute difference between the second instantaneous frequency variability and blood pressure (systolic and diastolic) variability is low in time-domain (0.191–0.221) and frequency-domain (0.406–0.636) parameters.
4. The results show that the characteristics estimated using the proposed algorithms can be used for measuring short-term heart rate variability during rest and in non-stationary conditions. The variability of pulse arrival time, first instantaneous frequency, and second instantaneous frequency show the same or opposite tendency as the variability of heart rate during the orthostatic test. The mean absolute difference between the variability of pulse arrival time, first and second instantaneous frequencies and the variability of heart rate is low (0.313–0.406) only for the SDNN parameter. In the case of thermal stress, the mean absolute difference between pulse arrival time and heart rate variability is low in time-domain (0.311 and 0.430) parameters.
5. The results indicate that the extracted characteristics (pulse arrival time and instantaneous frequencies) better reflect short-term heart rate and blood pressure variability during an orthostatic test than during a thermal stress test because each organism is different and respond to stress in a unique manner. Moreover, the database of thermal stress test is not large enough, the data is from a narrow age group and from subjects in different physical

shapes. Additionally, the thermal stress test is very complex and difficult for the human body.

6. Two physiological tests (orthostatic test and thermal stress test) were performed and two physiological signal databases were collected. The database of the thermal stress test is unique and collected under extreme conditions.
7. Based on investigations and conclusions 4–6, it is recommended:
    - To evaluate short-term systolic blood pressure variability to use pulse arrival time (for SDNN, RMSSD, and LF) and first instantaneous frequency (for SDNN, RMSSD, LF, and HF) parameters at rest or during low stress, pulse arrival time (for SDNN and RMSSD) and second instantaneous frequency (for SDNN, RMSSD, LF, and HF) parameters during high stress.
    - To evaluate short-term diastolic blood pressure variability using pulse arrival time (for SDNN, RMSSD, and LF), first instantaneous frequency (for SDNN, LF, and HF), and second instantaneous frequency (for RMSSD) parameters at rest or during low stress, pulse arrival time (for SDNN and RMSSD) and second instantaneous frequency (for SDNN, RMSSD, LF, and HF) parameters during high stress.
    - To evaluate short-term heart rate variability using pulse arrival time, first instantaneous frequency, and second instantaneous frequency (for SDNN) parameters at rest or during low stress, pulse arrival time (for SDNN and RMSSD) and second instantaneous frequency (for SDNN, RMSSD, LF, and HF) parameters during high stress.

REFERENCES

1. Ahlstrom, C., Johansson, A., Uhlin, F., Länne, T., Ask, P. (2005). Noninvasive investigation of blood pressure changes using the pulse wave transit time: a novel approach in the monitoring of hemodialysis patients. *Journal of Artificial Organs, 8*(3), 192-197. ISSN 1619-0904.

2. Akinci, A., Çeliker, A., Baykal, E., Teziç, T. (1993). Heart rate variability in diabetic children: sensitivity of the time- and frequency-domain methods. *Pediatric Cardiology, 14*(3), 140-146. ISSN 1432-1971.

3. Akselrod, S., Gordon, D., Madwed, J. B., Snidman, N. C., Shannon, D. C., Cohen, R. J. (1985). Hemodynamic regulation: investigation by spectral analysis. *American Journal of Physiology - Heart and Circulatory Physiology, 249*(4), H867-H875. ISSN 1522-1539.

4. Akselrod, S., Gordon, D., Ubel, F. A., Shannon, D. C., Berger, A. C., Cohen, R. J. (1981). Power spectrum analysis of heart rate fluctuation: a quantitative probe of beat-to-beat cardiovascular control. *Science, 213*(4504), 220-222. ISSN 1095-9203.

5. Allen, J. (2007). Photoplethysmography and its application in clinical physiological measurement. *Physiological Measurement, 28*(3), R1-R39. ISSN 1361-6579.

6. Allen, J., Di Maria, C., Mizeva, I., Podtaev, S. (2013). Finger microvascular responses to deep inspiratory gasp assessed and quantified using wavelet analysis. *Physiological Measurement, 34*(7), 769-779. ISSN 1361-6579.

7. Allen, R. A., Schneider, J. A., Davidson, D. M., Winchester, M. A., Taylor C. B. (1981). The Covariation of Blood Pressure and Pulse Transit Time in Hypertensive Patients. *Psychophysiology, 18*(3), 301-305. ISSN 1469-8986.

8. Aubert, A. E., Beckers, F., Ramaekers, D. (2000). Short-term heart rate variability in young athletes. *Journal of Cardiology, 37*, 85-88. ISSN 1876-4738.

9. Aubert, A. E., Seps, B., Beckers, F. (2003). Heart rate variability in athletes. *Sports Medicine, 33*(12), 889-919. ISSN 1179-2035.

10. Bekheit, S., Tangella, M., el-Sakr, A., Rasheed, Q., Craelius, W., El-Sherif, N. (1990). Use of heart rate spectral analysis to study the effects of calcium channel blockers on sympathetic activity after myocardial infarction. *American Heart Journal, 119*(1), 79-85. ISSN 0002-8703.

11. Bernardi, L., Ricordi, L., Lazzari, P., Soldá, P., Calciati, A., Ferrari, M. R., Vandea, I., Finardi, G., Fratino, P. (1992). Impaired circadian modulation of sympathovagal activity in diabetes. A possible explanation for altered temporal onset of cardiovascular disease. *Circulation, 86*(5), 1443-1452. ISSN 1524-4539.

12. Bilo, G., Giglio, A., Styczkiewicz, K., Caldara, G., Maronati, A., Kawecka-Jaszcz, K., Mancia, G., Parati, G. (2007). A new method for assessing 24-h blood pressure variability after excluding the contribution of nocturnal blood pressure fall. *Journal of Hypertension, 25*(10), 2058-2066. ISSN 1473-5598.

13. Blum, N., Blum, A. (2007). Beneficial effects of sauna bathing for heart failure patients. *Experimental and Clinical Cardiology, 12*(1), 29-32. ISSN 1918-1515.

14. Boggia, J., Li, Y., Thijs, L., Hansen, T. W., Kikuya, M., Björklund-Bodegård, K., Richart, T., Ohkubo, T., Kuznetsova, T., Torp-Pedersen, C., Lind, L., Ibsen, H., Imai, Y., Wang, J., Sandoya, E., O'Brien, E., Staessen, J. A. (2007). Prognostic accuracy of day versus night ambulatory blood pressure: a cohort study. *The Lancet, 370*(9594), 1219-1229. ISSN 0140-6736.

15. Brazaitis, M., Skurvydas, A., Pukenas, K., Daniuseviciute, L., Mickeviciene, D., Solianik, R. (2012). The effect of temperature on amount and structure of motor variability during 2-minute maximum voluntary contraction. *Muscle and Nerve, 46*(5), 799-809. ISSN 1097-4598.

16. Carter, J. B., Banister, E. W., Blaber, A. P. (2003). The effect of age and gender on heart rate variability after endurance training. *Medicine and Science in Sports and Exercise, 35*(8), 1333-1340. ISSN 0195-9131.

17. Cattivelli, F. S., Garudadri, H. (2009). Noninvasive Cuffless Estimation of Blood Pressure from Pulse Arrival Time and Heart Rate with Adaptive Calibration. *In Proceedings of 2009 sixth International Workshop on Wearable and Implantable Body Sensor Networks* (pp. 114-119). Berkeley: IEEE. ISSN 2376-8886.

18. Chen, W., Kobayashi, T., Ichikawa, S., Takeuchi, Y., Togawa, T. (2000). Continuous estimation of systolic blood pressure using the pulse arrival time and intermittent calibration. *Medical and Biological Engineering and Computing, 38*(5), 569-574. ISSN 1741-0444.

19. Cloutier, J., Norman, G. J., Li, T., Berntson, G. G. (2013). Person perception and autonomic nervous system response: The costs and benefits of possessing a high social status. *Biological Psychology, 92*(2), 301-305. ISNN 0301-0511.

20. Conway, J., Boon, N., Davies, C., Jones, J. V., Sleight, P. (1984). Neural and humoral mechanisms involved in blood pressure variability. *Journal of Hypertension, 2*(2), 203-208. ISSN 1473-5598.

21. Coumel, P., Hermida, J. S., Wennerblöm, B., Leenhardt, A., Maison-Blanche, P., Cauchemez, B. (1991). Heart rate variability in left ventricular hypertrophy and heart failure, and the effects of beta-blockade a non-spectral analysis of heart rate variability in the frequency domain and in the time domain. *European Heart Journal, 12*(3), 412-422. ISSN 1522-9645.

22. Cowan, M. J. (1995). Measurement of Heart Rate Variability. *Western Journal of Nursing Research, 17*(1), 32-48. ISNN 1552-8456.

23. C-Shop. (2007). *ANAM4: Software User Manual.* Norman, OK: Center for the Study of Human Operator Performance, University of Oklahoma.

24. De Boer, R. W. (1985). Beat-to-beat blood-pressure fluctuations and heart-rate variability in man: physiological relationships, analysis techniques and a simple model. University of Amsterdam, Department of Physiology.

25. De Boer, R. W., Karemaker, J. M., Strackee, J. (1985). Relationships between short-term blood-pressure fluctuations and heart-rate variability in resting subjects I: a spectral analysis approach. *Medical and Biological Engineering and Computing, 23*(4), 352-358. ISSN 1741-0444.

26. De La Cruz Torres, B., López, C. L., Orellana, J. N. (2008). Analysis of heart rate variability at rest and during aerobic exercise: a study in healthy people and cardiac patients. *British Journal of Sports Medicine, 42*(9), 715-720. ISSN 1473-0480.

27. Elgendi, M. (2012). On the Analysis of Fingertip Photoplethysmogram Signals. *Current Cardiology Reviews, 8*(1), 14-25. ISSN 1875-6557.

28. Ewing, D. J., Winney, R. (1975). Autonomic Function in Patients with Chronic Renal Failure on Intermittent Haemodialysis. *Nephron, 15*(6), 424-429. ISSN 2235-3186.

29. *Finapres Medical Systems | Portapres*. (2015). Retrieved from http://www.finapres.com

30. Forsström, J., Forsström, J., Heinonen, E., Välimäki, I., Antila, K. (1986). Effects of haemodialysis on heart rate variability in chronic renal failure. *Scandinavian Journal of Clinical and Laboratory Investigation, 46*(7), 665-670. ISSN 1502-7686.

31. Friedman, O., Logan, A. G. (2009). Nocturnal blood pressure profiles among normotensive, controlled hypertensive and refractory hypertensive subjects. *Canadian Journal of Cardiology, 25*(9), S312-S316. ISNN 0828-282X.

32. Fujii, T., Uzu, T., Nishimura, M., Takeji, M., Kuroda, S., Nakamura, S., Inenaga, T., Kimura, G. (1999). Circadian rhythm of natriuresis is disturbed in nondipper type of essential hypertension. *American Journal of Kidney Diseases, 33*(1), 29-35. ISSN 0272-6386.

33. Fukui, M., Ushigome, E., Tanaka, M., Hamaguchi, M., Tanaka, T., Atsuta, H., Ohnishi, M., Oda, Y., Hasegawa, G., Nakamura, N. (2013). Home blood pressure variability on one occasion is a novel factor associated with arterial stiffness in patients with type 2 diabetes. *Hypertensios Research, 36*(3), 219-225. ISSN 1348-4214.

34. Gargasas, L., Jurkonis, V., Bikulčienė, L., Zvironiene, A., Daukantas, S. (2012). Functional state evaluation system with distributed intellect for elderly and disabled persons. *Scientific Journal of RTU: Technologies of Computer Control, 13*, 57-62. ISSN 2255-9108.

35. Gesche, H., Grosskurth, D., Kuchler, G., Patzak, A. (2012). Continuous blood pressure measurement by using the pulse transit time: comparison to a cuff-based method. *European Journal of Applied Physiology, 112*(1), 309-315. ISSN 1439-6327.

36. Greiser, K. H., Kluttig, A., Schumann, B., Kors, J. A., Swenne, C. A., Kuss, O., Werdan, K., Haerting, J. (2005). Cardiovascular disease, risk factors and heart rate variability in the elderly general population: Design and objectives of the CARdiovascular disease, Living and Ageing in Halle (CARLA) Study. *BMC Cardiovascular Disorders, 5:33*. ISSN 1471-2261.

37. Gribbin, B., Steptoe, A., Sleight, P. (1976). Pulse wave velocity as a measure of blood pressure change. *Psychophysiology, 13*(1), 86-90. ISSN 1469-8986.

38. Guzmán, C. E., Sánchez, G. M., Márquez, M. F., Hermosillo, A. G., Cárdenas, M. (1999). Differences in Heart Rate Variability Between Cardioinhibitory and Vasodepressor Responses to Head-Up Tilt Table Testing. *Archives of Medical Research, 30*(3), 203-211. ISSN 0188-4409.

39. Guzzetti, S., Cogliati, C., Broggi, C., Carozzi, C., Caldiroli, D., Lombardi, F., Malliani, A. (1994). Influences of neural mechanisms on heart period and arterial pressure variabilities in quadriplegic patients. *American Journal of Physiology - Heart and Circulatory Physiology, 266*(3), H1112-H1120. ISSN 1522-1539.

40. Guzzetti, S., Piccaluga, E., Casati, R., Cerutti, S., Lombardi, F., Pagani, M., Malliani, A. (1988). Sympathetic predominance an essential hypertension: a study employing spectral analysis of heart rate variability. *Journal of Hypertension, 6*(9), 711-717. ISSN 1473-5598.

41. Hayano, J., Yamada, M., Sakakibara, Y., Fujinami, T., Yokoyama, K., Watanabe, Y., Takata, K. (1990). Short-and long-term effects of cigarette smoking on heart rate variability. *The American Journal of Cardiology, 65*(1), 84-88. ISNN 0002-9149.

42. Haynes, W. G. (2005). Role of leptin in obesity-related hypertension. *Experimental Physiology, 90*(5), 683-688. ISSN 1469-445X.

43. Hamilton, P. S., Tompkins, W. J. (1986). Quantitative investigation of qrs detection rules using the mit/bih arrhythmia database. *IEEE Transactions on Biomedical Engineering , BME-33*(12), 1157-1165. ISSN 0018-9294.

44. Hannuksela, M. L., Ellaham, S. (2001). Benefits and risks of sauna bathing. *The American Journal of Medicine, 110*(2), 118-126. ISSN 0002-9343.

45. Hansen, T. W., Li, Y., Boggia, J., Thijs, L., Richart, T., Staessen, J. A. (2011). Predictive Role of the Nighttime Blood Pressure. *Hypertension, 57*(1), 3-10. ISSN 1524-4563.

46. Heard, S. O., Lisbon, A., Toth, I., Ramasubramanian, R. (2000). An Evaluation of a New Continuous Blood Pressure Monitoring System in Critically Ill Patients. *Journal of Clinical Anesthesia, 12*(7), 509-518. ISSN 0952-8180.

47. Hey, S., Gharbi, A., von Haaren, B., Walter, K., König, N., Löffler, S. (2009). Continuous noninvasive Pulse Transit Time Measurement for Psychophysiological Stress Monitoring. *In Proceedings of 2009 International Conference on eHealth, Telemedicine, and Social Medicine* (pp. 113-116). Cancun: IEEE. ISSN 2308-4359.

48. Hillebrand, S., Gast, K. B., de Mutsert, R., Swenne, C. A., Jukema, J. W., Middeldorp, S., Rosendaal, F. R., Dekkers, O. M. (2013). Heart rate variability and first cardiovascular event in populations without known cardiovascular disease: meta-analysis and dose–response meta-regression. *Europace, 15*(5), 742-749. ISSN 1532-2092.

49. Hilz, M. J., Stemper, B., Sauer, P., Haertl, U., Singer, W., Axelrod, F. B. (1999). Cold face test demonstrates parasympathetic cardiac dysfunction in familial dysautonomia. *American Journal of Physiology - Regulatory Integrative and Comparative Physiology, 276*(6), R1833-R1839. ISSN 1522-1490.

50. Hirsh, J. A., Bishop, B. (1981). Respiratory sinus arrhythmia in humans; how breathing pattern modulates heart rate. *American Journal of Physiology - Heart and Circulatory Physiology, 241*(4), H620-H629. ISSN 1522-1539.

51. Höcht, C. (2013). Blood Pressure Variability: Prognostic Value and Therapeutic Implications. *ISRN Hypertension, 2013*, 1-16. ISSN 2090-8709.

52. Holt-Lunstad, J., Steffen, P. R. (2007). Diurnal Cortisol Variation is Associated With Nocturnal Blood Pressure Dipping. *Psychosomatic Medicine, 69*(4), 339-343. ISSN 1534-7796.

53. Huang, N. E., Shen, Z., Long, S. R., Wu, M. C., Shih, H. H., Zheng, G., Yen, N., Tung, C. C., Liu, H. H. (1998). The empirical mode decomposition and hilbert spectrum for nonlinear and non-stationary time series analysis. *Proceedings of The Royal Society A Mathematical Physical and Engineering Sciences, 454*(1971), 903-995. ISSN 1471-2946.

54. Huang, N. E., Wu, Z., Long, S. R., Arnold, K. C., Chen, X., Blank, K. (2009). On Instantaneous Frequency. *Advances in Adaptive Data Analysis, 1*(2), 177-229. ISSN 1793-7175.

55. Hughes, D. J., Babbs, C. F., Geddes, L. A., Bourland, J. D. (1979). Measurements of Young's modulus of elasticity of the canine aorta with ultrasound. *Ultrason Imaging, 1*(4), 356-367. ISSN 1096-0910.

56. Huikuri, H. V., Pikkujämsä, S. M., Airaksinen, K. E., Ikäheimo, M. J., Rantala, A. O., Kauma, H, Lilja, M., Kesäniemi, Y. A. (1996). Sex-related differences in autonomic modulation of heart rate in middle-aged subjects. *Circulation, 94*(2), 122-125. ISSN 1524-4539.

57. Ye, S., Kim, G., Jung, D., Baik, S., Jeon, G. (2010). Estimation of systolic and diastolic pressure using the pulse transit time. *International Journal of Medical, Health, Biomedical, Bioengineering and Pharmaceutical Engineering, 4*(7), 303-308. ISSN 2010-3778.

58. Yen, J. R., Shieh, J. S., Huang, N. E. (2010). Complementary Ensemble Empirical Mode Decomposition: A Novel Noise Enhanced Data Analysis Method. *Advances in Adaptive Data Analysis, 2*(2), 135-156. ISSN 1793-7175.

59. Younessi, M. A., Khalilzadeh, M. A., Joharinia, S. (2014). Continuous and Cuffless Blood Pressure Monitoring Based on ECG and SpO2 Signals by Using Microsoft Visual C Sharp. *Journal of Biomedical Physics and Engineering, 4*(1), 27-32. ISSN 2251-7200.

60. Janušauskas, A., Marozas, V., Lukoševičius, A. (2013). Ensemble empirical mode decomposition based feature enhancement of cardio signals. *Medical Engineering and Physics, 35*(8), 1059-1069. ISSN 1741-0444.

61. Johansson, A., Ahlstrom, C., Lanne, T., Ask, P. (2006). Pulse wave transit time for monitoring respiration rate. *Medical and Biological Engineering and Computing, 44*(6), 471-478. ISSN 1741-0444.

62. Kamen, P. W., Krum, H., Tonkin, A. M. (1996). Poincaré Plot of Heart Rate Variability Allows Quantitative Display of Parasympathetic Nervous Activity in Humans. *Clinical Science, 91*(2), 201-208. ISSN 1470-8736.

63. Kaplan, D. T., Furman, M. I., Pincus, S. M., Ryan, S. M., Lipsitz, L. A., Goldberger, A. L. (1991). Aging and the complexity of cardiovascular dynamics. *Biophysical Journal, 59*(4), 945-949. ISSN 0006-3495.

64. Kautzner, J., Camm, J. A. (1997). Clinical relevance of heart rate variability. *Clinical Cardiology, 20*(2), 162-168. ISSN 1932-8737.

65. Kazanavicius, E., Gircys, R., Vrubliauskas, A., Lugin, S. (2005). Mathematical Methods for Determining the Foot Point of the Arterial Pulse Wave and Evaluation of Proposed Methods. *Information Technology And Control, 34*(1), 29-36. ISSN 2335-884X.

66. Klabunde, R. E. (2011). *Cardiovascular Physiology Concepts.* Lippincott: Williams & Wilkins. ISSN 978-1451113846.

67. Koh, J., Brown, T. E., Beightol, L. A., Ha, C. Y., Eckberg, D. L. (1994). Human autonomic rhythms: vagal cardiac mechanisms in tetraplegic subjects. *The Journal of Physiology, 474*(3), 483-495. ISSN 1469-7793.

68. Kotsis, V., Stabouli, S., Karafillis, I., Papakatsika, S., Rizos, Z., Miyakis, S., Goulopoulou, S., Parati, G., Nilsson, P. (2011). Arterial stiffness and 24h ambulatory blood pressure monitoring in young healthy volunteers: The early vascular ageing Aristotle University Thessaloniki Study (EVA-ARIS Study). *Atherosclerosis, 219*(1), 194-199. ISSN 0021-9150.

69. Kukkonen-Harjula, K., Kauppinen K. (2006). Health effects and risks of sauna bathing. *International Journal of Circumpolar Health, 65*(3), 195-205. ISSN 2242-3982.

70. Lagi, A., Tamburini, C., Cipriani, M., Fattorini, L. (1997). Vagal control of heart rate variability in vasovagal syncope: studies based on 24-h electrocardiogram recordings. *Clinical Autonomic Research, 7*(3), 127-130. ISSN 1619-1560.

71. Lane, J. D., Greenstadt, L., Shapiro, D., Rubinstein, E. (1983). Pulse transit time and blood pressure: an intensive analysis. *Psychophysiology, 20*(1), 45-49. ISSN 1469-8986.

72. Lazzeri, C., La Villa, G., Barletta, G., Franchi, F. (2000). 24-Hour Heart Rate Variability in Patients with Vasovagal Syncope. *Pacing and Clinical Electrophysiology, 23*(4), 463-468. ISSN 1540-8159.

73. Lerma, C., Minzoni, A., Infante, O., José, M. V. (2004). A Mathematical Analysis for the Cardiovascular Control Adaptations in Chronic Renal Failure. *Artificial Organs, 28*(4), 398-409. ISSN 1525-1594.

74. Liu, Y., Poon, C. C. Y., Zhang, Y. T., Yip, G. W. K., Yu, C. M. (2009). A Novel Method for Assessing Arterial Stiffness by a Hydrostatic Approach. *In Proceedings of 31st Annual International Conference of the IEEE Engineering in Medicine and Biology Society* (pp. 1789-1791). Minneapolis: IEEE. ISSN 1094-687X.

75. Liu, Q. Poon, C. C. Y., Zhang, Y. (2012). A Novel Method to Estimate Baroreflex Sensitivity Based on Pulse Transit Time. *In Proceedings of 2012 IEEE-EMBS International Conference on Biomedical and Health Informatics* (pp. 432-434). Hong Kong: IEEE. ISSN 2168-2194.

76. Lucini, D., Bertocchi, F., Malliani, A., Pagani, M. (1996). A controlled study of the autonomic changes produced by habitual cigarette smoking in healthy subjects. *Cardiovascular Research, 31*(4), 633-639. ISSN 1755-3245.

77. Lurbe, E., Redon, J., Kesani, A., Pascual, J. M., Tacons, J., Alvarez, V., Batlle, D. (2002). Increase in Nocturnal Blood Pressure and Progression to Microalbuminuria in Type 1 Diabetes. *The New England Journal of Medicine, 347*(11), 797-805. ISSN 1533-4406.

78. Lutter, N., Engl, H. G. Fischer, F., Bauer, R. D. (1996). Noninvasive continuous blood pressure control by pulse wave velocity. *Zeitschrift fur Kardiologie, 85*(3), 124-126. ISSN 0300-5860.

79. Ma, H. T. (2014). A Blood Pressure Monitoring Method for Stroke Management. *BioMed Research International, 2014*, 1-7. ISSN 2314-6141.

80. Malik, M., Bigger, J. T., Camm, A. J., Kleiger, R. E., Malliani, A., Moss, A. J., Schwartz, P. J. (1996). Heart rate variability: standards of measurement, physiological interpretation and clinical use. Task Force of the European Society of Cardiology and the North American Society of Pacing and Electrophysiology. *European Heart Journal, 17*(3), 354-381. ISSN 1522-9645.

81. Malik, M., Padmanabhan, V., Olson, W. H. (1999). Automatic measurement of long-term heart rate variability by implanted single-chamber devices. *Medical and Biological Engineering and Computing, 37*(5), 585-594. ISSN 1741-0444.

82. Malliani, A., Pagani, M., Lombardi, F., Cerutti, S. (1991). Cardiovascular Neural Regulation Explored in the Frequency Domain. *Circulation, 84*(2), 482-492. ISSN 1524-4539.

83. Mancia, G. (2012). Short- and Long-Term Blood Pressure Variability: Present and Future. *Hypertension, 60*(2), 512-517. ISSN 1524-4563.

84. Mancia, G., di Rienzo, M., Parati, G. (1993). Ambulatory Blood Pressure Monitoring Use in Hypertension Research and Clinical Practice. *Hypertension, 21*(4), 510-524. ISSN 1524-4563.

85. Mancia, G., Ferrari, A., Gregorini, L., Parati, G., Pomidossi, G., Bertinieri, G., Grassi, G., di Rienzo, M., Pedotti, A., Zanchetti, A. (1983). Blood Pressure and Heart Rate Variabilities in Normotensive and Hypertensive Human Beings. *Circulation Research, 53*(1), 96-104. ISSN 1524-4571.

86. Mancia, G., Grassi, G. (2000). Mechanisms and Clinical Implications of Blood Pressure Variability. *Journal of Cardiovascular Pharmacology, 35*(7), S15-S19. ISSN 1533-4023.

87. Mancia, G., Parati, G., Pomidossi, G., Casadei, R., di Rienzo, M., Zanchetti, A. (1986). Arterial Baroreflexes and Blood Pressure and Heart Rate Variabilities in Humans. *Hypertension, 8*(2), 147-153. ISSN 1524-4563.

88. Masè, M., Mattei, W., Cucino, R., Faes, L., Nollo, G. (2011). Feasibility of cuff-free measurement of systolic and diastolic arterial blood pressure. *Journal of Electrocardiology, 44*(2), 201-207. ISSN 0022-0736.

89. McEniery, C. M, Yasmin, McDonnell, B., Munnery, M., Wallace, S. M., Rowe, C. V., Cockcroft, J. R., Wilkinson, I. B., on Behalf of the Anglo-Cardiff Collaborative Trial Investigators. (2008). Central pressure: variability and impact of cardiovascular risk factors: The Anglo-Cardiff Collaborative Trial II. *Hypertension, 51*(6), 1476-1482. ISSN 1524-4563.

90. Mena, L., Pintos, S., Queipo, N., V., Aizpúrua, J. A., Maestre, G., Sulbarán, T. (2005). A reliable index for the prognostic significance of blood pressure variability. *Journal of Hypertension, 23*(3), 505-511. ISSN 1473-5598.

91. Montano, N., Ruscone, T. G., Porta, A., Lombardi, F., Pagani, M., Malliani, A. (1994). Power Spectrum Analysis of Heart Rate Variability to Assess the Changes in Sympathovagal Balance During Graded Orthostatic Tilt. *Circulation, 90*(4), 1826-1831. ISSN 1524-4539.

92. Moran, D. S., Castellani, J. W., O'Brien, C., Young, A. J., Pandolf, K. B. (1999). Evaluating physiological strain during cold exposure using a new cold strain index. *American Journal of Physiology - Regulatory Integrative and Comparative Physiology, 277*(2), R556-R564. ISSN 1522-1490.

93. Moran, D. S., Shitzer, A., Pandolf, K. B. (1998). A physiological strain index to evaluate heat stress. *American Journal of Physiology - Regulatory Integrative and Comparative Physiology, 275*(1), R129-R134. ISSN 1522-1490.

94. Muehlsteff, J., Aubert, X. L., Schuett, M. (2006). Cuffless estimation of systolic blood pressure for short effort bicycle tests: the prominent role of the pre-ejection period. *In Proceedings of the 28th annual conference of Engineering in Medicine and Biology Society* (pp. 5088-5092). New York City, USA: IEEE. ISSN 1094-687X.

95. Muehlsteff, J., Ritz, A., Drexel, T., Eickholt, C., Carvalho, P., Couceiro, R., Kelm, M., Meyer, C. (2012). Pulse Arrival Time as Surrogate for Systolic Blood Pressure Changes during Impending Neurally Mediated Syncope. *In Proceedings of 34th Annual International Conference of the IEEE Engineering in Medicine and Biology Society. 2012*, pp. 4283-4286. San Diego: IEEE. ISSN 1094-687X.

96. Mukai, S., Hayano, J. (1995). Heart rate and blood pressure variability during graded head-up tilt. *Journal of Applied Physiology, 78*(1), 212-216. ISSN 1522-1601.

97. Mukkamala, R., Hahn, J. O., Inan, O. T., Mestha, L. K., Kim, C. S., Toreyin, H., Kyal, S. (2015). Toward Ubiquitous Blood Pressure Monitoring via Pulse Transit Time: Theory and Practice. *IEEE Transactions on Biomedical Engineering, 62*(8), 1879-1901. ISSN 0018-9294.

98. Murakami, K., Yoshioka, M. (2015). Pulse Transit Time Variability on a Range of Heart Rates between Resting and Elevated States. *IEEE International Conference on Systems, Man, and Cybernetics* (pp. 1579-1582). Hong Kong: IEEE. ISBN 978-1-4799-8697-2.

99. Nagy, E., Orvos, H., Bárdos, G., Molnár, P. (2000). Gender Related Heart Rate Differences in Human Neonates. *Pediatric Research, 47*(6), 778-780. ISSN 1530-0447.

100. Narkiewicz, K., Winnicki, M., Schroeder, K., Phillips, B. G., Kato, M., Cwalina, E., Somers, V. K. (2002). Relationship Between Muscle Sympathetic Nerve Activity and Diurnal Blood Pressure Profile. *Hypertension, 39*(1), 168-172. ISSN 1524-4563.

101. Naschitz, J. E, Rosner I. (2007). Orthostatic hypotension: framework of the syndrome. *Postgraduate Medical Journal, 83*, ISSN 1469-0756.

102. Nybo, L., Nielsen, B. (2001). Hyperthermia and central fatigue during prolonged exercise in humans. *Journal Applied Physiology, 91*(3), 1055-1060. ISSN 1055-1060.

103. Nichols, M., Townsend, N., Luengo-Fernandez, R., Leal, J., Gray, A., Scarborough, P., Rayner, M. (2012). *European Cardiovascular Disease Statistics 2012*. European Heart Network, Brussels, European Society of Cardiology, Sophia Antipolis. ISBN 978-2-9537898-1-2.

104. National Heart Foundation of Australia. (2016). Guidelines for the diagnosis and management of hypertension in adults – 2016. Melbourne: National Heart Foundation of Australia. ISBN 978-1-74345-110-6.

105. Obrist, P. A., Light, K. C., McCubbin, J. A., Hutcheson, J. S., Hoffer, J. L. (1978). Pulse transit time: Relationship to blood pressure. *Behavior Research Methods and Instrumentation, 10*(5), 623-626. ISSN 1554-3528.

106. Ochiai, R., Takeda, J., Hosaka, H., Sugo, Y., Tanaka, R., Soma, T. (1999). The relationship between modified pulse wave transit time and cardiovascular changes in isoflurane anethetized dogs. *Journal of Clinical Monitoring and Computing, 15*(7). ISSN 1573-2614.

107. O'Rourke, M. F., Pauca, A., Jiang, X. (2001). Pulse wave analysis. *British Journal of Clinical Pharmacology, 51*(6), 507-522. ISSN 1365-2125.

108. Osterhues, H. H., Hanzel, S. R., Kochs, M., Hombach, V. (1997). Influence of Physical Activity on 24-Hour Measurements of Heart Rate Variability in Patients with Coronary Artery Disease. *The American Journal of Cardiology, 80*(11), 1434-1437. ISNN 0002-9149.

109. Oweis, R. J., Al-Tabbaa, B. O. (2014). QRS Detection and Heart Rate Variability Analysis: A Survey. *Biomedical Science and Engineering, 2*(1), 13-34. ISSN 1937-688X.

110. Pagani, M., Lombardi, F., Guzzetti, S., Rimoldi, O., Furlan, R., Pizzinelli, P., Sandrone, G., Malfatto, G., Dell'Orto, S., Piccaluga, E., Turiel, M., Baselli, G., Cerutti, S., Malliani, A. (1986). Power Spectral Analysis of Heart Rate and Arterial Pressure Variabilities as a Marker of Sympatho-Vagal Interaction in Man and Conscious Dog. *Circulation Research, 59*(2), 178-193. ISSN 1524-4571.

111. Pan, J., Tompkins, W. J. (1985). A Real Time QRS Detection Algorithm. *IEEE Transactions on Biomedical Engineering, BME-32*(3), 230-236. ISSN 0018-9294.

112. Parati, G., Castiglioni, P., di Rienzo, M., Omboni, S., Pedotti, A., Mancia, G. (1990). Sequential Spectral Analysis of 24-Hour Blood Pressure and Pulse Interval in Humans. *Hypertension, 16*(4), 414-421. ISSN 1524-4563.

113. Parati, G., Faini, A., Valentini, M. (2006). Blood pressure variability: its measurement and significance in hypertension. *Current Hypertension Reports, 8*(3), 199-204. ISSN 1534-3111.

114. Parati, G., Ochoa, J. E., Bilo, G. (2012). Blood Pressure Variability, Cardiovascular Risk, and Risk for Renal Disease Progression. *Current Hypertension Reports, 14*(5), 421-431. ISSN 1534-3111.

115. Parati, G., Ochoa, J. E., Lombardi, C., Bilo, G. (2013a). Assessment and management of blood-pressure variability. *Nature Reviews Cardiology, 10*(3), 143-155. ISSN 1759-5010.

116. Parati, G., Ochoa, J. E., Salvi, P., Lombardi, C., Bilo, G. (2013b). Prognostic Value of Blood Pressure Variability and Average Blood Pressure Levels in Patients With Hypertension and Diabetes. *Diabetes Care, 36*(Suppl 2), S312-S324. ISSN 1935-5548.

117. Parati, G., Omboni, S., Rizzoni, D., Agabiti-Rosei, E., Mancia, G. (1998). The smoothness index: a new, reproducible and clinically relevant measure of the homogeneity of the blood pressure reduction with treatment for hypertension. *Journal of Hypertension, 16*(11), 1685-1691. ISSN 1473-5598.

118. Parati, G., Pomidossi, G., Albini, F., Malaspina, D., Mancia, G. (1987). Relationship of 24-Hour Blood Pressure Mean and Variability to Severity of Target-Organ Damage in Hypertension. *Journal of Hypertension, 5*(1), 93-98. ISSN 1473-5598.

119. Parati, G., Saul, J. P., di Rienzo, M., Mancia, G. (1995). Spectral Analysis of Blood Pressure and Heart Rate Variability in Evaluating Cardiovascular Regulation. A Critical Appraisal. *Hypertension, 25*(6), 1276-1286. ISSN 1524-4563.

120. Pfeifer, M. A., Cook, D., Brodsky, J., Tice, D., Reenan, A., Swedine, S., Halter, J. B., Porte, D. (1982). Quantitative evaluation of cardiac parasympathetic activity in normal and diabetic man. *Diabetes, 31*(4), 339-345. ISSN 1939-327X.

121. Pickering, T. G., Hall, J. E., Appel, L. J., Falkner, B. E., Graves, J., Hill, M. N., Jones, D. W., Kurtz, T., Sheps, S. G., Roccella, E. J. (2005). Recommendations for Blood Pressure Measurement in Humans and Experimental Animals. Part 1: Blood Pressure Measurement in Humans: A Statement for Professionals From the Subcommittee of Professional and Public Education of the American Heart Association Cou. *Hypertension, 45*(1), 142-161. ISSN 1524-4563.

122. Pikkujämsä, S. M., Mäkikallio, T. H., Sourander, L. B., Räihä, I. J., Puukka, P., Skyttä, J., Huikuri, H. V. (1999). Cardiac interbeat interval dynamics from childhood to senescence comparison of conventional and new measures based on fractals and chaos theory. *Circulation, 100*(4), 393-399. ISSN 1524-4539.

123. Pilch, W., Szyguła, Z., Palka, T., Pilch, P., Cison, T., Wiecha, S., Tota, Ł. (2014). Comparison of Physiological Reactions and Physiological Strain in Healthy Men under Heat Stress in Dry and Steam Heat Saunas. *Biology of Sport, 31*(2), 145-149. ISSN 2083-1862.

124. Pomeranz, B., Macaulay, R. J., Caudill, M. A., Kutz, I., Adam, D., Gordon, D., Kilborn, K. M., Barger, A. C., Shannon, D. C., Cohen, R. J., Benson, H. (1985). Assessment of autonomic function in humans by heart rate spectral analysis. *American Journal of Physiology - Heart and Circulatory Physiology, 248*(1), H151-H153. ISSN 1522-1539.

125. Poon, C. C. Y., Zhang, Y. T. (2005). Cuff-less and Noninvasive Measurements of Arterial Blood Pressure by Pulse Transit Time. *In Proceedings of the 27th Annual conference of IEEE Engineering in Medicine and Biology* (pp. 5877-5880). Shanghai: IEEE. ISSN 1094-687X.

126. Quinaglia, T., Martins, L. C., Figueiredo, V. N., Santos, R. C., Yugar-Toledo, J. C., Vilela Martin, J. F., Demacq, C., Pimenta, E., Calhoun, D. A., Moreno Jr, H. (2011). Non-dipping pattern relates to endothelial dysfunction in patients with uncontrolled resistant hypertension. *Journal of Human Hypertension, 25*(11), 656-664. ISSN 1476-5527.

127. Racinais, S., Gaoua, N., Grantham, J. (2008). Hyperthermia impairs short-term memory and peripheral motor drive transmission. *Journal of Physiology, 586*(19), 4751-4762. ISSN 00-3751.

128. Ramaekers, D., Ector, H., Aubert, A. E., Rubens, A., Van de Werf, F. (1998). Heart rate variability and heart rate in healthy volunteers. Is the female autonomic nervous system cardioprotective? *European Heart Journal, 19*(9), 1334-1341. ISSN 1522-9645.

129. Rapalis, A., Janušauskas, A., Lukoševičius, A., Marozas, V. (2014). Noise resistant method for cardiac pulse wave arrival time estimation. *Elektronika ir elektrotechnika, 20*(8), 59-62. ISSN 2029-5731.

130. Rapalis, A., Janušauskas, A., Marozas, V., Lukoševičius, A. (2016). Estimation of blood pressure variability during orthostatic test using instantaneous photoplethysmogram frequency and pulse arrival time. *Biomedical Signal Processing and Control*. ISSN 1746-8094.

131. Rapalis, A., Marozas, V. (2012). Nuolatinis kraujo spaudimo registravimas remiantis pulso bangos sklidimo laiku. *In Proceedings of Telecomunications and Electronics – 2012* (pp. 73-77). Kaunas: Technologija. ISBN 978-6-0902030-4-0.

132. Remington, J. W. (1963). The Physiology of the Aorta and Major Arteries. In W. F. Hamilton, *Handbook of Physiology* (Vol. 2, pp. 799-838). Washington, DC, USA: American Physiology Society.

133. Rothwell, P. M., Howard, S. C., Dolan, E., O'Brien, E., Dobson, J. E., Dahlöf, B., Sever, P. S., Poulter, N. R. (2010). Prognostic significance of visit-to-visit variability, maximum systolic blood pressure, and episodic hypertension. *The Lancet, 375*(9718), 895-905. ISSN 0140-6736.

134. Sahoo, A., Manimegalai, P., Thanushkodi, K. (2011). Wavelet Based Pulse Rate and Blood Pressure Estimation System from ECG and PPG Signals. *In Proceedings of International Conference on Computer, Communication and Electrical Technology – ICCCET2011* (pp. 285-289). Tamilnadu: IEEE. ISBN 978-1-4244939-4-4.

135. Sayers, B. M. (1973). Analysis of heart rate variability. *Ergonomics, 16*(1), 17-32. ISSN 1366-5847.

136. Sands, K. E., Appel, M. L., Lilly, L. S., Schoen, F. F., Mudge, G. H., Cohen, R. J. (1989). Power Spectrum Analysis of Heart Rate Variability in Human Cardiac Transplant Recipients. *Circulation, 79*(1), 76-82. ISSN 1524-4539.

137. Schillaci, G., Bilo, G., Pucci, G., Laurent, S., Macquin-Mavier, I., Boutouyrie, P., Battista, F., Settimi, L., Desamericq, G., Dolbeau, G., Faini, A., Salvi, P., Mannarino, E., Parati, G. (2012). Relationship Between Short-term Blood Pressure Variability and Large-Artery Stiffness in Human Hypertension: Findings From 2 Large Databases. *Hypertension, 60*(2), 369-377. ISSN 1524-4563.

138. Singh, J. P., Larson, M. G., O'Donnell, C. J., Wilson, P. F., Tsuji, H., Lloyd-Jones, D. M., Levy, D. (2000). Association of hyperglycemia with reduced heart rate variability (The Framingham Heart Study). *The American Journal of Cardiology, 86*(3), 309-312. ISNN 0002-9149.

139. Sinnreich, R., Kark, J. D., Friedlander, Y., Sapoznikov, D., Luria, M. H. (1998). Five minute recordings of heart rate variability for population studies: repeatability and age–sex characteristics. *Heart, 80*(2), 156-162. ISSN 1468-201X.

140. Sloan, R. P., Shapiro, P. A., Bagiella, E., Myers, M. M., Bigger, J. T., Steinman, R. C. (1994). Brief interval heart period variability by different methods of analysis correlates highly with 24-h analyses in normal. *Biological Psychology, 38*(2-3), 133-142. ISSN 0301-0511.

141. Smith, R. P., Argod, J., Pepin, J. L., Levy, P. A. (1999). Pulse transit time: an appraisal of potential clinical applications. *Thorax, 54*(3), 452-458. ISSN 1468-3296.

142. Sohar, E., Shoenfeld, Y., Shapiro, Y., Ohry, A., Cabili, S. (1976). Effects of exposure to Finnish sauna. *Israel Journal of Medical Sciences, 12*(11), 1275-1282. ISSN 0021-2180.

143. Spallone, V., Bernardi, L., Ricordi, L., Soldà, P., Maiello, M. R., Calciati, A., Gambardella, S., Fratino, P., Menzinger, G. (1993). Relationship between the circadian rhythms of blood pressure and sympathovagal balance in diabetic autonomic neuropathy. *Diabetes, 42*(12), 1745-1752. ISSN 1939-327X.

144. Stauss, H. M. (2007). Identification of blood pressure control mechanisms by power spectral analysis. *Clinical and Experimental Pharmacology and Physiology, 34*(4), 362-368. ISSN 1440-1681.

145. Stein, P. K., Kleiger, R. E., Rottman, J. N. (1997). Differing effects of age on heart rate variability in men and women. *The American Journal of Cardiology, 80*(3), 302-305. ISNN 0002-9149.

146. Stephenson, L. A., Kolka, M. A. (1988). Plasma volume during heat stress and exercise in women. *European Journal of Applied Physiology, 57*(4), 373-381. ISSN 1439-6327.

147. Stolarz-Skrzypek, K., Thijs, L., Richart, T., Li, Y., Hansen, T. W., Boggia, J., Kuznetsova, T., Kikuya, M., Kawecka-Jaszcz, K., Staessen, J. A. (2010). Blood pressure variability in relation to outcome in the International Database of Ambulatory blood pressure in relation to Cardiovascular Outcome. *Hypertension Research, 33*(8), 757-766. ISSN 1348-4214.

148. Sugo, Y., Ukawa, T., Takeda, S., Ishihara, H., Kazama, T., Takeda, J. (2010). A Novel Continuous Cardiac Output Monitor Based on Pulse Wave Transit Time. *In Proceedings of 32nd Annual International Conference of the IEEE Engineering in Medicine and Biology* (pp. 2853-2856). Buenos Aires: IEEE. ISSN 1094-687X.

149. Sutkowy, P., Woźniak, A., Boraczyński, T., Mila-Kierzenkowska, C., Boraczyński, M. (2014). The effect of a single Finnish sauna bath after aerobic exercise on the oxidative status in healthy men. *Scandinavian Journal of Clinical and Laboratory Investigation, 74*(2), 89-94. ISSN 1502-7686.

150. Špulák, D., Čmejla, R., Fabián, V. (2011). Parameters for mean blood pressure estimation based on electrocardiography and photoplethysmography. *In Proceedings of International Applied Electronics Conference* (pp. 1-4). Pilsen: IEEE. ISSN 1803-7232.

151. Teng, X. F., Poon, C. C. Y., Zhang, C., Zhang, Y. T. (2004). Study on the Effect of Contacting Force on Pulse Transit Time. *In proceedings of Internaional IEEE-EMBS International Workshop on Computer Architectures for Machine Perception* (pp. 111-114). Hong Kong: IEEE. ISBN 0-7803861-2-4.

152. Thayera, J. F., Yamamotob, S. S., Brosschotc, J. F. (2010). The relationship of autonomic imbalance, heart rate variability and cardiovascular disease risk factors. *International Journal of Cardiology, 141*(2), 122-131. ISSN 0167-5273.

153. Tsui, P. H., Chang, C. C., Huang, N. E. (2010). Noise-Modulated Empirical Mode Decomposition. *Advances in Adaptive Data Analysis, 2*(1), 25-37. ISSN 1793-7175.

154. Uehara, A., Kurata, C., Sugi, T., Mikami, T., Shouda, S. (1999). Diabetic cardiac autonomic dysfunction: parasympathetic versus sympathetic. *Annals of Nuclear Medicine, 13*(2), 95-100. ISSN 1864-6433.

155. Umetani, K., Singer, D. H., McCraty, R., Atkinson, M. (1998). Twenty-Four Hour Time Domain Heart Rate Variability and Heart Rate: Relations to Age and Gender Over Nine Decades. *Journal of the American College of Cardiology, 31*(3), 593-601. ISSN 0735-1097.

156. van Ravenswaaij-Arts, C., Hopman, J. C., Kollée, L. A., van Amen, J. P., Stoelinga, G., van Geijn, H. P. (1991). Influences on Heart Rate Variability in Spontaneously Breathing Preterm Infants. *Early Human Development, 27*(3), 187-205. ISSN 0378-3782.

157. Vardoulis, O., Papaioannou, T. G., Stergiopulos, N. (2013). Validation of a novel and existing algorithms for the estimation of pulse transit time: advancing the accuracy in pulse wave velocity measurement. *American Journal of Physiology - Heart and Circulatory Physiology, 304*(11), H1558-H1567. ISSN 1522-1539.

158. Verdecchia, P., Angeli, F., Mazzotta, G., Garofoli, M., Ramundo, E., Gentile, G., Ambrosio, G., Reboldi, G. (2012). Day-Night Dip and Early-Morning Surge in Blood Pressure in Hypertension: Prognostic Implications. *Hypertension, 60*(1), 34-42. ISSN 1524-4563.

159. Verdecchia, P., Schillaci, G., Gatteschi, C., Zampi, I., Battistelli, M., Bartoccini, C., Porcellati, C. (1993). Blunted nocturnal fall in blood pressure in hypertensive women with future cardiovascular morbid events. *Circulation, 88*(3), 986-992. ISSN 1524-4539.

160. Wennerblom, B., Lurje, L., Tygesen, H., Vahisalo, R., Hjalmarson, A. (2000). Patients with uncomplicated coronary artery disease have reduced heart rate variability mainly affecting vagal tone. *Heart, 83*(3), 290-294. ISSN 1468-201X.

161. Wheeler, T., Watkins, P. J. (1973). Cardiac denervation in diabetes. *British Medical Journal, 4*(5892), 584-586. ISSN 007-1447.

162. WHO. (2013). A *global brief on HYPERTENSION. Silent killer, global public health crisis. G*eneva, Switzerland: World Health Organization.

163. WHO. (2014a). *Global health estimates for deaths by cause, age, and sex for years 2000- 2012.* Geneva: World Health Organization. Retrieved from http://www.who.int/healthinfo/global_burden_disease/estimates/en/index1.html

164. WHO. (2014b). *GLOBAL STATUS REPORT on noncommunicable diseases 2014: Attaining the nine global noncommunicable diseases targets; a shared responsibility.* Geneva, Switzerland: World Health Organization. ISBN 978-92-4-156485-4.

165. Wibmer, T., Doering, K., Kropf-Sanchen, C., Rudiger, S., Blanta, I., Stoiber, K. M., Rottbauer, W., Shumann, C. (2014). Pulse transit time and blood pressure during cardiopulmonary exercise tests. *Physiological Research, 63*(3), 287-296. ISSN 1802-9973.

166. Wong, M. Y. M., Pickwell-MacPherson, E., Zhang, Y. T. (2009a). The acute effects of running on blood pressure estimation using pulse transit time in normotensive subjects. *European Journal of Applied Physiology, 107*(2), 169-175. ISSN 1439-6327.

167. Wong, M. Y. M., Pickwell-MacPherson, E., Zhang, Y. T., Cheng, J. C. Y. (2011). The effects of pre-ejection period on post-exercise systolic blood pressure estimation using the pulse arrival time technique. *European Journal of Applied Physiology, 111*(1), 135-144. ISSN 1439-6327.

168. Wong, M. Y. M., Poon, C. C. Y., Zhang, Y. T. (2009b). An evaluation of the cuffless blood pressure estimation based on pulse transit time technique: A half year study on normotensive subjects. *Cardiovascular Engineering, 9*(1), 32-38. ISSN 1573-6806.

169. Wu, D., Yang, P., Liu, G. Z., Zhang, Y. T. (2012). Automatic Estimation of Respiratory Rate from Pulse Transit Time in Normal Subjects at Rest. *Proceedings of the IEEE-EMBS International Conference on Biomedical and Health Informatics (BHI 2012)* (pp. 779-781). Hong Kong: IEEE. ISSN 2168-2194.

170. Wu, Z., Huang, N. E. (2009). Ensemble Empirical Mode Decomposition: A Noise-Assisted Data Analysis Method. *Advances in Adaptive Data Analysis, 1*(1), 1-41. ISSN 1793-7175.

171. Zanoli, L., Rastelli, S., Inserra, G., Castellino, P. (2015). Arterial structure and function in inflammatory bowel disease. *World Journal of Gastroenterology, 21*(40), 11304-11311. ISSN 2219-2840.

172. Zeskind, P. S., Gingras, J. L. (2006). Maternal cigarette-smoking during pregnancy disrupts rhythms in fetal heart rate. *Journal of Pediatric Psychology, 31*(1), 5-14. ISSN 1465-735X.

173. Zhang, J. (2007). Effect of age and sex on heart rate variability in healthy subjects. *Journal of Manipulative and Physiological Therapeutics, 30*(5), 374-379. ISSN 0161-4754.

174. Zhang, Q., Shi, Y., Teng, D., Dinh, A., Ko, S. B., Chen, L., Basran, J., Bello-Haas, V. D., Choi, Y. (2009). Pulse Transit Time-based Blood Pressure Estimation Using Hilbert-Huang Transform. *In Proceedings of 31st Annual International Conference of the IEEE Engineering in Medicine and Biology Society. 2009*, pp. 1785-1788. Minneapolis: IEEE. ISSN 1094-687X.

175. Zhang, R., Zuckerman, J. H., Levine, B. D. (1998). Deterioration of cerebral autoregulation during orthostatic stress: insights from the frequency domain. *Journal of Applied Physiology, 85*(3), 1113-1122. ISSN 1522-1601.

176. Zheng, Y. L., Yan, B. P., Zhang, Y. T., Poon, C. C. Y. (2014). An Armband Wearable Device for Overnight and Cuff-Less Blood Pressure Measurement. *IEEE Transactions on Biomedical Engineering, 61*(7), 2179-2186. ISSN 0018-9294.

177. Zielinski, T. P. (1996). Instantaneous Phase Shift Estimation Methods. *In Proceedings of the Instrumentation and Measurement Technology Conference. 1*, pp. 162-167. Brussels: IEEE. ISBN 0-7803-3312-8.

178. Zygmunt, A., Stanczyk, J. (2010). Methods of evaluation of autonomic nervous system function. *Archives of Medical Science, 6*(1), 11-18. ISSN 1896-9151.

179. Zoccali, C., Ciccarelli, M., Maggiore, Q. (1982). Defective Reflex Control of Heart Rate in Dialysis Patients: Evidence for an Afferent Autonomic Lesion. *Clinical Science, 63*(3), 285-292. ISSN 1470-8736.

180. Zong, W., Moody, G. B., Mark, R. G. (1998). Effects of vasoactive drugs on the relationship between ECG-pulse wave delay time and arterial blood pressure in ICU patients. *In Proceedings of Computers in Cardiology Conference. 25*, pp. 673-676. Cleveland: IEEE. ISSN 0276-6547.

LIST OF THE PUBLICATIONS RELATED TO THE DOCTORAL THESIS

Publications referred in Journals on the master list of Thomson Reuters Web of Science (with impact factor)

1. Rapalis, A., Janušauskas, A., Lukoševičius, A., Marozas, V., Noise resistant method for cardiac pulse wave arrival time estimation // Elektronika ir elektrotechnika. Kaunas: KTU. ISSN 1392-1215. 2014, Vol. 20, No. 8, p. 59-62. DOI: http://dx.doi.org/10.5755/j01.eee.20.8.8442. [Science Citation Index Expanded (Web of Science); Academic Search Premier; Compendex; Inspec; MEDLINE; Science Direct]. [IF (E): 0.561 (2014)].
2. Rapalis, A., Janušauskas, A., Marozas, V., Lukoševičius, A., Estimation of Blood Pressure Variability during Orthostatic Test Using Instantaneous Photoplethysmogram Frequency and Pulse Arrival Time // *Biomedical Signal Processing and Control*. ISSN 1746-8094. 2016, DOI: 10.1016/j.bspc.2016.10.014. [Science Citation Index Expanded (Web of Science); Academic Search Premier; Compendex; Inspec; MEDLINE; Science Direct]. [IF (E): 1.521 (2015)].

Publications in Reviewed Proceedings of International Scientific Conferences

1. Rapalis, A., Janušauskas, A., Marozas, V., Pulse arrival time estimation based on fundamental frequency component extraction // *Biomedical Engineering - 2013: Proceedings of International Conference, Kaunas University of Technology, 28, 29 November, 2013* / Kaunas University of Technology. Kaunas: Technologija. ISSN 2029-3380. 2013, pp. 82-86.
2. Rapalis, A., Marozas, V., Kraujo spaudimo pulsinės bangos atvykimo laiko vertinimas panaudojant multimodalinius fiziologinius signalus, *Mokslas – sveikatai: Proceedings of Conference, Lithuanian University of Health Sciences, 9 April, 2014* / Lithuania University of Health Sciences. Kaunas.
3. Rapalis, A., Janušauskas, A., Lukoševičius, A., Marozas, V., Noise Resistant Method for Cardiac Pulse Wave Arrival Time Estimation // *ELECTRONICS 2014*, 16-18 June, 2014 / Kaunas University of Technology. Palanga.
4. Černych, M., Šatas, A., Rapalis, A., Baranauskienė, N., Paulauskas, H., Eimantas, N., Brazaitis, M., Effects of the induced evening thermal stress for nightly and morning functional efficiency of cognitive system // *Current Issues and New Ideas in Sport Science: Proceedings of 9th conference of the Baltic sport science society, Lithuanian Sports University, 27-29 April, 2016* / Lithuanian Sports University. Kaunas: Lithuanian Sports University. ISBN: 978-609-8040-96-8. 2016, pp. 107-108.

5. Lázaro, Jesús; Bailón, Raquel; Laguna, Pablo; Marozas, Vaidotas; Rapalis, Andrius; Gil, Eduardo. Difference in pulse arrival time at forehead and at finger as a surrogate of pulse transit time // *Computing in cardiology 2016: [43th conference], September 11-14, 2016 Vancouver, Canada*. New York: IEEE. ISSN 2325-8861. 2016, vol. 43, p. 269-272.
6. Patašius, Martynas; Kriščiūnas, Andrius; Rapalis, Andrius; Barauskas, Rimantas; Janušauskas, Artūras; Čalnerytė, Dalia; Nečiūnas, Audrius. Exploration of modelling of blood flow through the arterial tree using phase error reducing finite element model // *Biomedical engineering 2016: proceedings of international conference / Kaunas University of Technology, Lithuanian Society for Biomedical Engineering*. Kaunas: Kauno technologijos universitetas. ISSN 2029-3380. 2016, p. 157-161.

SL344. 2017-05-03, 16,75 leidyb. apsk. l., Tiražas 12 egz.
Išleido Kauno technologijos universitetas, K. Donelaičio g. 73, 44249 Kaunas
Spausdino leidyklos „Technologija“ spaustuvė, Studentų g. 54, 51424 Kaunas

APPENDIX

Study No. 1: orthostatic test

Time-domain parameters of RRI, SBP, DBP, PAT, IF1, and IF2 during the orthostatic test. The results are expressed as box plots with a median (line inside box), 25% and 75% quartiles (box), range (whiskers) and outliers (plus).

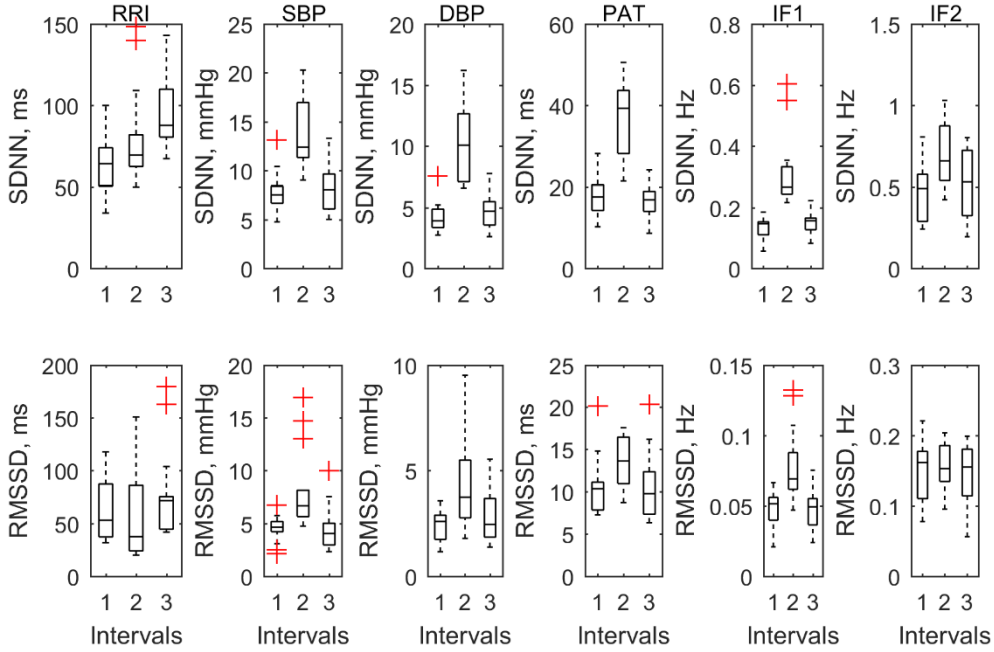

The changes of time-domain parameters between intervals I–II and II–III (data normalized by interval II (standing).

	SDNN Intervals			RMSSD Intervals		
	I	II	III	I	II	III
RRI	0.81 ±0.24	1	1.21 ±0.32	1.10 ±0.51	1	1.35 ±0.76
SBP	0.57 ±0.16	1	0.59 ±0.17	0.55 ±0.15	1	0.55 ±0.26
DBP	0.42 ±0.12	1	0.46 ±0.14	0.53 ±0.18	1	0.61 ±0.26
PAT	0.49 ±0.13	1	0.46 ±0.12	0.80 ±0.26	1	0.79 ±0.30
IF1	0.43 ±0.11	1	0.48 ±0.13	0.61 ±0.17	1	0.61 ±0.18
IF2	0.68 ±0.24	1	0.75 ±0.30	0.98 ±0.29	1	0.93 ±0.29

Frequency-domain parameters of RRI, SBP, DBP, PAT, IF1, and IF2 during the orthostatic test. The results are expressed as box plots with a median (line inside box), 25% and 75% quartiles (box), range (whiskers) and outliers (plus).

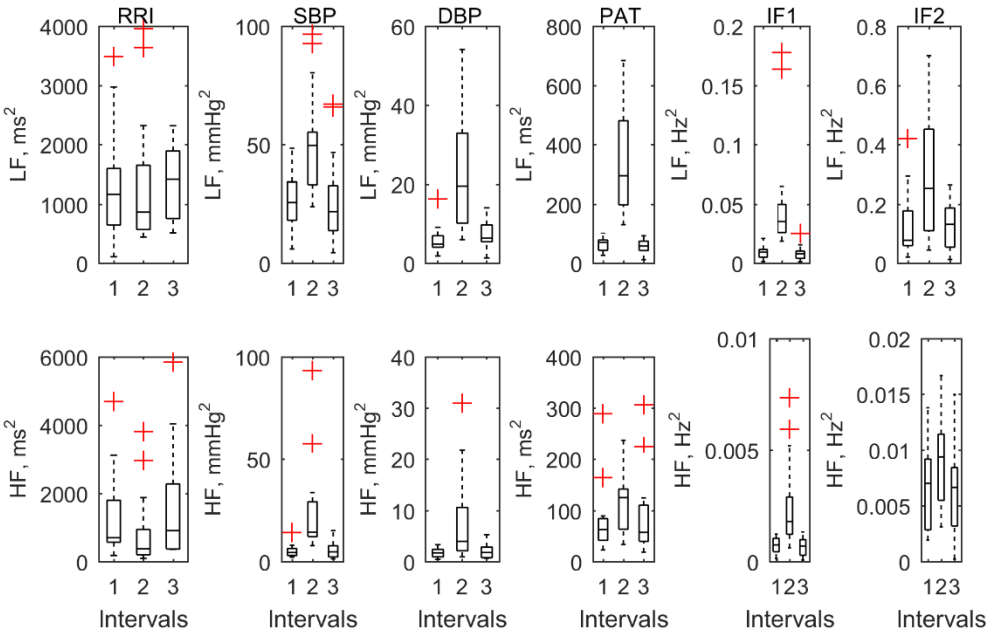

The changes of frequency-domain parameters between intervals I–II and II–III (data normalized by interval II (standing).

	LF Intervals			HF Intervals		
	I	II	III	I	II	III
RRI	0.99 ± 0.78	1	1.01 ± 0.43	1.40 ± 1.37	1	1.69 ± 1.78
SBP	0.51 ± 0.23	1	0.54 ± 0.38	0.21 ± 0.13	1	0.23 ± 0.16
DBP	0.26 ± 0.15	1	0.31 ± 0.17	0.22 ± 0.12	1	0.26 ± 0.18
PAT	0.19 ± 0.07	1	0.17 ± 0.07	0.69 ± 0.60	1	0.76 ± 0.71
IF1	0.17 ± 0.10	1	0.16 ± 0.12	0.28 ± 0.13	1	0.26 ± 0.16
IF2	0.44 ± 0.38	1	0.44 ± 0.28	0.77 ± 0.42	1	0.70 ± 0.44

Study No. 2: thermal stress test

Mean of RRI, SBP, DBP, PAT, IF1, and IF2 of all subjects of experiment E1D2. * – statistically significant difference ($p \leq 0.05$) between a particular interval and interval I.

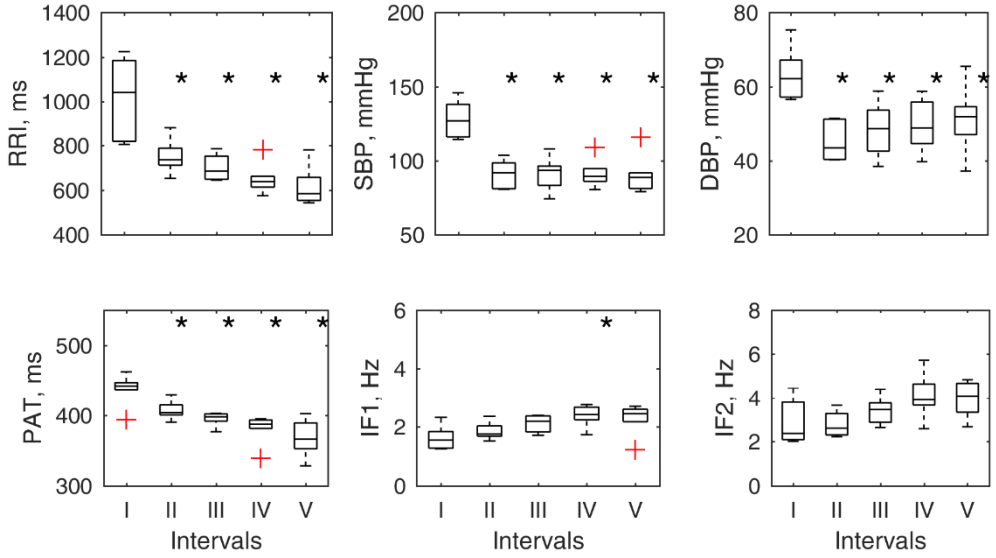

Mean of RRI, SBP, DBP, PAT, IF1, and IF2 of all subjects of experiment E2D1. * – statistically significant difference ($p \leq 0.05$) between a particular interval and interval I.

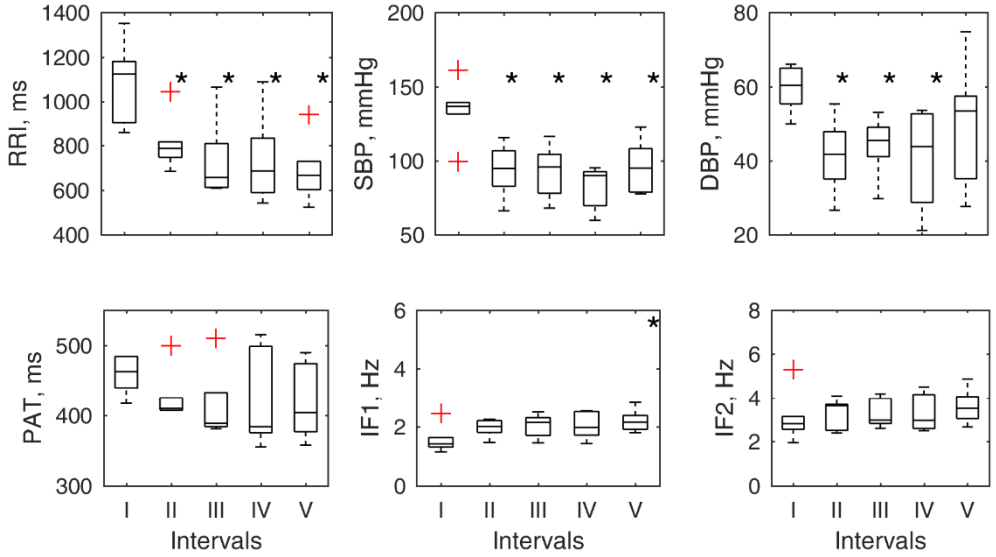

Mean of RRI, SBP, DBP, PAT, IF1, and IF2 of all subjects of experiment E2D2. * – statistically significant difference ($p \leq 0.05$) between a particular interval and interval I.

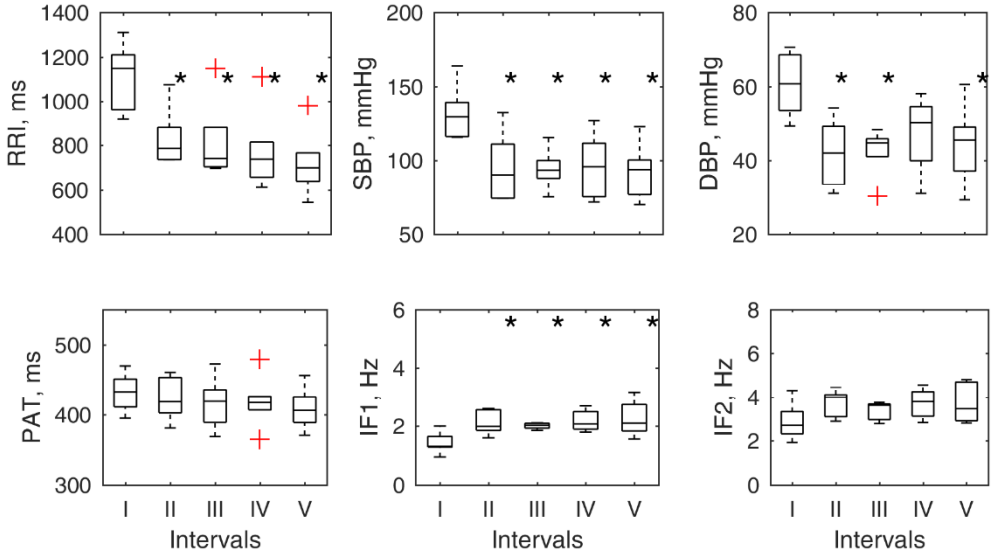

Mean of RRI, SBP, DBP, PAT, IF1, and IF2 of all subjects of experiment C1D1. * – statistically significant difference ($p \leq 0.05$) between a particular interval and interval I.

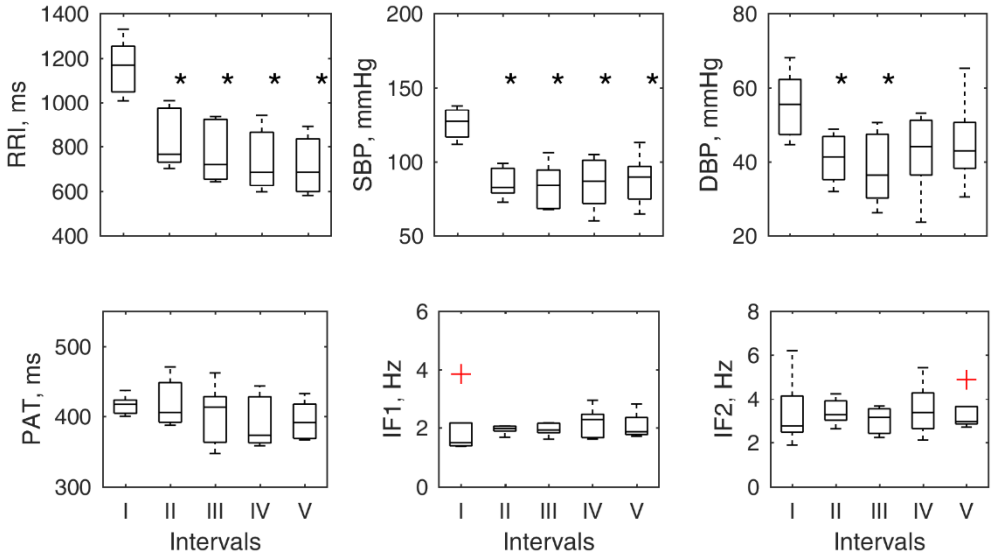

Mean of RRI, SBP, DBP, PAT, IF1, and IF2 of all subjects of experiment C1D2. * – statistically significant difference ($p \leq 0.05$) between a particular interval and interval I.

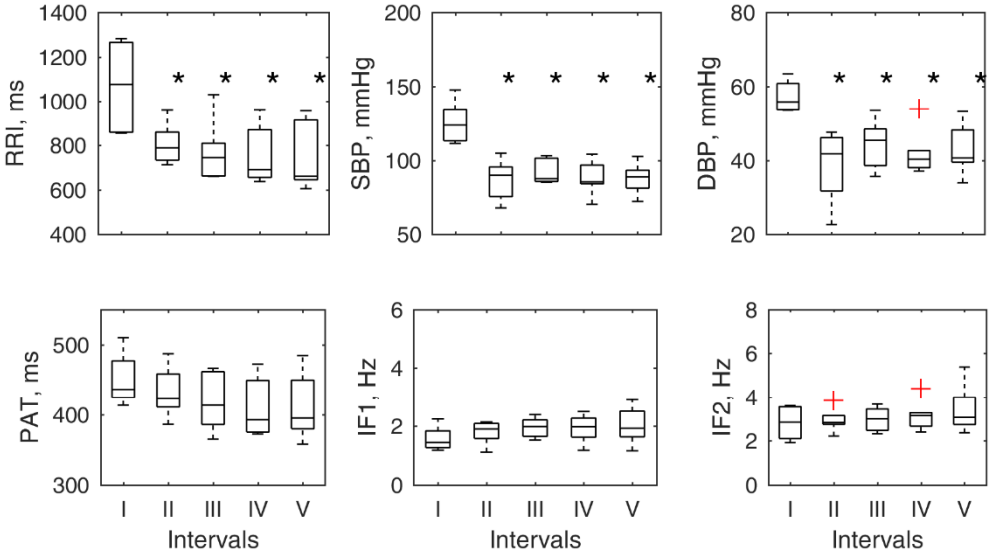

Time-domain parameters of RRI, SBP, DBP, PAT, IF1, and IF2 at five rest intervals of all experiments E1D1. The results are expressed as box plots with a median (line inside box), 25% and 75% quartiles (box), range (whiskers) and outliers (plus).

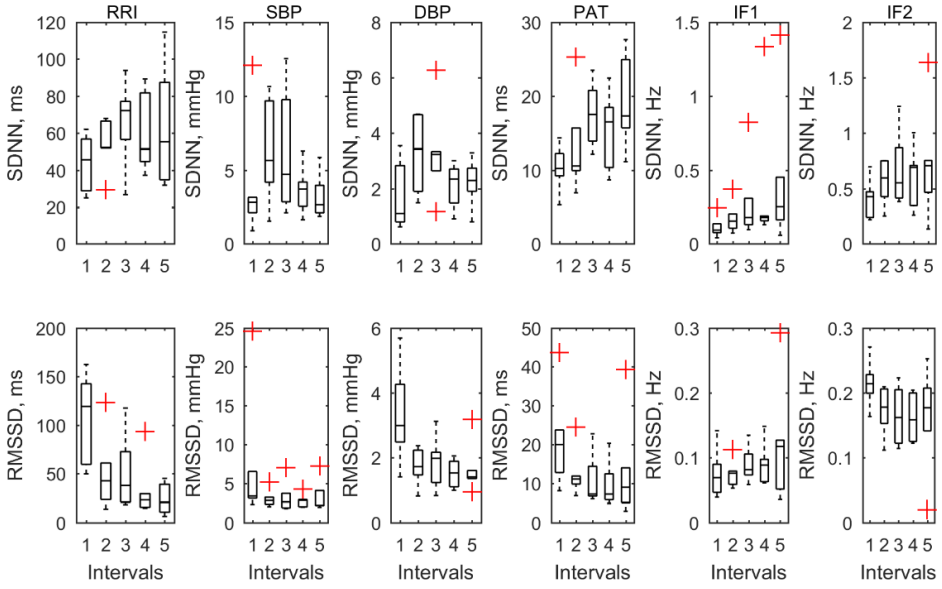

Time-domain parameters of RRI, SBP, DBP, PAT, IF1, and IF2 at five rest intervals of all experiments E1D2. The results are expressed as box plots with a median (line inside box), 25% and 75% quartiles (box), range (whiskers) and outliers (plus).

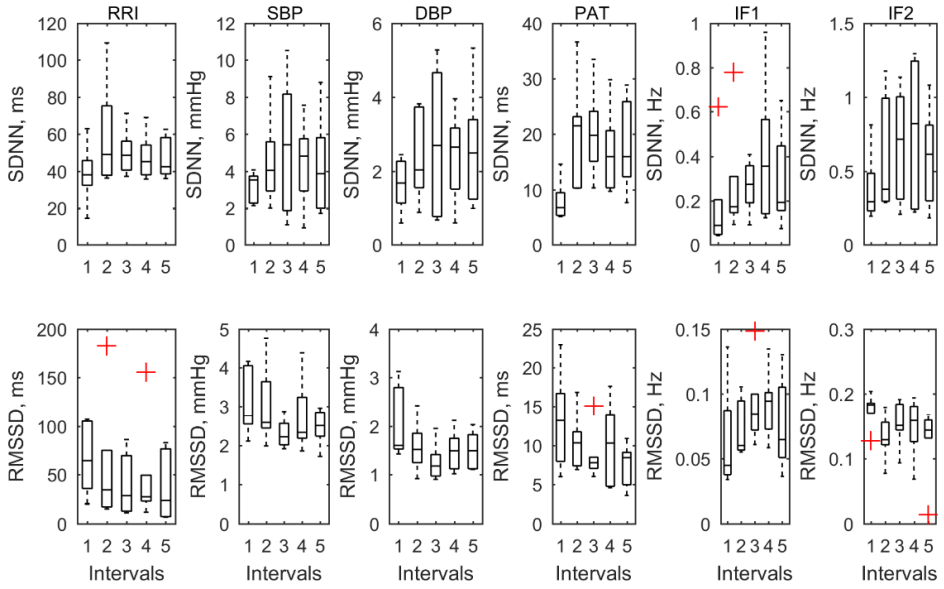

Time-domain parameters of RRI, SBP, DBP, PAT, IF1, and IF2 at five rest intervals of all experiments E2D1. The results are expressed as box plots with a median (line inside box), 25% and 75% quartiles (box), range (whiskers) and outliers (plus).

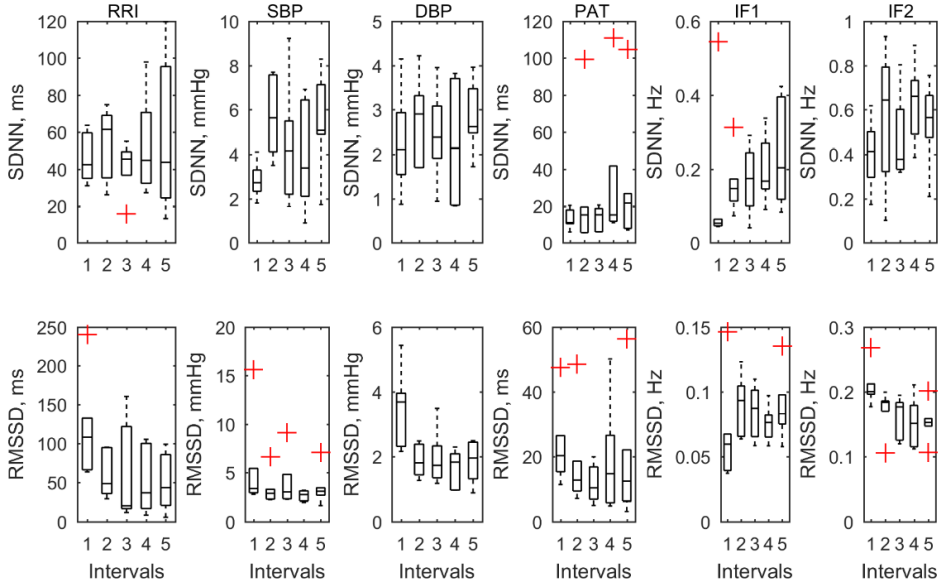

Time-domain parameters of RRI, SBP, DBP, PAT, IF1, and IF2 at five rest intervals of all experiments E2D2. The results are expressed as box plots with a median (line inside box), 25% and 75% quartiles (box), range (whiskers) and outliers (plus).

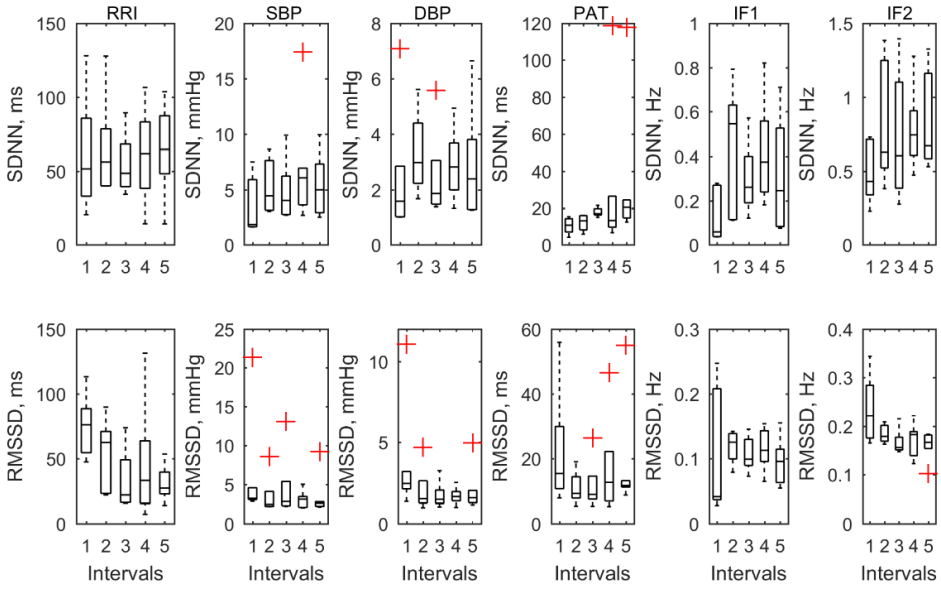

Time-domain parameters of RRI, SBP, DBP, PAT, IF1, and IF2 at five rest intervals of all experiments C1D1. The results are expressed as box plots with a median (line inside box), 25% and 75% quartiles (box), range (whiskers) and outliers (plus).

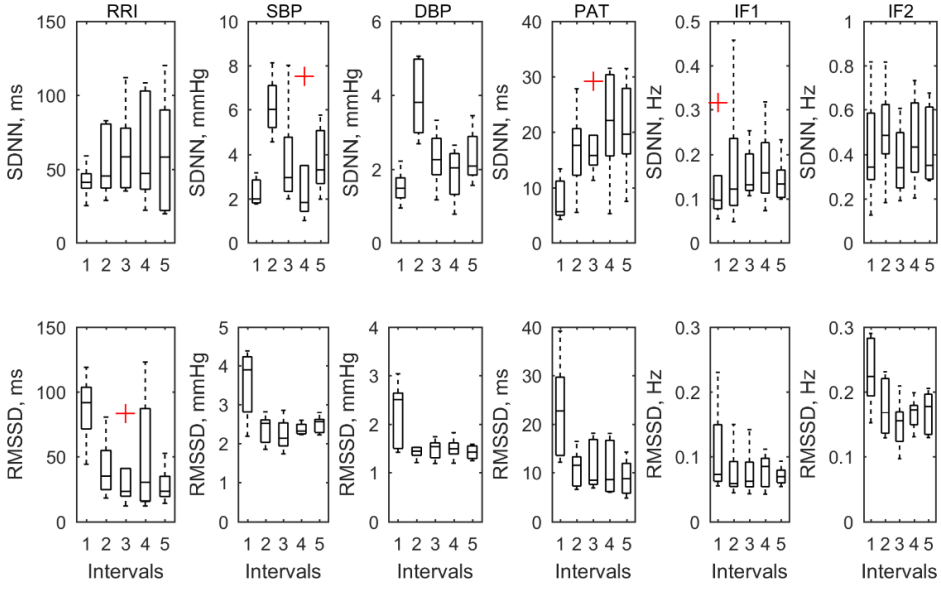

Time-domain parameters of RRI, SBP, DBP, PAT, IF1, and IF2 at five rest intervals of all experiments C1D2. The results are expressed as box plots with a median (line inside box), 25% and 75% quartiles (box), range (whiskers) and outliers (plus).

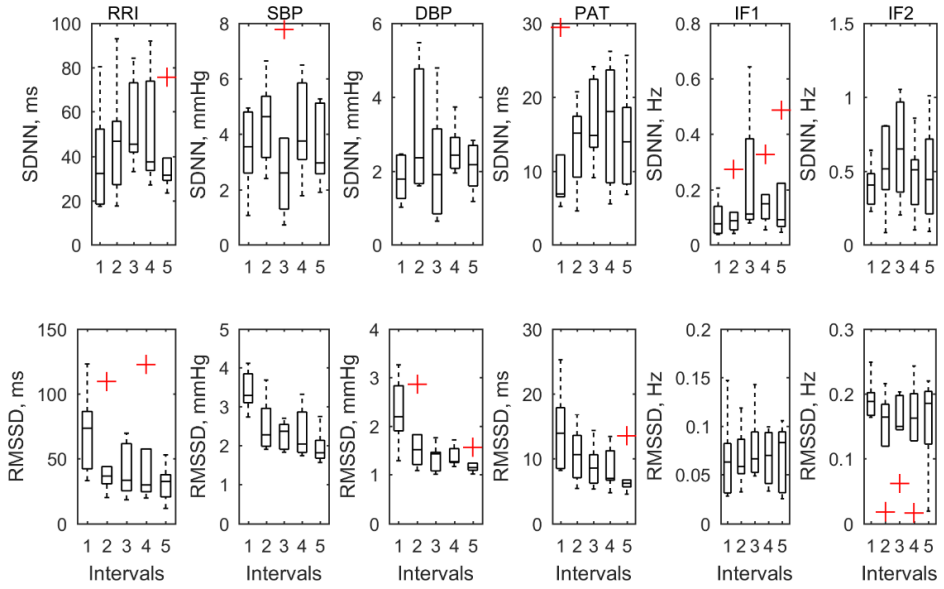

The changes between intervals of time-domain parameters (SDNN and RMSSD) of experiment E1D1 (data normalized by interval I).

			SDNN Intervals		
	I	II	III	IV	V
RRI	1	0.81 ± 0.21	0.88 ± 0.24	0.73 ± 0.26	0.74 ± 0.35
SBP	1	1.23 ± 0.73	1.21 ± 0.73	0.92 ± 0.54	0.82 ± 0.40
DBP	1	1.05 ± 0.45	1.02 ± 0.31	0.78 ± 0.23	0.82 ± 0.28
PAT	1	1.12 ± 0.45	1.11 ± 0.32	1.10 ± 0.41	1.49 ± 1.26
IF1	1	2.17 ± 2.49	2.53 ± 2.07	2.81 ± 2.15	2.82 ± 2.40
IF2	1	1.25 ± 0.73	1.28 ± 0.52	1.32 ± 0.39	1.26 ± 0.52
			RMSSD Intervals		
	I	II	III	IV	V
RRI	1	0.45 ± 0.24	0.45 ± 0.22	0.32 ± 0.20	0.25 ± 0.14
SBP	1	0.68 ± 0.32	0.68 ± 0.35	0.65 ± 0.36	0.69 ± 0.39
DBP	1	0.56 ± 0.15	0.59 ± 0.15	0.52 ± 0.19	0.52 ± 0.14
PAT	1	0.64 ± 0.18	0.52 ± 0.16	0.51 ± 0.28	0.83 ± 1.11
IF1	1	1.23 ± 0.84	1.36 ± 0.64	1.38 ± 0.65	1.66 ± 1.17
IF2	1	0.81 ± 0.19	0.76 ± 0.15	0.75 ± 0.14	0.73 ± 0.33

The changes between intervals of time-domain parameters (SDNN and RMSSD) of experiment E1D2 (data normalized by interval I).

			SDNN Intervals		
	I	II	III	IV	V
RRI	1	1.18 ± 0.47	0.93 ± 0.24	0.99 ± 0.42	0.83 ± 0.26
SBP	1	1.08 ± 0.34	1.08 ± 0.49	1.09 ± 0.51	1.01 ± 0.51
DBP	1	0.95 ± 0.33	0.97 ± 0.46	0.98 ± 0.42	1.01 ± 0.50
PAT	1	1.50 ± 0.58	1.39 ± 0.45	1.50 ± 0.57	1.30 ± 0.22
IF1	1	2.35 ± 2.02	3.05 ± 2.25	3.61 ± 2.96	3.33 ± 3.21
IF2	1	1.31 ± 0.78	1.57 ± 0.57	1.60 ± 0.54	1.36 ± 0.67
			RMSSD Intervals		
	I	II	III	IV	V
RRI	1	1.04 ± 1.22	0.67 ± 0.54	1.00 ± 1.08	0.63 ± 0.57
SBP	1	0.99 ± 0.25	0.78 ± 0.16	0.94 ± 0.41	0.84 ± 0.23
DBP	1	0.80 ± 0.19	0.65 ± 0.13	0.83 ± 0.37	0.81 ± 0.28
PAT	1	0.99 ± 0.63	0.76 ± 0.37	0.92 ± 0.70	0.65 ± 0.38
IF1	1	1.41 ± 0.74	1.97 ± 1.32	1.86 ± 1.07	1.68 ± 1.34
IF2	1	0.75 ± 0.15	0.86 ± 0.14	0.82 ± 0.18	0.69 ± 0.30

The changes between intervals of time-domain parameters (SDNN and RMSSD) of experiment E2D1 (data normalized by interval I).

			SDNN Intervals		
	I	II	III	IV	V
RRI	1	0.78 ± 0.28	0.73 ± 0.50	0.75 ± 0.40	0.78 ± 0.56
SBP	1	1.31 ± 0.57	1.12 ± 0.56	1.03 ± 0.29	1.19 ± 0.58
DBP	1	0.90 ± 0.37	0.77 ± 0.16	0.74 ± 0.19	1.89 ± 0.36
PAT	1	1.11 ± 0.56	0.99 ± 0.09	1.28 ± 0.80	1.34 ± 0.87
IF1	1	2.09 ± 0.90	2.14 ± 1.10	2.21 ± 1.42	2.76 ± 1.50
IF2	1	1.25 ± 0.43	1.17 ± 0.48	1.43 ± 0.36	1.30 ± 0.45
			RMSSD Intervals		
	I	II	III	IV	V
RRI	1	0.53 ± 0.24	0.68 ± 1.04	0.55 ± 0.59	0.55 ± 0.56
SBP	1	0.75 ± 0.28	0.74 ± 0.24	0.76 ± 0.18	0.76 ± 0.31
DBP	1	0.54 ± 0.09	0.51 ± 0.14	0.53 ± 0.23	0.56 ± 0.25
PAT	1	0.73 ± 0.24	0.62 ± 0.23	0.61 ± 0.29	0.67 ± 0.35
IF1	1	1.54 ± 0.54	1.48 ± 0.78	1.16 ± 0.38	1.58 ± 0.72
IF2	1	0.83 ± 0.20	0.77 ± 0.20	0.73 ± 0.18	0.75 ± 0.19

The changes between intervals of time-domain parameters (SDNN and RMSSD) of experiment E2D2 (data normalized by interval I).

			SDNN		
			Intervals		
	I	II	III	IV	V
RRI	1	0.87 ± 0.19	0.69 ± 0.25	0.79 ± 0.39	0.76 ± 0.32
SBP	1	1.25 ± 0.47	1.20 ± 0.53	1.25 ± 0.30	1.10 ± 0.29
DBP	1	0.96 ± 0.27	0.90 ± 0.46	0.89 ± 0.27	0.89 ± 0.18
PAT	1	0.93 ± 0.45	1.25 ± 0.46	1.65 ± 1.67	2.46 ± 3.00
IF1	1	4.24 ± 4.08	3.89 ± 2.32	3.63 ± 2.60	4.39 ± 4.08
IF2	1	1.35 ± 0.55	1.33 ± 0.53	1.27 ± 0.33	1.41 ± 0.69
			RMSSD		
			Intervals		
	I	II	III	IV	V
RRI	1	0.78 ± 0.54	0.45 ± 0.26	0.63 ± 0.60	0.43 ± 0.17
SBP	1	0.66 ± 0.21	0.79 ± 0.15	0.73 ± 0.30	0.70 ± 0.18
DBP	1	0.61 ± 0.11	0.59 ± 0.17	0.62 ± 0.22	0.64 ± 0.17
PAT	1	0.61 ± 0.36	0.65 ± 0.21	1.02 ± 1.08	1.21 ± 1.30
IF1	1	2.16 ± 1.56	2.27 ± 0.88	1.97 ± 1.06	2.14 ± 1.76
IF2	1	0.77 ± 0.18	0.79 ± 0.09	0.77 ± 0.20	0.72 ± 0.26

The changes between intervals of time-domain parameters (SDNN and RMSSD) of experiment C1D1 (data normalized by interval I).

			SDNN		
			Intervals		
	I	II	III	IV	V
RRI	1	0.86 ± 0.35	0.93 ± 0.54	1.02 ± 0.50	0.91 ± 0.64
SBP	1	1.51 ± 0.54	1.14 ± 0.70	1.07 ± 0.65	1.06 ± 0.41
DBP	1	1.27 ± 0.34	0.98 ± 0.38	0.89 ± 0.30	0.93 ± 0.23
PAT	1	1.00 ± 0.40	1.16 ± 0.53	1.24 ± 0.56	1.20 ± 0.74
IF1	1	1.09 ± 0.50	1.27 ± 0.92	1.43 ± 1.19	1.26 ± 0.73
IF2	1	1.09 ± 0.48	1.07 ± 0.76	1.25 ± 0.68	1.07 ± 0.18
			RMSSD		
			Intervals		
	I	II	III	IV	V
RRI	1	0.47 ± 0.18	0.39 ± 0.25	0.58 ± 0.45	0.35 ± 0.20
SBP	1	0.69 ± 0.10	0.68 ± 0.26	0.72 ± 0.24	0.76 ± 0.27
DBP	1	0.69 ± 0.20	0.74 ± 0.30	0.73 ± 0.19	0.71 ± 0.25
PAT	1	0.53 ± 0.21	0.53 ± 0.16	0.51 ± 0.21	0.47 ± 0.30
IF1	1	0.81 ± 0.36	0.79 ± 0.35	0.96 ± 0.70	0.84 ± 0.43
IF2	1	0.78 ± 0.20	0.67 ± 0.22	0.76 ± 0.26	0.75 ± 0.16

The changes between intervals of time-domain parameters (SDNN and RMSSD) of experiment C1D2 (data normalized by interval I).

			SDNN Intervals		
	I	II	III	IV	V
RRI	1	0.92 ± 0.26	0.93 ± 0.23	0.97 ± 0.40	0.72 ± 0.27
SBP	1	0.98 ± 0.41	0.76 ± 0.33	0.83 ± 0.24	0.77 ± 0.33
DBP	1	0.98 ± 0.45	0.75 ± 0.31	0.81 ± 0.11	0.74 ± 0.24
PAT	1	1.13 ± 0.44	1.15 ± 0.36	1.17 ± 0.48	1.01 ± 0.36
IF1	1	1.96 ± 1.72	2.26 ± 1.30	2.07 ± 1.40	2.27 ± 1.52
IF2	1	1.16 ± 0.53	1.30 ± 0.63	1.27 ± 0.80	1.35 ± 0.80
			RMSSD Intervals		
	I	II	III	IV	V
RRI	1	0.67 ± 0.34	0.62 ± 0.32	0.77 ± 0.63	0.54 ± 0.37
SBP	1	0.74 ± 0.15	0.68 ± 0.13	0.68 ± 0.17	0.58 ± 0.09
DBP	1	0.77 ± 0.29	0.63 ± 0.14	0.64 ± 0.17	0.57 ± 0.22
PAT	1	0.78 ± 0.33	0.66 ± 0.25	0.61 ± 0.21	0.51 ± 0.16
IF1	1	1.38 ± 0.98	1.48 ± 0.80	1.34 ± 0.99	1.32 ± 0.85
IF2	1	0.76 ± 0.36	0.79 ± 0.25	0.80 ± 0.40	0.82 ± 0.39

Frequency-domain parameters of RRI, SBP, DBP, PAT, IF1, and IF2 at five rest intervals of all experiments E1D1. The results are expressed as box plots with a median (line inside box), 25% and 75% quartiles (box), range (whiskers) and outliers (plus).

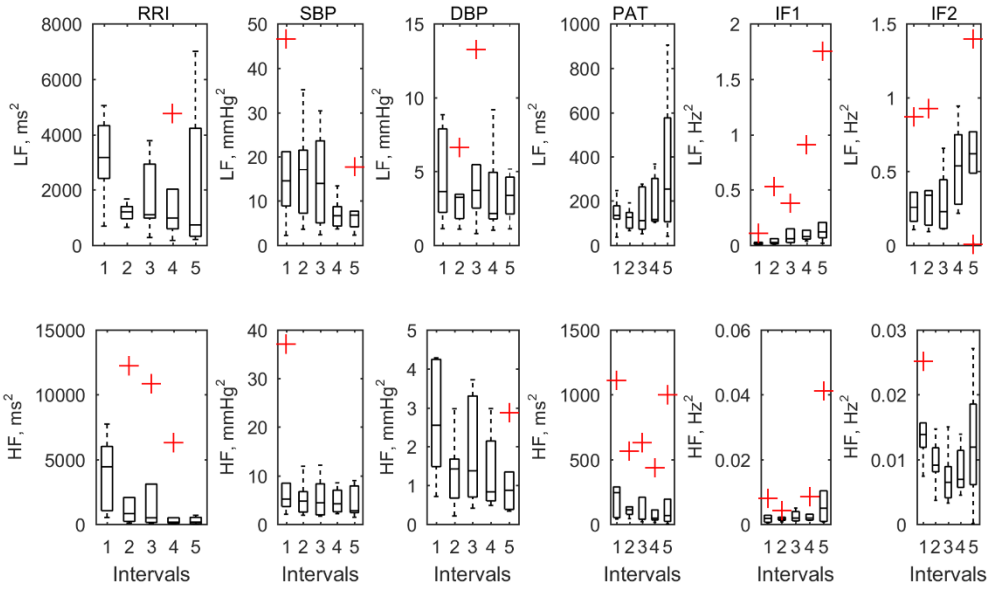

Frequency-domain parameters of RRI, SBP, DBP, PAT, IF1, and IF2 at five rest intervals of all experiment E1D2. The results are expressed as box plots with a median (line inside box), 25% and 75% quartiles (box), range (whiskers) and outliers (plus).

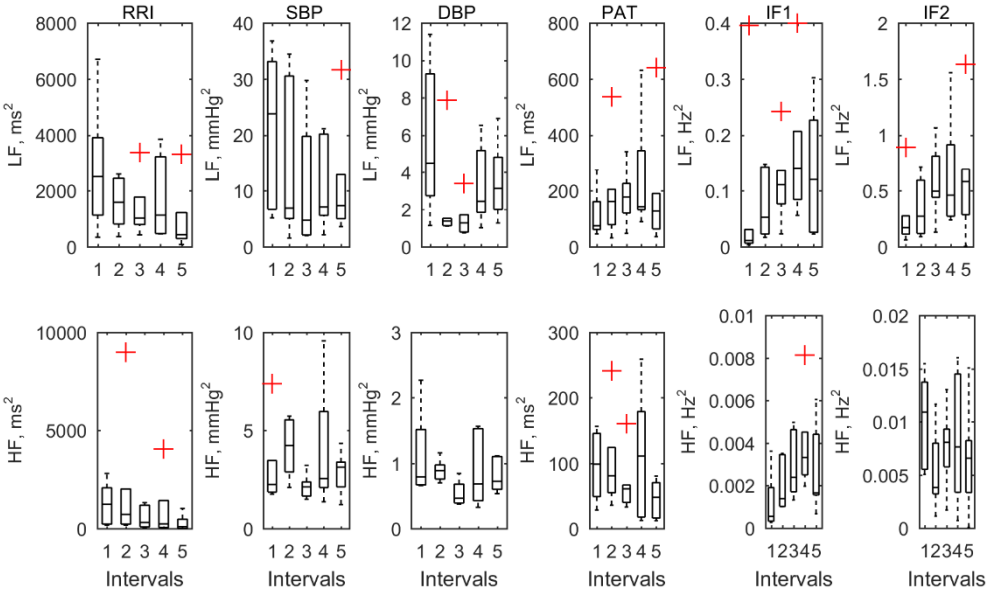

Frequency-domain parameters of RRI, SBP, DBP, PAT, IF1, and IF2 at five rest intervals of all experiment E2D1. The results are expressed as box plots with a median (line inside box), 25% and 75% quartiles (box), range (whiskers) and outliers (plus).

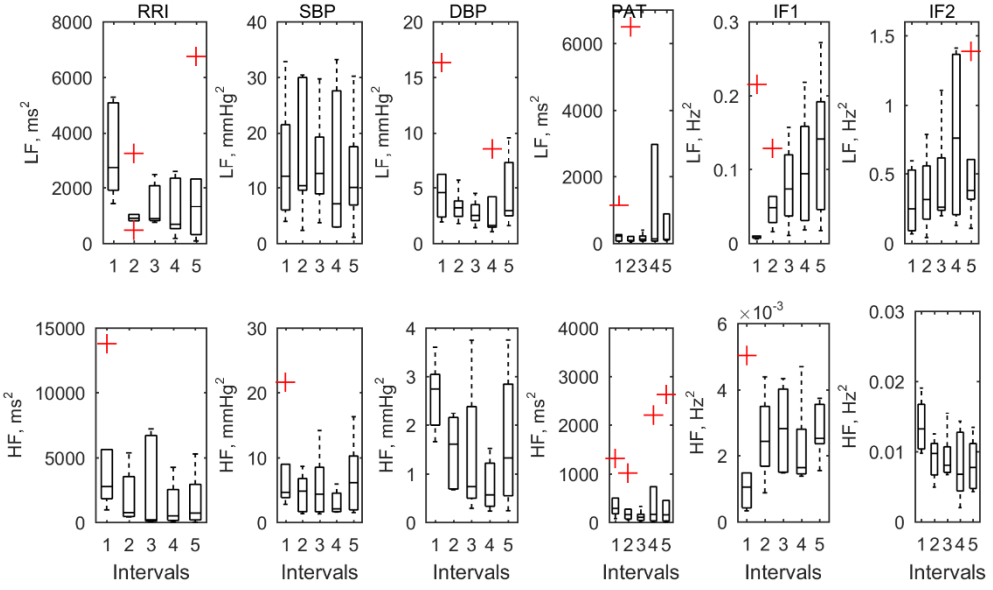

Frequency-domain parameters of RRI, SBP, DBP, PAT, IF1, and IF2 at five rest intervals of all experiment E2D2. The results are expressed as box plots with a median (line inside box), 25% and 75% quartiles (box), range (whiskers) and outliers (plus).

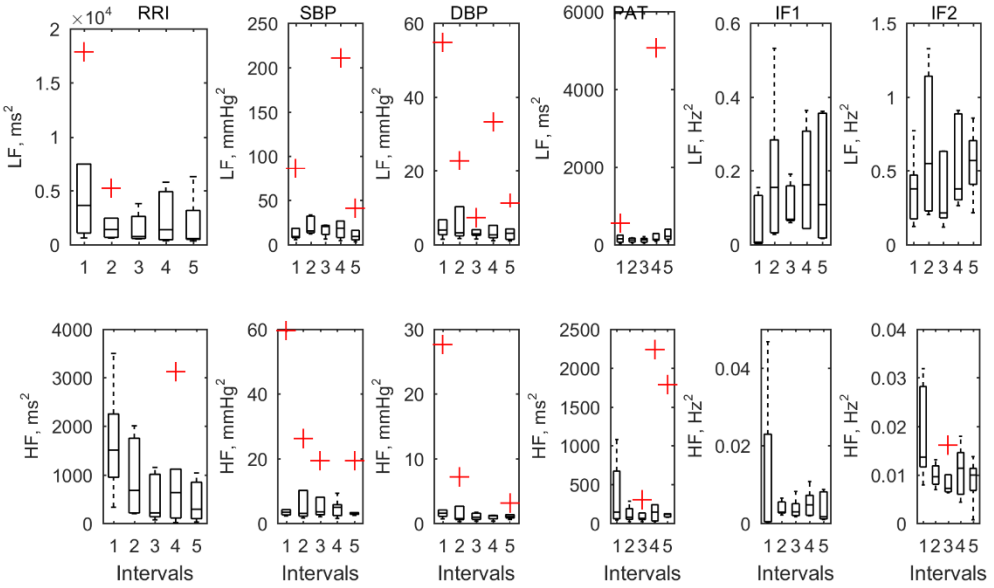

Frequency-domain parameters of RRI, SBP, DBP, PAT, IF1, and IF2 at five rest intervals of all experiment C1D1. The results are expressed as box plots with a median (line inside box), 25% and 75% quartiles (box), range (whiskers) and outliers (plus).

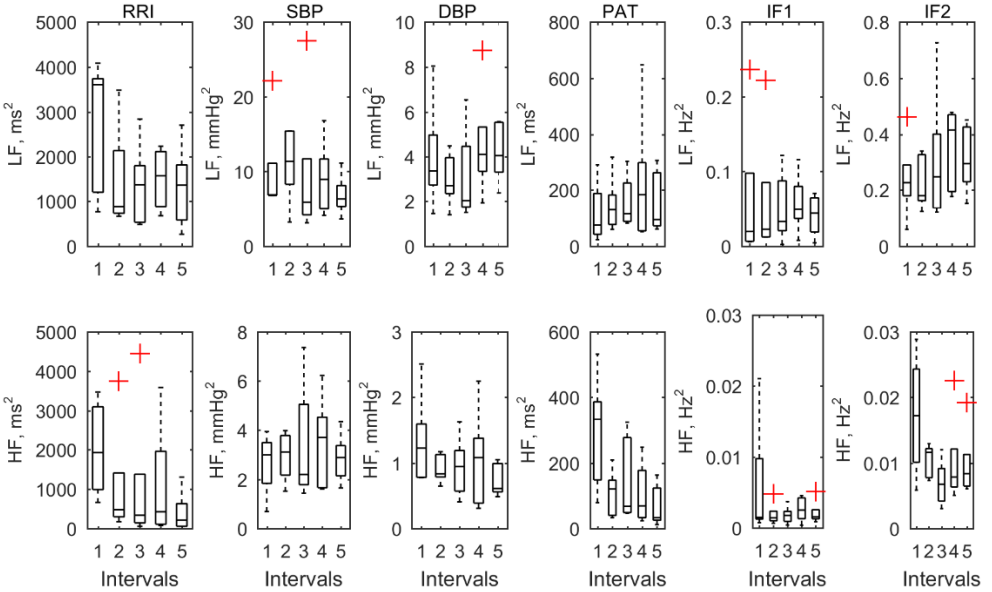

Frequency-domain parameters of RRI, SBP, DBP, PAT, IF1, and IF2 at five rest intervals of all experiment C1D2. The results are expressed as box plots with a median (line inside box), 25% and 75% quartiles (box), range (whiskers) and outliers (plus).

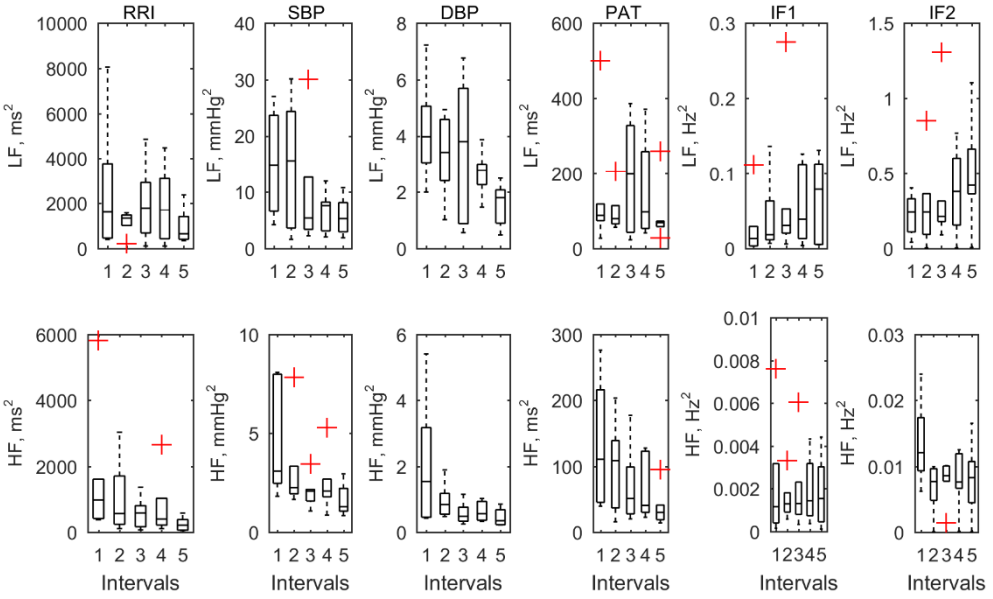

The changes between intervals of frequency-domain parameters (LF and HF) of experiment E1D1 (data normalized by interval I).

			LF Intervals		
	I	II	III	IV	V
RRI	1	1.15 ± 0.83	0.96 ± 0.75	0.73 ± 0.70	0.68 ± 0.66
SBP	1	1.17 ± 1.25	0.69 ± 0.62	0.90 ± 1.21	1.12 ± 1.22
DBP	1	0.87 ± 0.76	0.68 ± 0.60	0.56 ± 0.41	0.87 ± 0.77
PAT	1	3.05 ± 3.94	1.40 ± 1.56	2.84 ± 5.15	10.59 ± 23.41
IF1	1	5.15 ± 9.66	3.97 ± 4.61	4.91 ± 5.42	5.56 ± 9.47
IF2	1	1.15 ± 1.07	0.78 ± 0.34	0.79 ± 0.46	0.78 ± 0.52
			HF Intervals		
	I	II	III	IV	V
RRI	1	0.48 ± 0.56	0.42 ± 0.51	0.21 ± 0.31	0.10 ± 0.09
SBP	1	0.97 ± 0.70	0.84 ± 0.73	0.94 ± 0.97	0.84 ± 0.81
DBP	1	0.57 ± 0.34	0.69 ± 0.36	0.64 ± 0.51	0.52 ± 0.39
PAT	1	0.79 ± 0.60	0.55 ± 0.36	0.63 ± 0.80	3.45 ± 7.84
IF1	1	2.44 ± 3.85	2.33 ± 2.49	2.17 ± 1.76	4.61 ± 5.83
IF2	1	0.68 ± 0.27	0.49 ± 0.12	0.57 ± 0.17	0.83 ± 0.72

The changes between intervals of frequency-domain parameters (LF and HF) of experiment E1D2 (data normalized by interval I).

			LF Intervals		
	I	II	III	IV	V
RRI	1	2.40 ± 3.53	0.79 ± 0.67	1.57 ± 1.93	0.39 ± 0.32
SBP	1	0.90 ± 0.59	0.66 ± 0.40	1.16 ± 1.11	0.80 ± 0.64
DBP	1	0.64 ± 0.61	0.42 ± 0.18	0.74 ± 0.81	0.53 ± 0.24
PAT	1	1.86 ± 2.20	1.27 ± 1.04	3.28 ± 3.31	1.69 ± 1.63
IF1	1	2.34 ± 2.00	7.38 ± 8.25	4.40 ± 4.38	5.93 ± 7.64
IF2	1	0.64 ± 0.18	1.06 ± 0.47	0.93 ± 0.39	0.76 ± 0.44
			HF Intervals		
	I	II	III	IV	V
RRI	1	3.09 ± 5.64	0.62 ± 0.77	1.47 ± 2.56	0.21 ± 0.19
SBP	1	1.52 ± 0.69	0.87 ± 0.43	1.79 ± 1.84	1.16 ± 0.68
DBP	1	0.98 ± 0.42	0.62 ± 0.39	1.11 ± 0.97	0.95 ± 0.56
PAT	1	1.72 ± 1.81	1.07 ± 0.97	1.76 ± 2.02	0.63 ± 0.49
IF1	1	3.91 ± 4.67	6.60 ± 6.27	8.05 ± 9.02	6.45 ± 7.38
IF2	1	0.63 ± 0.61	0.81 ± 0.49	0.73 ± 0.37	0.63 ± 0.43

The changes between intervals of frequency-domain parameters (LF and HF) of experiment E2D1 (data normalized by interval I).

			LF Intervals		
	I	II	III	IV	V
RRI	1	1.19 ± 1.30	1.69 ± 2.21	1.46 ± 1.48	1.51 ± 1.50
SBP	1	1.11 ± 0.84	1.58 ± 1.45	1.34 ± 1.03	1.56 ± 1.43
DBP	1	0.67 ± 0.36	0.91 ± 0.67	0.87 ± 0.86	0.79 ± 0.52
PAT	1	1.77 ± 1.52	1.99 ± 2.05	3.31 ± 3.34	2.99 ± 3.10
IF1	1	3.47 ± 2.30	4.14 ± 3.95	2.08 ± 1.36	4.10 ± 3.22
IF2	1	1.09 ± 0.42	0.88 ± 0.44	0.69 ± 0.30	0.75 ± 0.43
			HF Intervals		
	I	II	III	IV	V
RRI	1	0.49 ± 0.43	1.62 ± 3.30	0.52 ± 0.86	0.68 ± 1.18
SBP	1	0.91 ± 0.79	0.76 ± 0.48	0.73 ± 0.47	1.14 ± 0.97
DBP	1	0.58 ± 0.26	0.49 ± 0.45	0.31 ± 0.24	0.67 ± 0.62
PAT	1	0.67 ± 0.40	0.57 ± 0.55	0.59 ± 0.65	0.73 ± 0.71
IF1	1	3.15 ± 2.55	3.56 ± 3.53	2.30 ± 2.41	3.41 ± 2.62
IF2	1	0.70 ± 0.25	0.70 ± 0.23	0.63 ± 0.45	0.61 ± 0.30

The changes between intervals of frequency-domain parameters (LF and HF) of experiment E2D2 (data normalized by interval I).

			LF		
			Intervals		
	I	II	III	IV	V
RRI	1	1.13 ± 0.66	0.52 ± 0.15	0.82 ± 0.63	0.60 ± 0.36
SBP	1	1.32 ± 0.87	1.11 ± 0.85	1.51 ± 1.29	1.33 ± 1.28
DBP	1	0.71 ± 0.39	0.54 ± 0.35	0.72 ± 0.46	0.70 ± 0.36
PAT	1	1.49 ± 1.86	1.45 ± 1.06	5.14 ± 10.19	17.62 ± 36.86
IF1	1	10.29 ± 9.84	10.24 ± 5.79	8.10 ± 6.13	13.79 ± 18.21
IF2	1	0.85 ± 0.27	0.83 ± 0.40	0.71 ± 0.38	0.85 ± 0.69
			HF		
			Intervals		
	I	II	III	IV	V
RRI	1	1.33 ± 2.09	0.33 ± 0.24	0.60 ± 0.79	0.28 ± 0.23
SBP	1	0.99 ± 0.69	0.92 ± 0.62	1.20 ± 0.98	0.88 ± 0.40
DBP	1	1.50 ± 0.17	0.48 ± 0.26	0.58 ± 0.33	0.69 ± 0.44
PAT	1	0.79 ± 1.07	0.62 ± 0.40	4.11 ± 9.04	3.71 ± 7.04
IF1	1	5.90 ± 5.93	6.00 ± 3.45	6.23 ± 5.25	10.56 ± 14.60
IF2	1	0.57 ± 0.21	0.61 ± 0.17	0.70 ± 0.40	0.61 ± 0.47

The changes between intervals of frequency-domain parameters (LF and HF) of experiment C1D1 (data normalized by interval I).

			LF		
			Intervals		
	I	II	III	IV	V
RRI	1	0.68 ± 0.43	0.64 ± 0.59	1.28 ± 1.33	0.84 ± 0.76
SBP	1	2.04 ± 1.83	1.41 ± 1.23	1.51 ± 1.52	1.31 ± 0.98
DBP	1	0.76 ± 0.56	0.78 ± 0.54	0.72 ± 0.64	0.72 ± 0.54
PAT	1	0.83 ± 1.02	1.09 ± 1.13	1.05 ± 0.53	1.00 ± 1.05
IF1	1	0.85 ± 0.70	0.94 ± 1.09	1.20 ± 1.70	1.00 ± 0.93
IF2	1	0.77 ± 0.51	0.60 ± 0.54	0.79 ± 0.50	0.70 ± 0.21
			HF		
			Intervals		
	I	II	III	IV	V
RRI	1	0.48 ± 0.40	0.43 ± 0.51	0.61 ± 0.57	0.23 ± 0.26
SBP	1	1.47 ± 1.13	2.06 ± 2.41	1.99 ± 2.15	1.55 ± 1.48
DBP	1	0.80 ± 0.29	0.88 ± 0.54	0.86 ± 0.66	0.70 ± 0.40
PAT	1	0.42 ± 0.22	0.50 ± 0.24	0.41 ± 0.31	0.40 ± 0.57
IF1	1	0.83 ± 0.77	0.87 ± 1.01	1.86 ± 2.38	1.32 ± 1.52
IF2	1	0.81 ± 0.66	0.56 ± 0.50	0.86 ± 0.80	0.76 ± 0.61

The changes between intervals of frequency-domain parameters (LF and HF) of experiment C1D2 (data normalized by interval I).

			LF Intervals		
	I	II	III	IV	V
RRI	1	0.95 ± 0.65	0.94 ± 0.56	1.79 ± 2.35	0.64 ± 0.45
SBP	1	0.88 ± 0.86	0.51 ± 0.18	0.69 ± 0.67	0.67 ± 0.61
DBP	1	0.46 ± 0.24	0.40 ± 0.08	0.44 ± 0.29	0.45 ± 0.24
PAT	1	1.24 ± 0.77	1.13 ± 0.57	1.13 ± 0.93	0.77 ± 0.46
IF1	1	5.61 ± 10.55	2.81 ± 1.91	3.51 ± 4.40	2.11 ± 2.18
IF2	1	0.87 ± 0.60	0.75 ± 0.39	0.93 ± 0.70	0.95 ± 0.67
			HF Intervals		
	I	II	III	IV	V
RRI	1	0.78 ± 0.64	1.01 ± 1.35	1.52 ± 2.71	0.36 ± 0.51
SBP	1	0.79 ± 0.28	0.63 ± 0.43	0.62 ± 0.24	0.51 ± 0.37
DBP	1	0.78 ± 0.52	0.51 ± 0.40	0.49 ± 0.27	0.40 ± 0.28
PAT	1	0.95 ± 0.80	0.67 ± 0.36	0.56 ± 0.23	0.41 ± 0.34
IF1	1	2.85 ± 4.30	1.62 ± 0.89	3.02 ± 3.96	2.25 ± 2.78
IF2	1	0.62 ± 0.52	0.70 ± 0.51	0.68 ± 0.47	0.71 ± 0.61